A CONSTITUTIVE EQUATION FOR MAMMALIAN SKELETAL MUSCLE TISSUE IN THE PASSIVE AND FULLY STIMULATED STATES

Dissertation for the Degree of Ph. D.
MICHIGAN STATE UNIVERSITY
DAVID L. BUTLER
1976





This is to certify that the

thesis entitled A CONSTITUTIVE EQUATION FOR MAMMALIAN SKELETAL MUSCLE TISSUE IN THE PASSIVE AND FULLY STIMULATED STATES presented by

David L. Butler

has been accepted towards fulfillment of the requirements for

Ph.D. degree in Mechanics

Major professor

Date May 21, 1976

O-7639

			•
			•
			i : :
			; ;
			, ,

(ph/43/)

ABSTRACT

A CONSTITUTIVE EQUATION FOR MAMMALIAN SKELETAL MUSCLE TISSUE IN THE PASSIVE AND FULLY STIMULATED STATES

By

David L. Butler

The purpose of this research is to construct a constitutive equation for unstimulated (passive) and tetanized skeletal muscle tissue. Results of experimental tests and anatomical studies provided the foundation for the development of the model. The anterior gracilis muscle was removed from the thigh of the Sprague-Dawley rat and placed in an oxygenated physiological salt solution at 25°C. Three kinds of mechanical tests were conducted on the passive muscle: stress relaxation tests using prescribed input strains and strain rates, loading and unloading tests at various strain rates, and sinusoidal tests, conducted at predetermined peak amplitudes and frequencies of oscillation. Tetanic stimuli generated force response curves and established the active mathematical model. Selected muscles were stained to determine muscle composition.

A model for the muscle was generated by the arrangement of three anatomic components: a connective tissue sheath composed of collagenous fibers was in parallel with muscle

cells and both were in series with collagenous tendon ends. The quasi-linear viscoelastic expression developed previously for collagenous tissue was utilized to develop the functional form of the constitutive equation for both the tendon ends and connective tissue sheath. Experimental stress relaxation tests were conducted on the muscle to determine the material parameters for the collagenous components in the model and to deduce the behavior of the muscle cells. The constitutive equations for the tissue components were mathematically combined to compute the stresses in the composite tissue and the computer was used to simplify the calculations. resulting composite constitutive equation was then used to predict the results of constant strain-rate loading, constant strain-rate loading and unloading and sinusoidal input deformation tests. Good agreement was found between theory and the passive experimental tests for peak strain levels below 40-45% and for strain rates less than 50%/min (20-30 rad./min. in the sinusoidal tests). The mathematical expression for the tetanic force-muscle length curves was generated from empirical tests on the tetanized gracilis muscle and agreement between the resulting tetanic stress-passive strain curves was observed for strains below 50%.

A CONSTITUTIVE EQUATION FOR MAMMALIAN SKELETAL MUSCLE TISSUE IN THE PASSIVE AND FULLY STIMULATED STATES

Вy

David L. Butler

A DISSERTATION

Submitted to
Michigan State University
in partial fulfillment of the requirements
for the degree of

DOCTOR OF PHILOSOPHY

Department of Metallurgy, Mechanics and Materials Science

ACKNOWLEDGEMENTS

I would like to thank a number of individuals for their financial, technical and moral support throughout my doctoral program:

Dr. Robert W. Little, my advisor, for assistance in the development of the mathematical formulation and preparation of the thesis as well as for frequent encouragement.

My other committee members, Dr. William Sharpe, Dr. Robert Echt and Dr. Richard Heisey, for their valuable comments during data collection and final thesis preparation.

The Department of Health, Education and Welfare for its NDEA Graduate Fellowship and the Division of Engineering Research for its research assistantships.

The National Institutes of Health for the grant to cover equipment costs.

Dr. Frank Kutyna and Mr. Roland Roy for help in developing surgical techniques.

Mr. Robert Wells and Mr. Bob Rose for assistance in instrumentation methods.

Mr. Don Childs and Mr. Stan Kurtz for machining of necessary parts.

Mr. Jon Tyner for photographic assistance and design of camera stand.

Mrs. Barb Wheaton for her help in histologic sectioning.

My wife, Sara, for her patience, encouragement, and technical assistance throughout this ordeal.

TABLE OF CONTENTS

		Page
LIST OF	TABLES	vi
LIST OF	FIGURES	vii
LIST OF	MATHEMATICAL SYMBOLS	хi
Chapter		
I.	INTRODUCTION	1
	1.1 Connective Tissue	2
	1.2 Muscle Tissue	4 5
II.	SKELETAL MUSCLE TISSUE	8
	2.1 Anatomy	8 11 14
III.	SURVEY OF LITERATURE	18
	3.1 Introduction	18 18 18
	3.2b. Unstimulated Skeletal Muscle	26 31 31 36
IV.	EXPERIMENTAL METHODS	41
	4.1 Nomenclature 4.2 Surgical Technique 4.3 In Vitro Muscle Chamber 4.4 Equipment Exterior to Chamber 4.4a. Visual Muscle Inspection 4.4b. Temperature Control 4.4c. Passive Testing	41 42 43 45 45 46 47
	4.4d. Active Testing	50 53

Chapter		Page
v.	MATHEMATICAL FORMULATION	74
	5.1 Development	74 98 99
	Test	99
	and Unloading Test	100 100 101
VI.	PRESENTATION AND DISCUSSION OF RESULTS	104
	6.1 Presentation	104
	Muscle	104
	Muscle	11/
VII.	CONCLUSIONS	148
BIBLIOGRA	АРНУ	153
APPENDICE	ES	
	A. Method for Neural Stimulation of the In Vitro Anterior Gracilis Muscle	161
	B. Visual Technique for Close Muscle Inspection	165
	Stimulator	168

LIST OF TABLES

Table		Page
3.1	The Ratio of the Resting Length (Corresponding to Peak Tetanic Tension) to the Passive Length (Corresponding to First Loading of Unstimulated Muscle) for Various Amphibian and Mammalian Muscles	. 20
3.2	Peak Isometric Tetanic Stress (Peak Force per Cross-sectional Area) for Different Amphibian and Mammalian Skeletal Muscles at Different Temperatures	. 25

LIST OF FIGURES

Figure		Page
3.1	Hill's three-element model	33
4.1	Thigh of a rat	56
4.2	Side view of Plexiglas test chamber	57
4.3	One stainless steel specimen clamp and two Plexiglas stimulator plates	58
4.4	Anterior gracilis muscle with pubic bone chip attached to one specimen clamp	59
4.5	Diagram of the anterior gracilis muscle fixed between the specimen bone clamps in the test chamber	60
4.6a	Photograph of anterior gracilis muscle taken using the camera stand	61
4.6b	Photograph of anterior gracilis muscle taken using the camera stand	62
4.7	Constant strain-rate test fixture	63
4.8	Test setup	64
4.9	Sinusoidal test fixture	65
4.10	Sanborn Recorder, Varian X-Y Recorder, Keithley Digital Multimeter and Rosemount Constant Temperature Ice Bath	66
4.11	Grass Stimulator, auxiliary stimulator and Tektronix Oscilloscope	67
4.12a	Sanborn record showing the effect of stimulus frequency variation upon the forcetime response of the isometrically	
	stimulated anterior gracilis muscle	68

Figure		Page
4.12b	Sanborn record showing the effect of muscle length upon the amplitude of the tetanic force-time response of isometrically stimulated gracilis muscle	69
4.13a	Anterior gracilis muscle cells in cross-section (hematoxylin and eosin stain)	70
4.13b	Anterior gracilis muscle cells in cross- section (trichrome stain)	71
4.14a	Anterior gracilis muscle cells in longitudinal view (trichrome stain)	72
4.14b	Anterior gracilis muscle cells in longitudinal view (H and E stain)	73
5.1	Model for skeletal muscle	77
5.2	Experimental stress relaxation test	99.
5.3	Constant strain rate test	99
5.4	Constant strain rate loading and unloading test	100
5.5	Sinusoidal strain input test	100
6.1	Stress plotted as a function of strain for different strain-rates shown for each curve	126
6.2	Stress plotted as a function of strain for a constant strain-rate of 6.0%/min	127
6.3	Stress plotted as a function of strain for a constant strain-rate of 16.0%/min	128
6.4	Stress plotted as a function of strain for a constant strain-rate of 35.0%/min	129
6.5	Stress plotted as a function of strain for a constant strain-rate of 46.5%/min	130
6.6	Stress plotted as a function of strain for a constant strain-rate of 58.5%/min	131
6.7	Stress plotted as a function of time for constant strain-rate loading at 5.5%/min. followed by stress relaxation at 45.0% strain	132
		102

Figure		Page
6.8	Stress plotted as a function of time for constant strain-rate loading at 16.5%/min. followed by stress relaxation at 41.0%	122
	strain	133
6.9	Stress plotted as a function of time for constant strain-rate loading at 30.0%/min. followed by stress relaxation at 42.5%	
	strain	134
6.10	Stress plotted as a function of time for constant strain-rate loading at 49.0%/min. followed by stress relaxation at 20.0%	
	strain	135
6.11	Stress plotted as a function of time for constant strain-rate loading at 56.5%/min. followed by stress relaxation at 28.0% strain	136
	strain	130
6.12	Stress plotted as a function of strain for constant strain-rate loading at 7.0%/min. to 46.5% strain followed by unloading at the same rate	137
	the same rate	137
6.13	Stress plotted as a function of strain for constant strain-rate loading at 15.5%/min. to 43.0% strain followed by unloading at the same rate	138
		130
6.14	Stress plotted as a function of strain for constant strain-rate loading at 35.0%/min. to 46.5% strain followed by unloading at	
	the same rate	139
6.15	Stress plotted as a function of strain for constant strain-rate loading at 65.5%/min. to 48.0% strain followed by unloading at	
	the same rate	140
6.16	Peak stress plotted as a function of cycle number for positive sinusoidally-varying	
	strains	141
6.17	Peak stress plotted as a function of cycle number for positive sinusoidally-varying	
	strains	142

Figure		Page
6.18	Peak stress plotted as a function of cycle number for positive sinusoidally-varying strains	143
6.19	Peak stress plotted as a function of cycle number for positive sinusoidally-varying strains	144
6.20	Peak stress plotted as a function of cycle number for positive sinusoidally-varying strains	145
6.21	Force plotted as a function of muscle length for tetanized and unstimulated (passive) muscle	146
6.22	Stress plotted as a function of strain for tetanized and unstimulated (passive) muscle	147
A.1	Suction electrode	164
B.1	(a) Photograph of camera stand and base and (b) sketch of apparatus	167
C.1	Circuit diagram of auxiliary stimulator	169

LIST OF MATHEMATICAL SYMBOLS

A	Ratio of effective cross-sectional area of the muscle cells; \textbf{A}^{m} divided by $\overline{\textbf{A}}$
\overline{A} , A^{te} , A^{m} , A^{c}	Initial cross-sectional areas of the composite tissue, tendon, muscle cells and connective tissue sheath, respectively
В	Ratio of effective cross-sectional area of the connective tissue sheath; A^{c} divided by \overline{A}
b	Constant in Fung's elastic stress develop- ment
С	Constant in Haut and Little's elastic stress expression and used in this study
D	Constant in Fung's elastic stress develop- ment
E	Constant in Haut and Little's stress expression and used in this study
F	Elastic constant relating the stress and strain in the muscle cells
G(t)	"Reduced" relaxation function developed by Fung and used in this study
i	Interval number in iterative process
I ₁ ,I ₂ ,,I ₅	Integrals in general stress expressions in Regions 1 and 2
$\overline{1}_1, \overline{1}_2, \dots, \overline{1}_5$	Integrals in general stress expressions in Region 2 (when $t = t_{i-NT} = t_k$)
j	Interval number in iterative process
k	Interval number in iterative process
K	Constant in Fung's elastic stress expression

$\kappa_1, \kappa_2, \kappa_3$	Constants in tetanic stress expression
KT	First interval in Region 2; NT + 1
1,1 ^{te} ,1 ^m ,1 ^c	Initial lengths of the composite tissue, tendon, muscle cells and connective tissue sheath, respectively
l (subscript)	<pre>Interval number in iterative process; j + NT</pre>
L	Current specimen length used by Haut and Little
L ₀	Original specimen length used by Haut and Little
М	Constant in Haut and Little's development of a relaxation function and used in this study
NT	Last interval in Region 1
P ₀	Peak tetanic force at the "resting length"
Pi	Group of terms for use in the quadratic formula and stress development in interval, i, Regions 1 and 2
QS _j	Group of terms for use in the quadratic formula and stress development in interval, j, Region 2
^{QT} j	Group of terms for use in the quadratic formula and stress development in interval, j, Region 2
S	Time-dependent constant in first interval of stress expression
t	Time course of test
t _i	Total time at end of interval, i
TAi	Group of terms for use in quadratic formula and stress development in interval, i, Region 2
Yi	Group of terms for use in quadratic formula and stress development in interval, i, Region 2

$\beta_{\mathbf{i}}, \beta_{\mathbf{i}}^{te}, \beta_{\mathbf{i}}^{m}, \beta_{\mathbf{i}}^{c}$	Strain rates in the interval, i, for the composite tissue, tendon, muscle cells and connective tissue sheath, respectively
$\Delta \varepsilon_{\mathbf{i}}, \Delta \varepsilon_{\mathbf{i}}^{\mathbf{te}}, \Delta \varepsilon_{\mathbf{i}}^{\mathbf{m}}, \Delta \varepsilon_{\mathbf{i}}^{\mathbf{c}}$	Strain increments in the interval, i, for the composite tissue, tendon, muscle cells and connective tissue sheath, respectively
$\Delta \sigma_{\mathbf{i}}, \Delta \sigma_{\mathbf{i}}^{te}, \Delta \sigma_{\mathbf{i}}^{m}, \Delta \sigma_{\mathbf{i}}^{c}$	Stress increments in the interval, i, for the composite tissue, tendon, muscle cells and connective tissue sheath, respectively
Δt _i	Time increment in interval, i
ε	Lagrangian strain; change in specimen length per original specimen length
$\varepsilon_{\mathbf{i}}^{,\varepsilon_{\mathbf{i}}^{te},\varepsilon_{\mathbf{i}}^{m},\varepsilon_{\mathbf{i}}^{c}$	Total strains at the end of the interval, i, for the composite tissue, tendon, muscle cells and connective tissue sheath, respectively
-m ε	Strain in the muscle cells at the transition between Regions 1 and 2
ε0	Peak strain in composite tissue during sinusoidal displacements
λ	Extension ratio; current specimen length per original specimen length as used by Fung
μ	Normalized slope of stress - ρ_m (time) curve employed by Haut and Little and used in this study
$\sigma^{\mathbf{e}}(\varepsilon)$, $\sigma_{\mathbf{e}}(\varepsilon)$	Elastic stress response, independent of time and a function of strain
σ (t)	Lagrangian or engineering stress; force per unit area
σ _i ,σ _i ,σ _i ,σ _i	Lagrangian stresses at the end of interval, i, for the composite tissue, tendon, muscle cells and connective tissue sheath, respectively
σ	Total stress in the composite tissue
$\sigma^{ extsf{stim}}$	Tetanic stress in the muscle cells
τ	Variable of integration
ω _i	Frequency of oscillation in composite tissue during sinusoidal displacements

CHAPTER I

INTRODUCTION

For over a century, biologists and engineers have studied the mechanical properties of healthy body tissues to better understand changes in mechanical properties which occur in disease or injury and to eventually find artificial replacements for these damaged components. Tissues are composed of cells embedded in varying amounts and types of intercellular substance. The four basic tissues are epithelial, nerve, connective and muscle and, in combination, they form the organs of the body. Connective and muscle tissues serve the major function of transmitting load or deformations and an understanding of their mechanical properties is essential.

Certain fibrous components in the intercellular substance of soft tissues have been found to carry the majority of mechanical loads. Epithelial and nerve tissues which contain numerous cells in a minimum of intercellular substance, are therefore unable to lend mechanical strength to an organ. However, extensive research has been conducted on connective and muscle tissues due to the loadbearing capacity of the former and the contractile ability

of the latter. This study will investigate the mechanical response of mammalian skeletal muscle.

A preliminary classification of the various types of connective and muscle tissues will first be given, followed by a statement of the purpose of this research. Skeletal muscle will be investigated in detail in Chapter II.

1.1 Connective Tissue

Connective tissue consists of living cells enveloped by intercellular substance or matrix. The latter is composed of fibers which are formed by cells known as fibroblasts, as well as extracellular fluid and an amorphous gel known as ground substance. The amount, type and orientation of the fibers determine the mechanical strength of the tissue. The three types of intercellular fibers which are found in connective tissue are collagenous, reticular and elastic fibers. Collagenous fibers consist of a protein known as collagen and contain parallel bundles of smaller fibrils. These fibers are quite resistant to stretch, displaying a large modulus or slope in the loading curves at higher loads. Reticular fibers resemble collagenous fibers and are thought to be smaller, immature collagen fibrils. These fibers usually appear in a two-dimensional network or reticulum surrounding structures such as blood vessels, muscle fibers and nerve fibers. Elastic fibers

are more extensible than the other types and retain their shape when released after loading. The strands are rather homogeneous in content, nonwavy, and are composed of the protein elastin (17, 50, 65, 74).

It is both the ratio of cells to intercellular substance and the relative packing that results in the connective tissue classifications of dense and loose. The dense varieties may be organized or unorganized. The dense organized types, having parallel bundles, include collagenous tendons connecting muscle to bone, collagenous and elastic ligaments linking bone to bone, and aponeuroses or flattened tendonous membranes. Dense unorganized tissue is termed fascia and contains interwoven, non-parallel fibers in the form of sheets which surround organs, blood vessels, bone and cartilage. Loose fibrous types normally contain elastic fibers and include:

1) fibroelastic tissue, with an abundance of elastic fibers

- fibroelastic tissue, with an abundance of elastic fibers in the matrix such as observed in capsules around organs;
- 2) areolar tissue containing spaces filled with ground substance; 3) reticular tissue containing reticular fibers; and 4) adipose tissue with a predominance of fat cells (65).

Other types of specialized connective tissue appear in the body. These kinds include cartilage and bone with minerals in the matrix adding strength, and blood, the only fluid variety (65).

1.2 Muscle Tissue

Muscle constitutes approximately 43% of the whole body weight of the human and the tissue has a predominance of living cells (also called muscle fibers) in a minimum of matrix. Muscle fibers respond by contracting when a nerve stimulus of sufficient intensity, duration and frequency is applied (81).

The three kinds of muscle tissue which are found in the body are smooth, cardiac and skeletal muscle. muscle is observed in the walls of hollow organs (visceral smooth muscle); in the interior of the eye, skin, and gland ducts (multi-unit smooth muscle); and in the urinary bladder. Smooth muscle cells are usually long and spindleshaped in appearance, are in close physical and chemical association with each other and each cell has a centrallylocated nucleus. In general, smooth muscle cells are partially contracted in the body. Visceral smooth muscle fibers spontaneously depolarize and contract and neural stimulation only modifies the speed of the contraction. Multi-unit smooth muscle cells require neural input to contract and the strength of the contraction is usually not extreme because there are few contractile elements within the cells (43, 78, 81).

Cardiac muscle is found in sheets in the muscle layer (myocardium) within the walls of the heart's chambers. Heart muscle contracts involuntarily like visceral smooth

muscle, and neural stimulation only alters the rate of the contractile process. The cells possess striations due to the presence of many contractile elements morphologically aligned, and only one central nucleus normally appears in each cell. Branching of the muscle fibers is evident and cells are in close physical contact. The strong coordinated contractions of cardiac muscle propel blood through the heart's chambers and the circulatory system (43, 81).

Skeletal muscle, the subject of this research, is found in the limbs, trunk and head. It represents the "flesh" or "meat" of most animals. Each muscle cell is long and cylindrical in shape and contains many nuclei along its outer edges. Skeletal muscle is voluntary because it requires stimuli from the voluntary nervous system to contract. Each cell, wrapped in a connective tissue sheath, is connected to one tendon fiber. Following stimulation, the muscle cells contract, generate a force, and transfer this force through the tendon fibers to bones or other types of connective tissue (81).

1.3 Statement of the Problem

Researchers have sought to determine the mechanical behavior of both passive and stimulated muscle. The mechanics of contraction have been especially important to physiologists, anatomists and biophysicists who have attempted to understand the processes involved in muscle

stimulation, in the generation of tension in the muscle and in the transfer of forces from muscle through connective tissue elements. Bioengineers have tested different types of connective tissues in uniaxial and biaxial loading and have also investigated muscle tissue in the passive state to determine force-extension curves. However, since a muscle contains both muscle tissue and connective tissue, the response of each has been hard to isolate.

A theoretical and experimental investigation of skeletal muscle will be made in the passive or unstimulated condition as well as in the fully stimulated or tetanic condition. A composite uniaxial stress-strain-time equation for a muscle containing parallel fibers will be derived using hereditary integrals to predict the response of passive tissue. The anatomic structure of muscle (assuming connective tissue in a parallel and series arrangement with muscle fibers) will be utilized to develop the mathematical model. In addition, the general shape of the tetanized muscle response curve will be found and expressed in terms of both the initial passive length and the cross-sectional area. Finally, the relative placement of the passive and tetanic stress-strain curves will be made. An iterative process will be employed using the computer to simplify the calculations.

The experimental procedure will specify uniaxial deflections of the muscle and the passive and tetanic force responses will be monitored. Cross-sectional areas and initial lengths of muscle fibers and connective tissue will be established by optical means and histologic sectioning. This procedure will permit the determination of stresses (forces per unit area) and strains (deformations per unit length).

CHAPTER II

SKELETAL MUSCLE TISSUE

2.1 Anatomy

Skeletal muscle is the most abundant of the muscle types in the body and makes its attachment to tendons or aponeuroses. A skeletal muscle may be either convex or flat in appearance and can vary in color from pale to dark red depending upon its composition and blood supply (81).

Each muscle, surrounded by a connective tissue sheath known as the epimysium, is composed of bundles of living cells or fibers. Divisions of the epimysium, called the endo- and perimysium, enclose each cell and groups of cells, respectively. Muscle cells are attached at their ends to fibrous connective tissue or tendons which are predominately composed of collagen. Each muscle fiber is comprised of bundles of long myofibrils and each myofibril, in turn, consists of a network of actin and myosin protein myofilaments which are arranged in fundamental contracting units called sarcomeres. The aligned filaments, giving a striped appearance to the muscle fiber, interact to form an actomyosin complex which contracts when activated (17, 50, 65, 74).

Recent studies have revealed that different fiber types may be distinguished in mammalian muscle and that more than just color distinctions can be made. As reported by Close (25), on the basis of the activities of certain enzymes, Dubowitz and Pearce and Engel et al. found that two kinds of fibers were present in muscle. Other researchers have noted that three types of muscle fibers exist due to differences in the cell ultrastructure, certain cell enzyme activities and the properties of the myosin filaments (25, 68). Close (25) has tabulated the morphological, physiological and histochemical properties of the different skeletal muscle fibers. In this review. it was reported that Padykula and Gauthier classified the three fiber types as white, intermediate and red, while Brooke and Kaiser labeled the intermediate fibers as Type I and the red and white fibers as Type IIA and IIB, respectively (25). Barnard et al. (15) determined the histochemical and physiological characteristics of all three kinds of fibers in both the rat and guinea pig. Intermediate fibers were identified as slow-twitch fibers and the red and white fibers were classified as fasttwitch fibers (see definition of muscle twitch in Section 2.3). However, further research is necessary to classify the fiber type proportions for various muscles of different species.

Changes have been found to occur in muscle fibers following exercise. Edgerton et al. determined that the percentage of red fibers increased in rat plantaris muscles following exercise while the white fibers showed a proportional decline (34). Barnard, Edgerton and Peter explored the effects of low-intensity exercise on the medial gastrocnemius muscle of the guinea pig and found an increase in red fiber population with a decrease in the percentage of white fibers. Barnard et al. concluded that an interconversion of white and red fibers occurred following exercise (13, 14).

The postnatal growth of skeletal muscle fibers causes a transition from immature myotubes to adult muscle fibers at different stages during animal development (25). The longitudinal growth of skeletal muscles has been investigated by Elliott and Crawford (35) who revealed that the individual sarcomeres were fully developed early after birth and future growth occurred at the ends of each fiber. Goldspink and Rowe (47) found that increases in the cross-sectional area of muscle were a result of the growth of individual fibers and not a proliferation of these cells. Goldspink (48) determined that increases observed in muscle fiber diameter were due to longitudinal splitting of the myofibrils. Muir (68) noted that skeletal muscle fibers from the pig are often arranged in "metabolic bundles," which contain a central region of slow-twitch oxidative

fibers surrounded first by fast-twitch oxidative glycolytic fibers and finally by a rim of fast-twitch glycolytic fibers. He revealed that this grouping might be a developmental process whereby primitive slow-twitch fibers are later surrounded by fast-twitch fibers. Davies, as reported by Muir (68), found that the number of slow-twitch fibers in the central core of the metabolic bundle increases during growth and the number of fast-twitch oxidative glycolytic fibers shows a proportional decline. He related this to the fact that the speed of contraction in the whole muscle decreased with increasing age.

2.2 Innervation and Activation

Skeletal muscle is not self-excitatory and requires impulses from the voluntary portion of the central nervous system to produce contractions. Motor nerves from the central nervous system contain numerous axons or fibers which supply from one to 200 muscle fibers. The distal end of each nerve fiber branch is buried in the sarcolemma or sheath of one muscle cell and the nerve fiber and its associated muscle fibers comprise one motor unit (17, 50, 81).

The neural disturbance sent by the central nervous system is known to generate a chemical change in the sarcolemmas of the muscle fibers. This disturbance is transmitted to the cell interior by a series of infoldings of

the sarcolemma known as the transverse tubules or T systems. The stimulus results in a release of calcium ions (stored in sacs around the myofibrils) which causes biochemical changes on the myofilament surfaces and a linkage of actin and myosin. Calcium ions are returned to storage locations when the neural stimulus ceases (17, 50, 51, 81).

What changes occur following denervation (cutting) and cross-union (transposition) of the motor nerves to the muscles? Close (24) and Peter (71) have found no conclusive evidence supporting significant alterations of contractile material in mammalian skeletal muscle after denervation. Eccles et al. (31) disputed this claim and have investigated cross-union of motor nerves in detail. They found that tonic motoneurons with discharge frequencies of 10-20/sec. innervate the intermediate, slow-twitch fibers while phasic motoneurons with discharge frequencies of 30/sec. and 60/sec. innervate the fast-twitch fibers. Buller et al. (20) determined that reciprocal changes occurred in the time course of twitch contractions when a cross-union of motor nerves to fast and slow muscles was performed. The originally slow-twitch fibers increased their speed of contraction while the fast-twitch fibers were slowed. Eccles et al. (32, 33) proposed two mechanisms for the changes in muscle response following cross-innervation; either the pattern of motor impulses is affected or a substance is generated by the motor nerve

and passed to the muscle, which results in changes in the rate of muscle contraction. Fex (38) found that the speed of contraction in rat soleus muscle was altered by the presence of fast nerve implants, lending credence to the second hypothesis proposed by Eccles. Barany and Close (12) showed that the velocity of contraction of the individual sarcomeres is altered by cross-union of the motor nerves. However, considerable research is still necessary regarding the area of dynamic changes in the contraction of muscle fibers and sarcomeres following cross-union.

Biochemical research has attempted to establish the differences between the processes of contraction in different muscles of the same species and the same muscles from different species (25). The myosin filaments of fast and slow muscles have the same molecular weight but vary in the ultrastructure, and the actin filaments are similar in molecular structure among different muscles (30). In addition, one enzyme, myosin ATPase, which is important in activation reacts with calcium at a much greater rate in fast-fibered muscles than in slow-fibered types (30). This finding might account for the differences in the speed of contraction. Attempts have been made to isolate fragments of myosin to determine how actin binds to myosin in both fast- and slow-fibered muscles (29).

2.3 Mechanical Testing and Response

Two methods for mechanically testing skeletal muscle are currently used. <u>In vivo</u> experiments are conducted when tissue specimens are tested in the body while <u>in vitro</u> tests are made on specimens which have been removed from the animal and have been placed in a physiological bath (7). The benefits of having an intact blood supply make the <u>in vivo</u> experiments appealing but for the purposes of this study, the <u>in vitro</u> conditions permit more accurate mechanical tests to be run.

Muscle tissue contracts when appropriate electrical, chemical, thermal or mechanical stimuli are applied either directly to the muscle or through the nerve trunk (81). Electrical stimulation was used in this research because it is simpler and more reliable to apply than the other methods. The response of the muscle cells to electrical stimuli depends upon the voltage intensity, time duration and frequency of the stimulus pulses. The magnitudes of these parameters are affected by whether the muscle is stimulated directly on its surface, through the nerve which innervates the muscle, or by another method. To ensure that the muscle remained undisturbed during the in vitro tests, the tissue was stimulated indirectly through the physiological bath.

The mechanical response which is evoked by the application of a single stimulus pulse is known as a muscle

twitch. When one end of a muscle is attached to a force transducer and the other end is connected to a displacement transducer, the twitch response may take the form of a change in external force and/or a shortening of the tissue (81). There is a minimum voltage which must be supplied to the muscle to yield a twitch response (threshold stimulus) in a minimum number of cells and each stimulus pulse must be of sufficient time duration.

Details of the relationships between voltage intensity and pulse duration and the characteristics of a muscle twitch have been studied (43, 81).

As the voltage level of the pulse is increased, a greater number of fibers are stimulated and, at some maximal voltage intensity, all fibers are contracting. Each cell obeys the all-or-none law and contracts completely or not at all. The magnitude of the whole muscle response is then dictated by the number of fibers which are stimulated (81). A supramaximal voltage level was maintained in this study so as to investigate the maximal response of the contracting muscle.

The frequency of stimulation also affects the magnitude of the recorded force or the degree of muscle shortening. Should a second stimulus pulse be supplied to the tissue before the muscle has completely recovered from the first, a second force response is seen on the force-time plot with a larger peak value. The force

increase occurs even though the first stimulus pulse may have been supramaximal and the change may be due to the presence of an increased amount of calcium ions around the myofilaments. A series of stimulus pulses at a moderate frequency causes a set of increasing force pulses over time which is known as the staircase phenomenon. the frequency of stimulation is augmented, the individual force pulses, which are recorded against time, approach each other and the muscle is said to be in a state of incomplete tetany. When the frequency of stimulation is such that a smooth or fused force-time plot is observed, a condition of complete tetany has been achieved (25, 81). This research is concerned with the recording of maximal tetanic forces corresponding to supramaximal voltage levels. Only the amplitudes of the tetanic forces are of interest here and no attempt was made to record the time course of the tetanic force response.

To better understand the contractile properties of muscle, two mechanical experiments have classically been employed and are known as the isometric and isotonic tests. In the isometric experiment, the muscle is fixed at both ends and a stimulus is applied either directly to the muscle or through its nerve trunk. A force transducer is attached to one end of the muscle and the force which is generated by the contracting muscle is monitored over

time. Though the length of the muscle is said to remain constant in an isometric test, a small amount of displacement does occur in the force transducer in order to record the force. An isotonic experiment is performed by stimulating a muscle that has a constant force applied along the central axis of the muscle and then recording the amount of shortening or displacement which occurs in time (43, 81). The isometric test was utilized and supramaximal indirect stimulation was applied to obtain isometric tetanic force values at various muscle lengths.

CHAPTER III

SURVEY OF LITERATURE

3.1 Introduction

Muscle resists stretch in the unstimulated or passive state and when activated, it can transfer its generated force through tendon ends to connective tissue such as bone or to other muscles. Though considerable research has been performed to understand the contractile action of muscle, the constitutive (stress-strain-history) expressions for passive skeletal muscle have not been fully explored. In addition, the positions of the unstimulated and the tetanic stress-strain curves have not been definitely related to the passive strain axis. Research on the mechanical characteristics of passive and tetanized skeletal muscle from both amphibians and mammals will be discussed along with some comparisons with cardiac muscle. Various discrete and continuous models for active and unstimulated muscle tissue will also be discussed.

3.2 Mechanical Properties

3.2a. Stimulated Skeletal Muscle

The <u>resting</u> (optimum or equilibrium) muscle length, corresponding to peak isometric tetanic tension has been

determined in numerous studies (7, 45, 59, 73, 76, 77, 80, 82). Hill (59) discovered that the tetanized frog and toad sartorius muscles developed maximum forces at about the standard length in the body. Both Schottelius and Senay (77) and Bahler (7) determined that previous stimulation of the muscle at various lengths increased the value of the resting Rosenblueth et al. (76) questioned the existence of the resting length for some cat and frog skeletal muscles since tetanic tests revealed that there was a range of lengths over which a peak tetanic tension could be recorded. Geffen (45) challenged their contention and found distinct resting lengths for the medial and lateral heads of the rat gastrocnemius muscle which were within the physiological range, and near the normal length in the body. The resting length has also been expressed as a percentage of the passive length at which unstimulated muscle tension is first recorded. In Table 3.1 a list of these percentages is given from various studies on amphibian and mammalian skeletal muscles as well as from two tests on cardiac muscles. In general, the resting length for skeletal muscle was between 107% and 130% of the passive length while the resting length percentages appeared to be higher for cardiac tissue. However two discrepancies are present in the table. The value given by Schottelius and Senay (77) should have been somewhat larger because a passive tension of 50 gm. was present in the muscle at the resting length, indicating that the passive length was

,

Table 3.1. The Ratio of the Resting Length (Corresponding to Peak Tetanic Tension) to the Passive Length (Corresponding to First Loading of Unstimulated Muscle) for Various Amphibian and Mammalian Muscles

Investigators	Reference	Muscle	Resting Length Passive Length (%)
Aubert et al.	6	frog sartorius	107
Evans and Hill	36	frog sartorius	112
Hartree and Hill (Geff	en) 45	frog sartorius	140-150
Hill (Geffen)	45	frog sartorius	107
Rosenblueth et al.	76	frog sartorius	129
Bahler	7	rat anterior gracilis	125
Geffen	45	rat gastrocnemius medial head	128
		lateral head	136
Rack and Westbury	73	cat soleus	107
Rosenblueth et al.	76	cat sartorius	112
		cat soleus	128
		cat gastrocnemius	121
Schottelius and Senay	77	rat gastrocnemius	97
Walker and Thomas	82	rat triceps surae	108
Parmley et al.	70	cat papillary (cardiac)	133
Sonneblick et al.	80	human papillary (cardiac)	151 <u>+</u> 11

shorter than the resting length. Also in tests on the rat triceps surae muscles by Walker and Thomas (82), the percentage of 108% was found using peak isometric twitch tensions and no percentage was quoted for any tetanic tests.

Numerous studies on the time course of the development of isometric tetanic tension have shown a steep initial rise to a force plateau (7, 9, 23, 44, 59, 63, 75, 76). Gasser and Hill (44) performed tests on frog sartorius muscle and found that the general shape of the isometric forcetime curve at any length was similar to the redevelopment of force when the tetanized muscle was released or extended to that same length. Releases of 30-35% of muscle length resulted in no regenerated isometric tension, however. Jewell and Wilkie (63) also conducted tests on the frog sartorius muscle and found that the tetanic tension reached a plateau within 120-150 msec. following stimulation. Hill (59) determined that when the initial length of the frog or toad sartorius muscle was shorter than the resting length, rapid but stable tetanic tensions were achieved. However, when stretched above the resting length, the muscle was said to be unstable and thought to undergo slow but steady permanent deformation. Tests by Rosenblueth et al. (75, 76) revealed that for various cat skeletal muscles, the isometric tetanic tension peaked much faster than maximum isotonic shortening could be completed. For the in vivo cat soleus muscle, they established that three seconds were required to attain a force

peak. Bahler (7, 9) discovered that a force plateau for the fast-fibered rat anterior gracilis muscle was reached within 100 msec. at 17.5°C. and Close (23) also found that 100 msec. were necessary for the establishment of force peaks for the rat extensor digitorum longus and soleus muscles at 35°C. For given lengths of the muscle relative to the resting length and for known muscle compositions, the general shapes of the isometric force-time curves were similar for both amphibian and mammalian skeletal muscles.

The shape of the isometric tetanic tension versus muscle length curve has also been of interest to investigators (7, 9, 10, 11, 44, 45, 56, 59, 73, 76, 77). Gasser and Hill (44) noted that a range of lengths existed over which the resting tension of frog sartorius muscle was minimal but the tetanic tension increased linearly with increasing length. Hill (56) made thermal measurements on the tetanized frog sartorius muscle and determined that the isometric heat rate first became greater as the length of the muscle was decreased, then reached a maximum and finally declined as the length was further decreased. As stated by Hill (56), Brown and Hill found that the heat evolved by the muscle could be related to the tension, indicating that a peak tetanic tension existed at a definite muscle length. Hill (59) later directly determined for frog and toad sartorius muscle that the developed tetanic force was a function of the muscle length, having a peak tetanic tension at about the standard

length in the body. Rosenblueth et al. (76) showed that no symmetry was present in the tetanic tension-muscle length curve about the maximum tension for various cat and frog muscles while Geffen (45) generated nearly symmetric bellshaped tetanic force-length curves for the medial and lateral heads of the rat gastrocnemius muscle. Bahler (7), Bahler et al. (10, 11) and Ernst (see Bahler (9)) claimed that the isometric tetanic tension versus length curve possessed a paraboloid shape. Schottelius and Senay (77) showed that previous stimulation of the rat gastrocnemius muscle caused a decrease in the complete tetanic tensionlength curve and they attributed this decline to either plastic deformation of the tissue or to contractile fatigue. Rack and Westbury (73) graphed the tetanic tension against the sarcomere length for in vivo cat soleus muscles and discovered that changing from synchronous stimulation of the nerve trunk to distributed stimulation of various fiber groups enabled a state of fused tetany to be established at lower frequencies. The general shapes of the force-length curves for both amphibian and mammalian muscles were quite similar and almost all curves revealed a very distinct force peak.

Peak tetanic tensions of amphibian and mammalian skeletal muscles have been cited by numerous researchers (10, 11, 45, 56, 63, 73, 77). A comparison of the tissue responses is difficult because the test animals have varied

in size and the resulting muscles have also deviated in size and total contractile strength. However some authors have also expressed the peak tetanic tensions per cross-sectional area of muscle (tetanic stress), given that the specimens had relatively uniform areas along their lengths. In Table 3.2 a listing of the peak tetanic stresses is shown for both amphibian and mammalian skeletal muscles and for one study on frog fibers (22). A great deal of variation exists in the stress values and even the results of studies on the same muscle are not comparable.

The effect of temperature is also noted in the table and it has been found by investigators that temperature increases result in higher peak tetanic tensions and stresses (22, 26, 27). Close and Hoh (26) displayed graphs of the peak tetanic stresses for temperatures between 20°C. and 35°C. for two muscles from the rat. The isometric tetanic stress for the rat extensor digitorum longus muscle was found to increase linearly with temperature throughout the temperature range while the stress in the rat soleus muscle increased from 20°C. to 25°C. but then remained constant above 25°C. Close and Hoh (26) also noted that an increase in the tetanic stress occurred as the temperature of the frog sartorius muscle was changed from 2°C. to 20-22°C. Cullingham et al. (27) supplied direct and indirect stimulation to in vivo cat tibialis muscles and found that the maximum isometric tetanic tensions were greatest at 38-40°C.

Table 3.2. Peak Isometric Tetanic Stress (Peak Force per Cross-sectional Area) for Different Amphibian and Mammalian Skeletal Muscles at Different Temperatures

Investigators	Reference	Muscle	Peak Tetanic Stress (dynes/6 cm. 2×10 ⁶)	Tempera- ture (°C.)
Casella	22	frog anterior tibialis	1.68	0
			2.45	20
		frog		_
		semitendinosus	1.06	0
			1.45	20
		frog fiber	2.70	0
			3.22	20
Close and Hoh	26	frog sartorius	2.33	2
			3.43	20-22
Hill	56	frog sartorius	1.08	0
Hill	59	forg sartorius	1.76	0
Jewell and Wilkie	63	frog sartorius	2.49	2
Bahler et al.	11	rat anterior gracilis	1.31	17.5
Close and Hoh	26	rat extensor digitorum		
		longus	2.16	20
			2.70	35
		rat soleus	1.57	20
			1.76	25-35

while only a five percent decrease in tension occurred when the temperature was lowered to 28°C. A further drop in temperature to 20°C. resulted in a 30-35% decrease in the peak isometric tetanic tension. Indirect stimulation also resulted in 2-4% lower tensions than direct stimulation at 40°C. and 7-8% lower values at 20°C. Casella (22) discovered that peak tetanic stresses for frog muscles at 0°C. and 20°C. were much lower than for the individual frog fibers at the same temperatures and indicated that the presence of passive connective tissue elements in a whole muscle decreased these peak stresses.

3.2b. Unstimulated Skeletal Muscle

The determination of the length at which the first indication of force is recorded during muscle extension has been discussed frequently (7, 42, 45, 59, 75, 76). Fung (42) recognized the difficulty in finding an initial length for biological materials since the tension changes only slightly for relatively large stretches. Geffen (45) arrived at the same conclusion for mammalian muscle and Rosenblueth et al. (75, 76) stated that a passive or standard length was impossible to determine for various cat skeletal muscles because the force-extension curve was asymptotic to the length axis as the loads approached zero. Instead Rosenblueth et al. concluded that only the initial tension and not the initial passive length was possible to specify. However Bahler (7) and Hill (59) had little

difficulty in specifying initial unstimulated lengths for the rat anterior gracilis and frog sartorius muscles, respectively.

Both direct force recordings and heat measurements have been employed to understand the loading characteristics of skeletal muscle. Various investigators, using the former technique, have displayed or discussed the mechanical loading-extension curves for skeletal and cardiac muscles (1, 3, 9, 40, 41, 63, 72, 75, 76, 80, 82). Fung (40) noted that many biological tissues such as muscle could be extended large amounts before the force-extension curves became nonlinear. Loading curves developed by Rosenblueth et al. (75, 76) for cat muscle and Walker and Thomas (82) for rat muscle revealed that a linear region was present in the loading curves up to 10-12% and 8-10% extension, respectively. Sonnenblick et al. (80) also observed a somewhat linear region in the force-extension curve for human papillary muscles up to 10% elongation.

As reported by Jewell and Wilkie (63), Hill found that the unstimulated force in the frog sartorius muscle increased exponentially with length and Matthews (see Rack (72)) obtained the same exponential relationship for cat soleus muscle, the curve becoming steeper as the maximum physiological length was approached. The loading curves which Matthews displayed were found to be relatively independent of the rate of extension up to 5 mm./sec. However,

Walker and Thomas (82) found that the higher the rate of passive loading of the rat triceps surae muscle, the larger the muscle tension and Abbott and Lowy (1) observed a similar rate dependency for amphibian muscle. Weiss et al. (see Abbott (3)) attributed the first exponential portion of the loading curve to the response of the muscle cells while the stiffer part of the curve at longer lengths was due to the behavior of the supporting connective tissue structures. Bahler (9) also noted that the resistance of the rat anterior gracilis muscle to large amounts of stretching occurred in the connective tissue around the muscle cells and in the sarcolemmas. Repeated loading of the muscle resulted in lower tensions at given lengths which Schottelius and Senay (77) and Walker and Thomas (82) attributed to either the viscous nature of muscle or the permanent damage which occurred from overextension of the tissue.

Heat measurements made by Hill and Hartree (54) on frog sartorius muscle and discussions by Wohlish (as reported by Abbott (3)) revealed that a linear relationship existed between the muscle temperature and the amount of muscle extension and was due to the thermoelastic properties of the tissue. Hill and Hartree (54) found that live or dead muscle resembled rubber in its thermal characteristics since the temperature increased when it was extended, indicating a negative coefficient of thermal expansion.

However, Abbott (3) reported that the temperature of muscle decreased with further extension since collagen was being stretched in this length region and had a positive coefficient of thermal expansion. The temperature of muscle also dropped as the muscle was returned to its original length. As stated by King and Lawton (64), Heidenhain and Feng also noticed the inversion in the coefficient of thermal expansion from a negative to a positive value at 25-30% extension, indicating the effects of connective tissue at greater muscle lengths.

To better understand the rate response of skeletal muscle, various authors (1, 5, 18, 60, 63, 82) have conducted stress relaxation tests on muscle whereby the muscle was extended to a certain length and the force decline was then measured over time at that length. Abbott and Lowy (1) determined that the tension decay in toad sartorius and tortoise iliofibularis muscles was extremely rapid during the first half-second of relaxation but then dropped more slowly over the next four to six seconds. Jewell and Wilkie (63) noted stress relaxation in frog sartorius muscle as did Buchthal et al. (18) during tests on amphibian muscles. Walker and Thomas (82) performed fast and slow stretches of rat triceps surae muscle and showed that the majority of stress relaxation occurred within one minute and the remainder of the decline during the next four minutes. After similar deformations, Walker and Thomas found that the

muscle tensions approached the same force value regardless of the rate of extension. Apter and Graessley (5) observed that stress relaxation occurred in cat gastrocnemius and cat cardiac muscles at 37°C. and Hoffman et al. (60) found that stress relaxation was greater in stimulated than unstimulated cat cardiac muscle.

Hysteresis curves are generated for passive muscle by loading and unloading the tissue at a constant rate and observing the size and shape of the closed loop which develops. The force during unloading of the tissue has been seen to be lower than the loading counterpart and has been attributed to the viscous nature of muscle (39). and Wilkie (63) developed hysteresis curves for slow stretches lasting 10 minutes and at this rate, the area of the loops was found to be quite small. Rosenblueth et al. (75) determined that the amount of hysteresis (i.e. area of the loops) for relaxed cat muscle was much less than that observed for tetanized muscle and Matthews (see Rack (72)) also noted minimal amounts of hysteresis in cat soleus muscle. Results of Fung's (40) studies on cat papillary muscle at three extension rates from 0.09% length/sec. to 9% length/sec. showed that the size of the hysteresis loops was independent of the extension rate of the tissue. Hoffman et al. (60) found that the hysteresis curves for the cat papillary muscle were affected by previous stimulation of the muscle.

Only two repeated cyclic extension tests of muscle were discovered in the literature. Gasser and Hill (44) used a vibrating spring to provide cyclic oscillations to passive and active frog sartorius muscle. The peak force in the stimulated tissue was found to decrease more rapidly than for passive muscle and was thought to be due to the more viscous nature of active muscle. Rack (72) used a rotating cam to cause sinusoidal stretches of passive and tetanized cat soleus muscle at different frequencies and amplitudes of oscillation. The resulting length-tension (L-T) and velocity-tension (V-T) plots revealed that very little change occurred in either the peak or trough passive muscle tensions with increasing frequency, indicating a relative insensitivity to rate. For the tetanized muscle, the trough tensions showed large decreases with increasing frequency with little change occurring in peak tension. In addition the tensions in the passive and active muscle were found to greatly increase with larger amplitudes of muscle stretch.

3.3 Modeling

3.3a. Stimulated Skeletal Muscle

Investigators have attempted to model the mechanical behavior of stimulated skeletal muscle using discrete model elements (8, 44, 55, 56, 57, 58, 59, 63, 66). According to Levin and Wyman (66), Weber first noted the mechanical similarity between active muscle and a stretched spring and

believed that the tension-length curves were identical in loading and unloading of muscle. Blix (see Levin and Wyman (66)) contended that stimulated muscle possessed viscous properties since extensions of the tissue resulted in larger tensions than releases of the muscle ends. Hill (55), after performing experiments on arm muscles of human subjects, concluded that the mechanical response of active muscle could be modeled by a spring and dashpot in parallel. Following quick release tests of tetanized isometric frog sartorius muscles, Gasser and Hill (44) developed a viscoelastic model for active muscle which was composed of a thin rubber tube filled with a viscous gel and tied firmly at the ends and Levin and Wyman (66) proposed still another model which contained a parallel combination of a linear spring and dashpot, both in series with an undamped spring. The latter was included to account for the immediate redevelopment of active tension following a rapid shortening or extension of initially isometric amphibian skeletal muscles.

Heat measurements of frog sartorius muscle led Hill (56) to propose a three-element conceptual model for amphibian skeletal muscle in which a contractile element (CE) was in series with a nonlinear elastic element (SE), both of which were in parallel with another nonlinear elastic element (PE) (see Fig. 3.1). The contractile element corresponded to the actomyosin complex within the

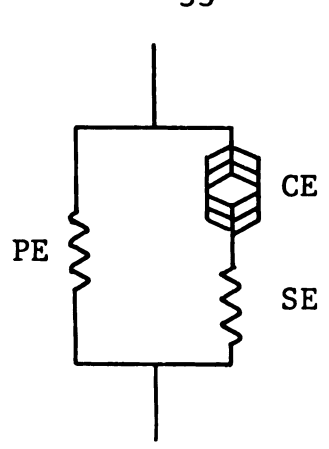


Figure 3.1
Hill's three-element model

muscle cells and the series element was thought to model the mechanical behavior of the tendon ends. The epi- and perimysium and sarcolemmas surrounding the muscle cells were then grouped together as the parallel element. In the unstimulated muscle, the parallel component was assumed to carry the total load in extension while the series element remained unloaded because the contractile element was free to extend. If the muscle was stimulated, the contractile component was forced to contract and extend the series element. The parallel element in the stimulated condition only contributed significant tension during large extensions of the muscle.

Researchers have attempted to isolate the contractile and series elements in Hill's model to better understand the development of muscle tension following stimulation and to discover the anatomic locations of each. Hill (57) suspected that the series elasticity was not restricted to the tendon

ends but might instead be an inherent property of the contractile component (i.e. the elasticity of the myofilaments). He emphasized that the series element was completely undamped and that the contractile component was better represented by a characteristic force-velocity relation than a damped spring. Hill (58) later labeled the series element as simply the tendon ends but realized that other undamped elastic elements could be present within the muscle fibers themselves. Hill further stated that the general force-extension response of the tendon was due to a statistical distribution of long and short tendon bundles. Hill (59) performed extremely quick release tests on active frog sartorius muscle and concluded that 1) any damping which was present in the series elastic elements was due to the response of the moist collagen fibers, and 2) no substantial amount of elastic shortening occurred within the contractile material following muscle release. Jewell and Wilkie (63), Bahler (8) and Fung (40) also conducted quick release experiments on active frog sartorius, rat anterior gracilis and cat papillary muscles, respectively, and developed mathematical load-extension expressions for the undamped series element. Fung (41) further found that the tension in the series element was also a function of the length of the parallel elastic element.

Changes have been made in the form of Hill's model to account for differences in the mechanical response of muscle.

Aubert et al. (6) described a model which was composed of

a series elastic element corresponding to the tendon ends, in series with a parallel arrangement of the contractile and parallel elements. Parmley et al. (70) and Hoffman et al. (60) concluded that Aubert's model was also appropriate for describing the mechanical response of cardiac muscle if additional viscous and elastic elements were placed in series with the parallel element and in parallel with the series element. Fung (41) showed the equivalence of the Hill and Aubert models if the magnitudes of the material parameters for the various elements were adjusted. Glantz (46) developed a three-element model for the series and parallel elements each of which included two linear elastic springs in parallel and in series with a dashpot. Bahler (9) constructed a three element model for rat anterior gracilis muscle which replaced Hill's contractile component with a parallel combination of a force generator and an internal viscous load and also included other viscous elements to pattern the damping effect of the tissue.

Other mathematical models have been employed to fit the response of stimulated muscle. Nubar (69) modeled the behavior of active skeletal muscle using a series expansion of the extension ratios of the muscle fibers. Each term in the expansion contained an elastic or viscous coefficient which could be adjusted to match the response. Aside from the development of force, stimulation of the muscle caused an increase in the thickness or diameter of the muscle fibers

which Nubar related to the longitudinal strain and extension ratio in the total muscle. Apter and Graessley (5) utilized the equation of motion to simulate the isometric tension versus time curve for cardiac muscle. A series of terms were generated containing elastic and viscous material parameters as well as a variable which depended upon the contractile state of the muscle.

3.3b. Unstimulated Skeletal Muscle

Preliminary attempts to model passive skeletal muscle have utilized discrete elastic and viscous elements. as discussed by Hill (56), determined that resting muscle acted like a spring moving in a viscous fluid. Hartree (54) recognized that a model for unstimulated frog sartorius muscle must contain viscoelastic elements to account for the rate dependency of muscle during loading and the change in the sizes and shapes of hysteresis loops during one cycle of loading. With the introduction of the three-element conceptual model, Hill (56) admitted that even though the parallel element was considered to be elastic, to a minor degree purely viscous and viscoelastic elements had to be added due to the irreversible thermo-elastic effects during stretch and the prolonged after-extension of resting muscle. Jewell and Wilkie (63), adopting Hill's three-element model, determined that the most important site of parallel elasticity was the nonliving connective tissue sheaths surrounding the cells. Therefore the parallel elastic element was the same in either

the resting or stimulated muscle and the behavior of the contractile mechanism could be found by subtracting the total muscle tension from the passive tension at any length.

Following numerous relaxation tests on amphibian muscle. Abbott and Lowy (1) suggested that a more reasonable discrete model for the unstimulated tissue would be to combine two models in parallel, each one composed of a spring and a dashpot in series. Abbott and Lowy then developed a relationship between the force and a product of the muscle extension and an exponential of the time and material parameters. Glantz (46) constructed a three-element conceptual model to simulate the response of unstimulated cardiac muscle. An exponential elastic spring was in parallel with a linear dashpot and both were connected in series with another exponential spring. The force in the model was found to be equal to the exponential of the muscle extension multiplied by an expression containing the time response of the tissue. Stress relaxation tests were used to compute the values of the viscous and elastic parameters in Glantz's model.

Some attempts have been made to describe the passive response of muscle by other mathematical methods. Nubar (69) developed a geometric method for determining the theoretical passive stress-strain relationship for pennate-shaped skeletal muscles, given that the muscle fibers underwent a lateral shrinkage (the Poisson effect) during muscle extension. In a review by King and Lawton (64) certain biological fibers

(composed of long protein molecular chains) were considered to be elastomers, exhibiting elastic behavior when extended anywhere from 30% to 100% of their initial unloaded lengths. The force in the fibers was related to the displacement using statistical mechanics. Though the mathematical expressions fit the experimental results for rubber and certain biological substances, some question remained about whether this treatment was applicable to both muscle fibers and whole muscle. Blatz, Chu and Wayland (16) defined a strain energy function to relate the maximum stresses to a power law of the extension ratios. The theoretical loading curves were found to be similar to the experimental data for various animal tissues including skeletal muscle fibers from the frog.

Fung (39) recognized the difficulties in applying classical linear elasticity to highly non-linear biological materials that experience large deformations. He realized that 1) a Young's Modulus was not applicable to biological materials because of the slope changes in the loading curve and, 2) strain rate, strain level and strain history were important in characterizing any passive biological tissue. He found that the slope of the $\mathrm{d}T/\mathrm{d}\lambda$ vs. T curve was constant for some specimens where T was the Lagrangian stress and λ was the extension ratio and the uniaxial stress was then related to the exponential of the extension ratio. Fung (40) applied the model for the general behavior of biological tissues to resting heart muscle and determined

a similar exponential relationship between the Lagrangian stress and the extension ratio. He also realized that an infinite number of springs and dashpots (i.e. a continuous model) was necessary to simulate the response of passive muscle tissue.

Fung (42) sought to include the viscous or history-dependent characteristics of biological tissues into the established elastic behavior developed previously. Following viscoelastic theory, he represented the stress history of a loaded material by a relaxation function of the separable form:

$$K(\varepsilon,t) = G(t)\sigma_{e}(\varepsilon)$$
 3.1

where $K(\epsilon,t)$ was the total relaxation function, G(t) was the reduced relaxation function, σ_e was the elastic response, ϵ was the strain and t was the time. By superimposing infinitesimal stretches at various times, τ , the stress became

$$\sigma(t) = \int_0^t G(t - \tau) d\sigma_e$$
 3.2

or in terms of strain history,

$$\sigma(t) = \int_0^t G(t-\tau) \frac{d\sigma_e(\varepsilon(\tau))}{d\varepsilon(\tau)} \frac{d\varepsilon(\tau)}{d\tau} d\tau. \qquad 3.3$$

Fung then presented methods for determining the relaxation function and the elastic stress and once these were found, the material response to any type of loading was known.

Haut and Little (53) were successful in analyzing collagen fibers using Fung's quasi-linear approach. The relaxation function and elastic stress took the form:

$$G(t) = A + B \ln t$$

$$\sigma^{e}(\epsilon) = C\epsilon^{2}$$
3.4

where the constants were obtained from loading at various strain rates to prescribed strains followed by stress relaxation at a fixed strain level. Jenkins and Little (62), while studying the ligamentum nuchae, found that the stress relaxation was highly strain level dependent. They therefore chose to modify Fung's relaxation function by not separating strain and time, giving

$$K(\varepsilon,t) = F(\varepsilon,t)\sigma^{e}(\varepsilon)$$
. 3.5

The "modified" relaxation function and elastic stress were then expressed as

$$F(\varepsilon,t) = 1 + \varepsilon^2 \ln t$$

 $\sigma^{e}(\varepsilon) = C\varepsilon + D\varepsilon^2$.

Utilizing Fung's quasi-linear viscoelastic approach, it is extremely valuable to predict the passive material response of mammalian skeletal muscle to all types of deformations. In addition, knowing the shape, magnitude and relative placement of the tetanic stress vs. passive strain curve with respect to the passive stress-strain curve, a more complete constitutive equation for muscle tissue could be established.

CHAPTER IV

EXPERIMENTAL METHODS

The anterior gracilis muscle was removed from the thigh of a rat and the passive (unstimulated) tissue was subjected to three types of mechanical tests to establish a uniaxial stress-strain-time expression. In addition, the tetanic tension curve was generated and aligned with the passive curve at various lengths in the physiological range. In this way the parameters in a composite quasilinear viscoelastic equation were obtained, satisfying the mechanical response of a parallel-fibered muscle in the passive and fully stimulated states.

4.1 Nomenclature

Force is the action of one body against another. The units may be in grams force, dynes, pounds, Newtons, etc. A force transducer was used to record the force in the muscle as a result of the changes in length imposed on the unstimulated muscle or the stimulation provided to the tissue. Passive length (gauge length) is the length of the tissue specimen at which force is first recorded during extension. Its units may be in mm., cm., inches, etc. Resting length is the length of the muscle at which

Engineering stress is the force (either unstimulated or stimulated) in the muscle divided by its perpendicular cross-sectional area at the gauge length. Its units may be in pounds/in.², dynes/cm.², gm./cm.², Newtons/m²(Pascals), etc. Engineering strain is the change in total muscle length divided by the original muscle length. Strain is, therefore, a dimensionless quantity but is usually expressed in inches per inch, cm./cm. or percent.

4.2 Surgical Technique

sprague-Dawley rats (130-180 grams) were anesthetized with sodium pentobarbital (35 mg./kg.; intraperitoneal). The animal was restrained on a board and a stereomicroscope (Leitz Model TS, E. Leitz Inc., Rockleigh, N.J.) was used with six-power magnification to perform the surgery. The skin from the medial side of the right thigh was cut and reflected, exposing the anterior gracilis muscle. The muscle has its origin at the pubis symphysis and its insertion on the upper crest on the tibia near the knee. It receives its innervation from the anterior obturator nerve and its blood supply from a branch of the femoral artery. The surface layer of fascia was separated from the pubis to the tibia. Fascia surrounding the gracilis was also cut without disturbing the artery or the nerve (Fig. 4.1). A scalpel was used to cut the surrounding

muscles at the tibia and a chip of bone was removed. A glass probe was inserted beneath the muscle and the anterior gracilis was carefully separated from the posterior gracilis. Muscles around the origin of the gracilis were cut, a chip of pubis was taken and the artery and nerve were severed. The muscle was transferred to a 300 c.c. Plexiglas chamber containing a physiological salt solution and the bone chips were trimmed. The animal was sacrificed following surgery with 0.4 c.c. sodium pentobarbital injected directly into the heart.

4.3 <u>In Vitro Muscle Chamber</u>

A Plexiglas test chamber with dimensions of 5.7 cm. \times 5.4 cm. \times 5.2 cm. was constructed to house the muscle during the experimental tests (Fig. 4.2). The 160 c.c. chamber was filled with a physiological salt bath called Tyrode's solution. Tyrode's solution is composed of 8.0 gm. NaCl, 0.2 gm. KCl, 0.2 gm. CaCl₂, 0.1 gm. MgCl₂, 0.05 gm. NaH₂PO₄, 1.0 gm. NaHCO₃, and 1.0 gm. glucose in one liter of distilled water. The solution was prepared in eight-liter quantities. A sintered-glass air stone was placed in one wall of the Plexiglas chamber and 95% O₂ - 5% CO₂ was bubbled into the bath for at least one hour before the insertion of the muscle.

Two stainless steel specimen grips were designed to clamp the gracilis bone chips and one grip is shown in

Figure 4.3. The pubic bone was inserted in a notch in one of the grips and clamped (Fig. 4.4). The muscle and grip were suspended in the chamber of oxygenated Tyrode's solution and a diagram of the muscle and test chamber appears in Figure 4.5. The temperature of the bath was regulated at $25 \pm 1^{\circ}\text{C}$. with a stainless steel heat exchanger. This temperature was chosen because the metabolic activity of the tissue could be slowed to decrease the oxygen uptake. The tibia bone chip was inserted in a second specimen grip fixed in the base of the test chamber (Fig. 4.2). The grip which was clamped to the pubic chip was attached to a fixed force transducer and was kept submerged in the solution throughout each mechanical test. The test chamber was connected to a lower moveable head capable of either constant strainrate or sinusoidal displacements.

Following attempts to directly stimulate the muscle in the test chamber (see Appendix A), an indirect method was selected similar to that used by Bahler (7). Two Plexiglas plates with long arms and paddle ends were designed to attach to the sides of the test chamber and holes were drilled in the paddles (Fig. 4.3). Silver wire of 0.005 in. diameter and 99.99% purity was electrically plated in 0.1 M HCl for one minute to prevent silver ions from destroying the muscle cells. The silver chloride coated wire was threaded in a grid pattern through the holes in the paddles and glued to the arms and all

wire except the grids facing the muscle was coated with an insulator (Insl-X Products Corp., Yonkers, N.Y.). The total grid area of each paddle was approximately 0.64 cm.². During the stimulation tests, the paddles in the test chamber were placed parallel to the face of the gracilis on each side of the central region of the muscle.

4.4 Equipment Exterior to Chamber

4.4a. Visual Muscle Inspection

Two procedures were employed to view the anterior gracilis muscle in the test chamber. The dimensions of the specimen were determined with a travelling microscope (see Fig. 4.8) equipped with Ames and Scherr Tumico dial gauges for measurement of specimen length and also equipped with a micrometer head (Model 465M, L.S. Starrett Co., Athol, Mass.) for measurements of width and thickness. The sensitivity or accuracy of each dial gauge was 0.001 inches and the micrometer was graduated in 0.002 millimeter increments. The specimen length was determined to be the distance between tendon-bone attachments and for 49 muscles, the mean + one standard deviation was 2.146 cm. + 0.096 cm. The thickness of the specimen was measured at eight to ten points along the length and the muscle, grips and chamber were then turned ninety degrees and the width measurements were made at the same length locations. An average width and thickness were computed to determine the cross-sectional area which was $0.0170 \text{ cm.}^2 + 0.0047 \text{ cm.}^2$ for 49 muscles.

A second method was utilized to photograph the gracilis muscle in the test chamber and to determine the relative lengths of the muscle cells and tendon ends. A camera, microscope and series of extension tubes were placed on a stand which was capable of vertical and horizontal movement (see Appendix B for description). Four muscles were inspected at magnifications of one to twelve times and the tendon-muscle boundary at each end was viewed and photographed (Figs. 4.6a-b). From these observations the ratio of tendon length to total muscle length was determined to be between six and ten percent and the muscle cell length ratio was found to be 90-96%. The relative lengths of both tendon ends were also determined. A larger portion of the tendon was found to occur at the origin of the muscle.

4.4b. Temperature Control

The stainless steel heat exchanger which was used to maintain the temperature of the Tyrode's solution in the test chamber, contained tap water pumped from a large six-gallon tank (see Fig. 4.8). The large tank temperature was maintained by use of a constant temperature circulator (Bronwill Model 20, Will Corp., Rochester, N.Y.). A linear relationship was found between the large tank and

'
T.
1
1
t
1
!
ļ.
l 1
(
1

test chamber temperatures between 20°C and 45°C. An ironconstantan thermocouple monitored the test bath temperature.

The hot junction was placed in the test chamber while the
cold junction was inserted in a constant temperature (ice
bath (Rosemount Model 911, Rosemount Engineering Co.,
Minneapolis, Minn.) held to 0 ± 1°C. The thermocouple output was read with a digital multimeter (Keithley Model 160,
Keithley Instruments, Cleveland, Ohio), accurate to a
microvolt. A linear relationship was found between the
thermocouple output and the recorded test chamber temperature
between 20°C and 35°C. The voltage level at 25°C was
1.90 mv + 0.05 mv.

4.4c. Passive Testing

The test bath containing the specimen was pinned to the lower, moveable head of one of the two testing fixtures employed in the study. The upper fixed support of the test fixture contained a force transducer (Statham Model UC3, Statham Instruments, Inc., Oxnard, Calif.) in tandem with a Statham UL4-0.5 load cell accessory (Fig. 4.7). A universal joint linked the upper bone grip to the transducer. A Statham Model SC1001 Universal Transducer Readout unit (Fig. 4.8), regulated by a constant voltage transformer (Sola Model F, Sola Electric Co., Chicago, Ill.), powered the transducer cell and recorded changes in force. A clip gauge was made from two strain gages (Micro-

Measurement EA-06-062AQ-350, Micro-Measurements, Romulus, Michigan) mounted on both sides of a thin, curved stainless steel strip, 0.25 inches wide and 0.008 inches thick. The clip was secured on a constant strain-rate fixture between the lower head which moved in threaded screws and the fixed base (Fig. 4.7). The strain gauges, when attached to a bridge amplifier meter (Ellis Model BAM-1, Ellis Associated, Pelham, N.Y.), accurately monitored displacements of the specimen ends (Fig. 4.8). A scotch yoke sinusoidal test fixture was utilized to produce variable amplitude cyclic deflections at the tibial or lower end of the muscle while the upper pubic end was fixed as before (Fig. 4.9). A second clip gauge of similar design was connected between the fixed and moveable heads of the sinusoidal fixture. A gearbox with gear ratios of 5 to 1, 3 to 1 and 1 to 1 was placed between the test fixture and a 1/70 horsepower shunt wound motor (Bodine Model NSR-12R, Bodine Electric Co., Chicago, Ill.) with a speed control (Minarik Model W-14, Minarik Electric Co., Los Angeles, Calif.) (Fig. 4.8). The motor was used to move the lower test fixture head and the attached test chamber. The speed control and gearbox ratios permitted a wide variety of displacement rates of the lower grip in the test chamber.

Outputs from the Statham and Ellis meters were first filtered for the passive tests using low pass filters

with cutoff frequencies of 0.34 Hz. These force and deflection signals were recorded on a dual channel DC amplifier recorder (Sanborn Model 322, Sanborn Co., Waltham, Mass.) and an X-Y recorder (Varian F-80A, Varian Associates, Walnut Creek, Calif.) which were connected in parallel (Fig. 4.10). The sensitivities of the load cell and clip gage were 34 dynes and 0.005 cm. as read from the Sanborn Recorder.

Stress relaxation tests were performed using the constant strain-rate fixture. The Minarik speed control and gearbox were set to give the desired strain rate, the motor speed control switch was turned on and the tissue was extended to a predetermined strain level. The motor was then turned off and the force decay was recorded for six to ten minutes at that peak strain. Constant strainrate loading and unloading tests were run by loading the tissue at constant strain rates to specified strain levels while recording the force, as in the stress relaxation tests. By reversing the switch on the Minarik speed control, the force was monitored during unloading at the same rate. Cyclic tests were conducted using the sinusoidal test fixture. The speed control and gearbox were adjusted to give the frequency of oscillation and the motor was The force in the muscle was recorded for the imposed sinusoidal deflections during 20-30 cycles.

It was discovered in preliminary tests that as the surface of the Tyrode's solution passed over the fixed grip and universal joint, the surface tension created an artificial linear force that affected the loading curves. The grip was therefore kept submerged during testing. In all passive experiments, the muscle was first tested and then, after removal of the tissue from the chamber, the test was rerun to determine the additional force caused by the grip moving in the bath. This drag force was then subtracted from the loading curves. The gauge length, or initial passive length, was then determined from the corrected curve.

4.4d. Active Testing

The leads from the Plexiglas stimulator plates were attached to a stimulator (Grass Model SD-9, Grass Instruments Co., Quincy, Mass.) with variable frequency, voltage intensity and stimulus duration (Fig. 4.11).

Biphasic stimulation was selected because net ionic polarization occurred between the plates with monophasic pulses. It was determined that insufficient current could be generated by the stimulator to maintain the voltage intensity of 60 to 100 volts necessary for tetanic stimulation. Therefore, to achieve maximum stimulation, a second stimulator was built to produce alternating square pulses of prescribed current level (See Appendix C for description).

The Grass Stimulator then monitored the stimulus duration and frequency of the pulses. One channel of an oscilloscope (Tektronix Type 532, Tektronix Inc., Portland, Oregon) (Fig. 4.11) was used to display the resulting pulse train.

The circuit, composed of the stimulator plates and stimulators, was calibrated in the following manner.

Since the bath resistance was approximately 50 Ohms, a 50 Ohm resistor was inserted across the terminals of the Grass Stimulator. The intensity dial of the auxiliary stimulator was adjusted until the voltage level of the square pulses appearing on the oscilloscope provided the desired current.

Preliminary tests on the gracilis muscle indicated that current levels, pulse durations and frequencies of 0.2 Amp., 2 milliseconds and 80-90 pulses per second, respectively, produced tetanic stimulation. The current density across the muscle (current level divided by the grid area of the stimulator plate) was thus 300-350 mA./cm.², for the given area of the plate grid.

Following the determination of the cross-sectional area, the gracilis was tetanically stimulated at various lengths above and below the gauge length. The length of the muscle was varied between 1.9 cm. and 3.3 cm. in 0.2 cm. increments. A tetanic pulse train lasting 3-5 seconds was supplied to the muscle. The force, recorded against time on the Sanborn Recorder, increased sharply

after muscle stimulation and a plateau was reached within one second following the first indication of force. This peak force was the tetanic force value used to develop tetanic force-muscle length curves. When the electrical stimulation to the muscle was removed, the force dropped to the original baseline within one second. Sample force-time plots for different stimulus frequencies and muscle lengths appear in Figures 6.12(a and b). A low-pass filter with a cutoff frequency of 77.0 Hz. was placed between the Statham Meter and the Sanborn Recorder to eliminate high frequency interference in the circuit.

The gracilis was stimulated twice at a particular length every half-hour and when force deviations of more than 25% occurred, no further tests were run. All useable values at a particular length were averaged to obtain the tetanic force and the stress was determined by dividing each force value by the initial cross-sectional area. The resting length at which peak tetanic force was developed occurred between 2.6 cm. and 2.8 cm. for the 8 muscles tested (see Fig. 6.21).

Following passive or active testing of the anterior gracilis muscle, the tibial and pubic bone chips were removed and the muscle was dried. The muscles were then weighed and the mean \pm one standard deviation for 49 muscles was found to be 0.0715 gm. \pm 0.0152 gm.

4.5 Histologic Methods

Four tissue specimens were subjected to histologic staining to determine the relative areas of collagenous tissue and muscle cells to total cross-sectional area and to inspect the muscle fiber orientation in longitudinal view. The computed collagenous and muscle cell area ratios were used as parameters in the mathematical model to be discussed in Chapter V.

A paraffin technique (67) was employed to obtain microscope slides in cross-sectional and longitudinal Immediately following surgery, the tissue was fixed in 10% formalin solution. After 24-48 hours, the muscle was removed, cut into six equal segments and each piece was placed in a metal cassette. The cassettes were inserted in an Ultratechnicon (Technicon Instruments Corp., Terrytown, N.Y.) for 24 hours where the muscle was dehydrated with alcohols, cleared with xylene and impregnated in a series of paraffin baths. A Lab Tech Tissue Tech 2 (Miles Labs., Elkart, Ind.) was then utilized to embed the prepared tissue in paraffin. micron thick sections were taken with the microtome and the slices were stained with both hematoxylin-eosin and Gomori's One Step Trichrome before mounting on slides. Eosin displayed the muscle cytoplasm in pink and red while hematoxylin revealed the nuclear constituents. trichrome stain clearly exhibited in blue the collagen

which was within the connective tissue surrounding the muscle cells. Two types of muscle fibers were observed. A greater proportion were large, lightly-stained cells which are believed to be fast-twitch fibers while a smaller number of darkly-stained cells are believed to be slower fibers (see Bahler (7)). The muscle cells are seen in cross-section in Figs. 4.13 (a and b) and appear longitudinally in Figs. 4.14 (a and b). The photographs were taken using a camera (Minolta SRT-102, Minolta, Tokyo, Japan) with a Minolta Universal Microscope Adapter. The combination was secured atop a Nikon Vertical Minocular Phototube (Cat. No. 77745) with a Nikon 10X High Eyepoint Compensating Wide Field Eyepiece (Cat. No. 77857) placed in the top of the phototube. The complete apparatus was then placed upon a Nikon Microscope Stand equipped with Koehler illumination and a moveable stage.

After inspection with a Bausch and Lomb light microscope under 3.5, 10 and 43 objective power, selected slides were placed in a Leitz-Wetzlar enlarger which projected the image of the slide onto white paper. The cross-section was traced, noting muscle cell types, collagenous tissue, blood vessels and tissue shrinkage. A planimeter was used to determine the relative proportion of muscle cells to total area as well as the percentage of collagenous tissue in the total area. From tests on the four muscles it was determined that the muscle cells

occupied $94.8 \pm 2.5\%$ of the total effective area (the total area minus blood vessels, nerve tissue and spaces left by shrinkage), while collagenous tissue occupied $6.5 \pm 2.8\%$ of the effective area. The proportions of the components showed little variation after inspection of the cross-sections at different locations along the muscle.

Another technique for determining the relative proportions of constituents in a tissue is a stereologic method which has been demonstrated by Weibel and Elias (84). A rectangular grid pattern is repeatedly superimposed on random cross-sections and the intersection of the points which are generated with the tissue components of interest are counted. The ratio of the component volume to total volume in the tissue is then equated by statistical methods to the ratio of counted points to total lattice points on the cross-section. This method is quite accurate as long as the distance between points is sufficiently small.



 $\overline{\text{Fig. 4.1.}}$ Thigh of a rat. A portion of the skin (1) has been removed revealing muscles (2), blood vessels (3) and fat (4). A retractor (5) on the right has been used to expose the area. The curved end of a glass probe (6) can be seen underneath the anterior gracilis muscle (7) which is less than one millimeter in thickness. Fascia surrounding the central portion of the gracilis has been removed. The anterior gracilis muscle has its insertion on the tibia (8) and its origin (not shown) on the pubis symphysis at the far right.

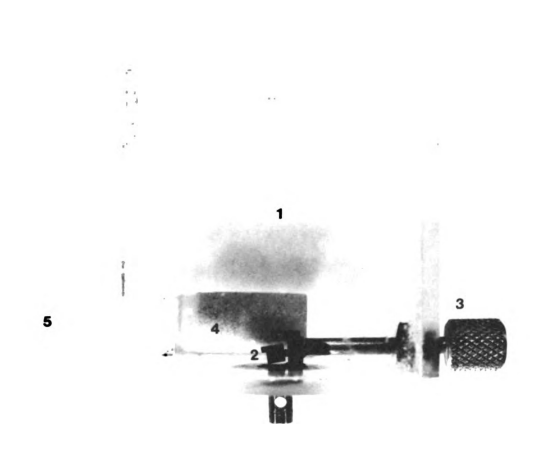


Fig. 4.2. Side view of Plexiglas test chamber (1). The dimensions of the 160 c.c. chamber are 5.7 cm. \times 5.4 cm. \times 5.2 cm. A specimen clamp (2) has been fixed in the chamber base. A screwdriver with knurled handle (3) has been secured in one wall of the chamber and was used to tighten the specimen grip screw. An air stone (4) is shown fixed in the opposite wall of the test chamber and polyethylene tubing (5) has been connected to the air stone. Oxygen in the form of 95% $0_2 - 5\%$ 0_2 was bubbled into the chamber through the air stone.

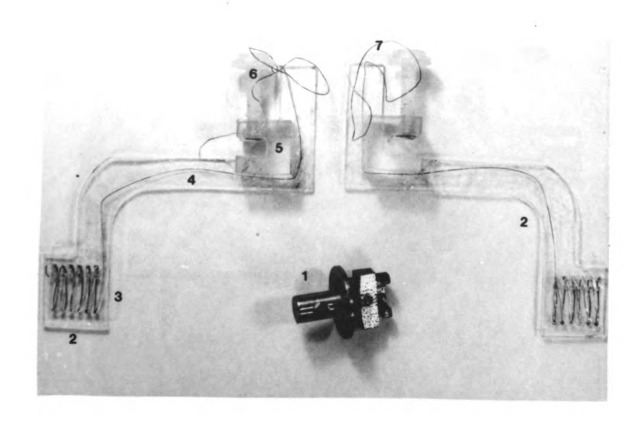
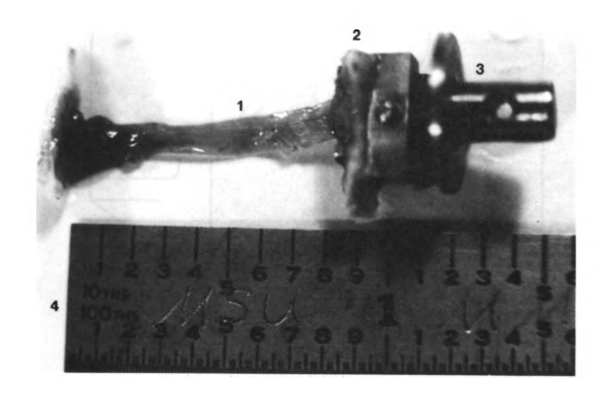


Fig. 4.3. One stainless steel specimen clamp (1) and two Flexiglas stimulator plates (2). The specimen clamp was used to grip the pubic bone chip and the top of the clamp was pinned to a force transducer. Each stimulator plate is composed of a paddle (3), a long arm (4) and a support (5) with Flexiglas set screw (6). Coated silver wire (7) was threaded in a grid in the paddle, glued along the arm and connected to stimulators. All wire except the grid facing the muscle was insulated. The stimulator plate was placed in the test chamber, the notch in the plate support was permitted to rest on the edge of the chamber and the set screw was used to fix the plate to the chamber wall.



 $\underline{Fig.~4.4.}$ Anterior gracilis muscle (1) with pubic bone chip (2) attached to one specimen clamp (3). A ruler (4) graduated in tenths and hundredths of an inch is shown next to the muscle which is approximately one inch long.

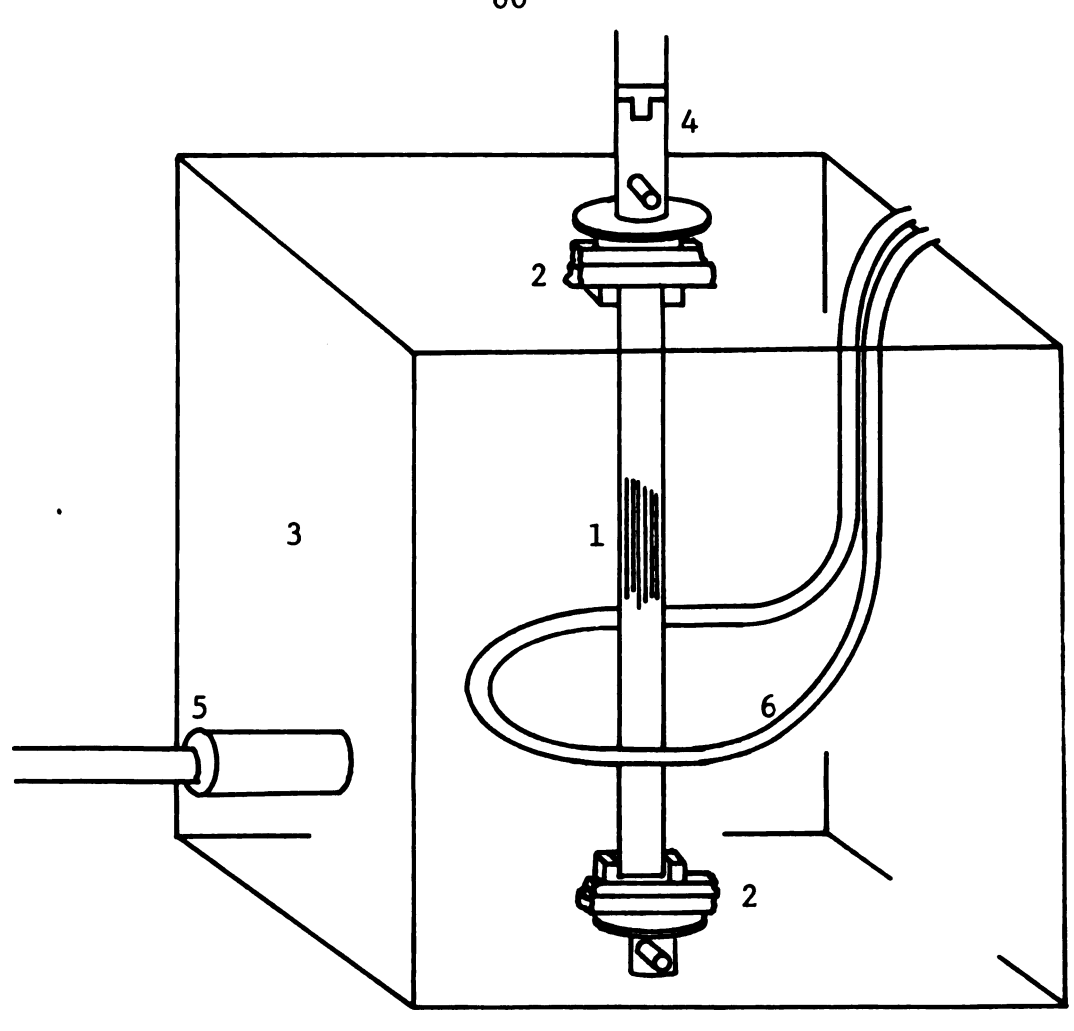
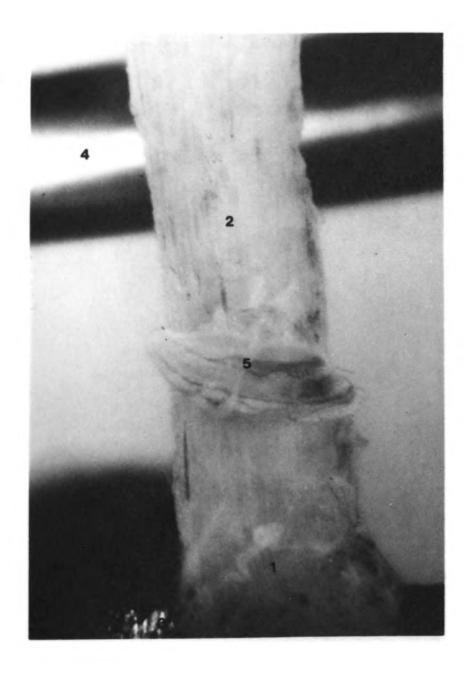


Fig. 4.5. Diagram of the anterior gracilis muscle (1) fixed between the specimen bone clamps (2) in the test chamber (3). Note the universal joint (4) attached to the upper clamp, the air stone and tubing (5) at the left and the heat exchanger (6) around the muscle.



<u>Fig. 4.6a.</u> Photograph of anterior gracilis muscle taken using the camera stand. Near the bottom, the muscletendon boundary (1) can be seen at the insertion of the gracilis muscle (2) on the tibia. Note the specimen clamp (3) fixed in the base of the chamber. Also note the heat exchanger (4) and the Sapphenous artery and vein (5) on the surface of the muscle. (2X)



Fig. 4.6b. Photograph of anterior gracilis muscle taken using the camera stand. Note the muscle fiber orientation (1) and bits of connective tissue (2). (7X)

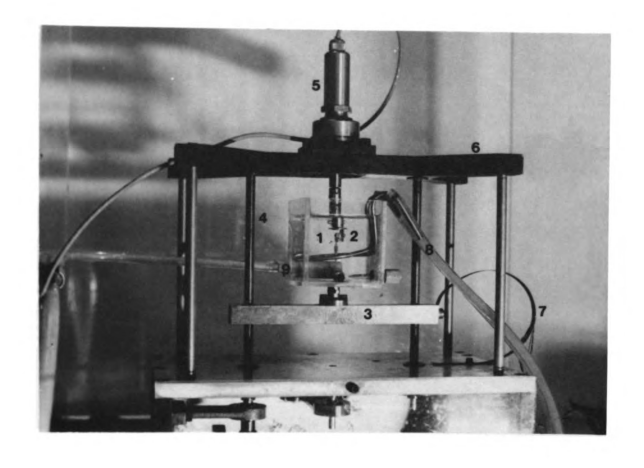


Fig. 4.7. Constant strain-rate test fixture. The test chamber (1), containing the muscle and specimen clamps (2), was pinned to the lower fixture head (3) which moved in threaded screws (4) at constant strain rates. Note the force transducer with load cell accessory (5) on the top support (6), used to measure the force and the clip gauge (7) which measured muscle displacements. Also note the heat exchanger and its tubing (8) and the air stone and tubing (9).

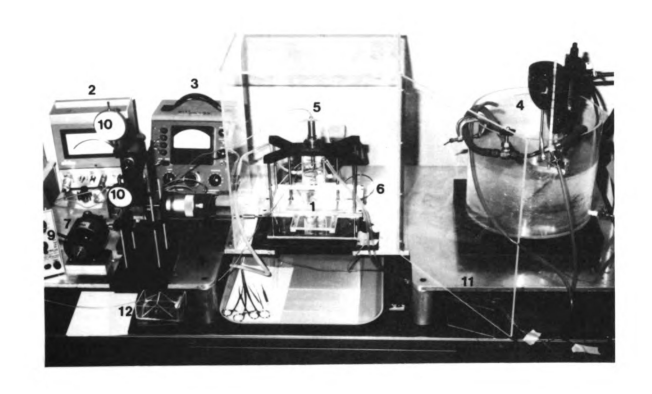


Fig. 4.8. Test setup. The test fixture (1) is shown in the center. The Statham meter (2) and Ellis meter (3) are shown at the left and the large tank and temperature regulator (4) appear at the right. The force transducer (5) to monitor force change was connected to the Statham meter and the clip gauge (6) to measure changes in displacement was connected to the Ellis meter. The motor (7) which drove the test fixture was first connected to a gearbox (8). A speed control (9) for the motor appears at the left and the travelling microscope (10) to measure muscle dimensions is also shown. Also note the thermocouple circuit (11) and the Plexiglas chamber for initial trimming of the bone chips (12).

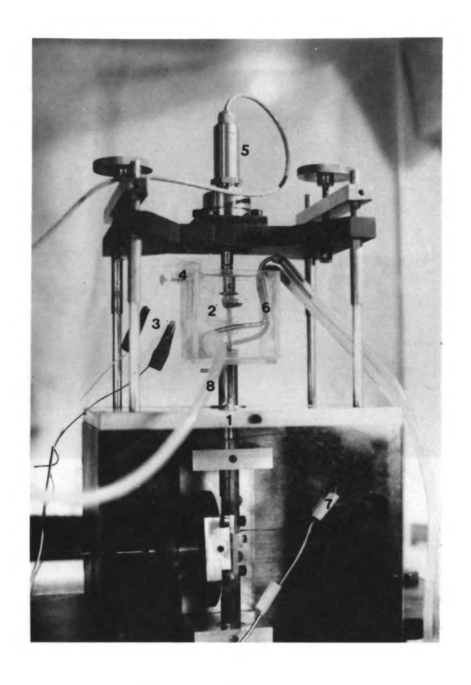


Fig. 4.9. Sinusoidal test fixture (1). Note the muscle in the test chamber (2) and the leads (3) from the stimulator plates (4) which are attached to the test chamber wall. Also note the force transducer (5), the heat exchanger (6), the clip gauge (7) in the fixture base and the tubing (8) for chamber oxygenation.

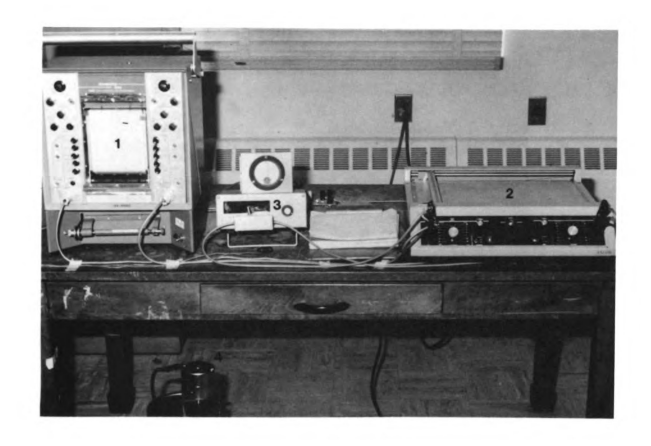


Fig. 4.10. Recording equipment. [Sanborn Recorder (1), Varian X-Y Recorder (2), Keithley Digital Multimeter (3)] and Rosemount Constant Temperature Ice Bath (4). The Sanborn Recorder displayed the force and deflection signals against time on two separate channels. The X-Y recorder was used to graph force against deflection and the multimeter indicated the voltage outputs from the Statham and Ellis meters and the thermocouple. The ice bath maintained the temperature of the cold junction of the thermocouple at 0 \pm 1°C.



Fig. 4.11. Grass Stimulator (1), auxiliary stimulator (2) and Tektronix Oscilloscope (3). The auxiliary stimulator provided alternating square pulses of sufficient current level to create tetanic forces in the muscle. The Grass Stimulator was used to vary the frequency and time duration of the pulses and the oscilloscope allowed for initial calibration of the stimulator circuit.

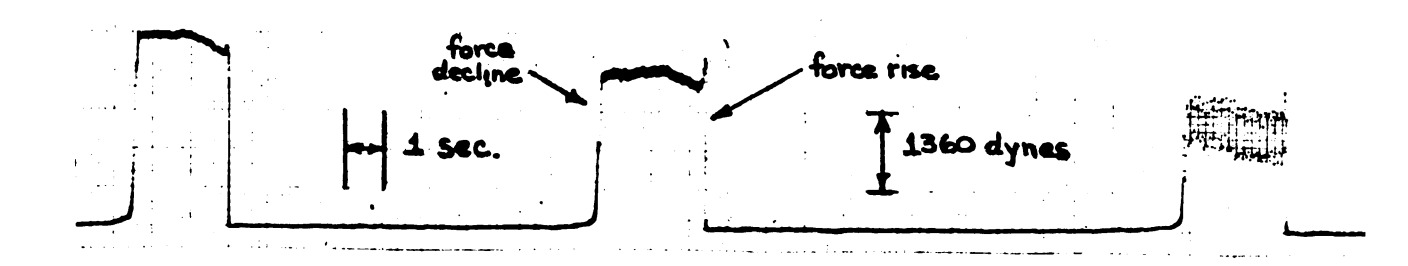


Fig. 4.12a. Sanborn record showing the effect of stimulus frequency variation upon the force-time response of the isometrically stimulated anterior gracilis muscle. The frequencies of stimulation are 20, 30 and 40 pulses per second and time (abscissa) is increasing from right to left. The force (ordinate) and time scale factors are also shown. Note the individual force twitches at 20/sec. and the development of a smoother force-time curve with increasing frequency of stimulation. The rise and fall times of the pulses each occur within 500 msec. The muscle length was 2.3 cm. and the amplitude and duration of the stimulus pulses were 0.2 A. and 2 msec., respectively.



Fig. 4.12b. Sanborn record showing the effect of muscle length upon the amplitude of the tetanic force-time response of isometrically stimulated gracilis muscle. The muscle length was 2.3 cm. for the test on the right and 2.7 cm. for the test at the left. Note the force (ordinate) scale factors are different for the curves and time (abscissa) is increasing to the left. The force used to develop the tetanic force-muscle length curve (Fig. 6.21) was measured when the curve attained a plateau. This peak force occurred within one second following the first indication of force. The amplitude, frequency and duration of the pulses were 0.2 A, 80/sec. and 2 msec., respectively for both tests.

Fig. 4.13a. Anterior gracilis muscle cells in crosssection (hematoxylin and eosin stain). Note muscle cells (1), multiple nuclei on periphery of cells (2), and capillaries (3). (100X)



Fig. 4.13b. Anterior gracilis muscle cells in crosssection (trichrome stain). Note muscle cells (1), collagenous tissue around muscle cell bundles (2), venule containing red blood cells (3), and nerve tissue (4). (100X)

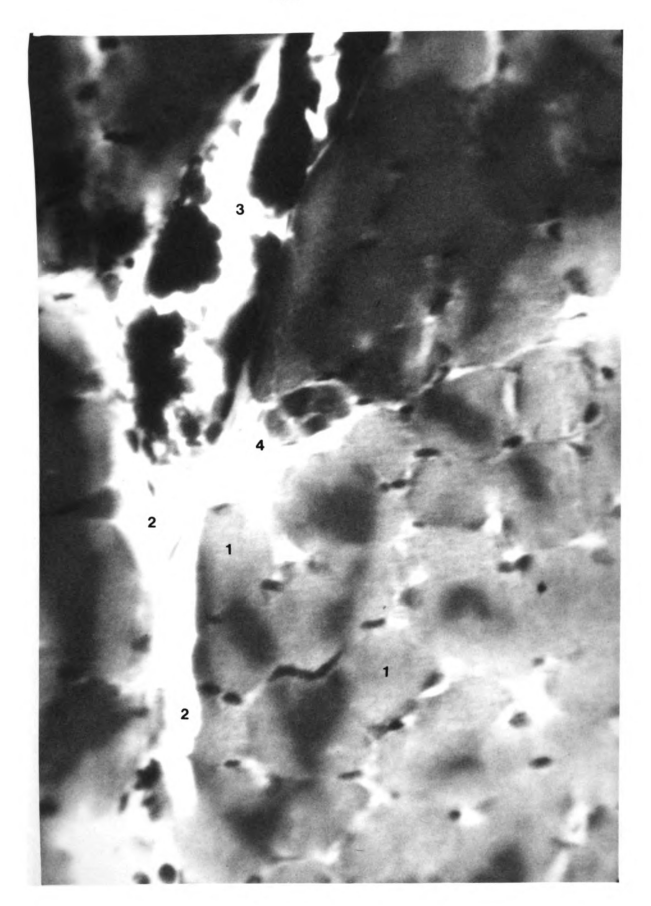


Fig. 4.14a. Anterior gracilis muscle cells in longitudinal view (trichrome stain). Note parallel fibers (1), collagenous tissue between cells (2), and vascular structures (3). (40X)

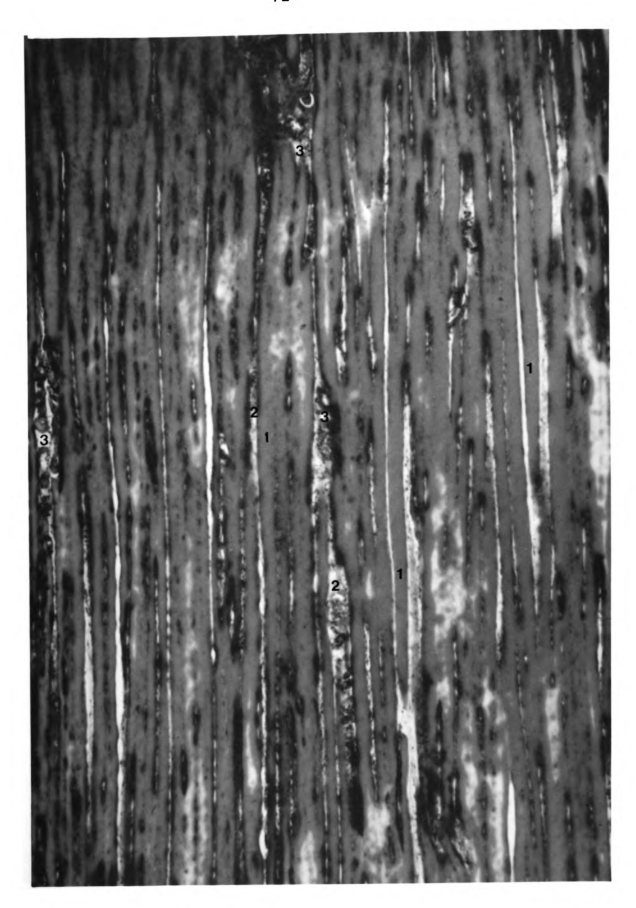
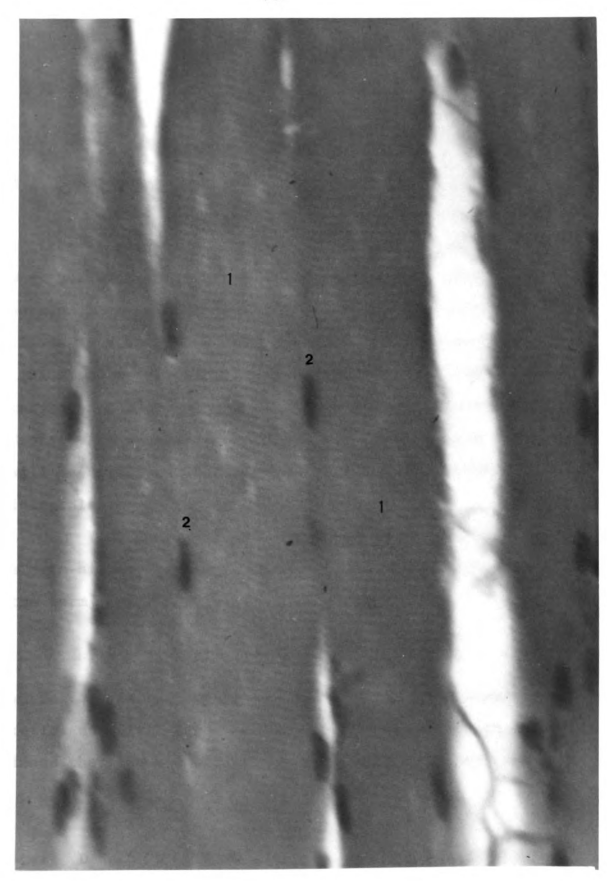


Fig. 4.14b. Anterior gracilis muscle cells in longitudinal view (H and E stain). Note muscle cells with cross-striations (1) and nuclei spaced along fibers (2). (400X)



CHAPTER V

MATHEMATICAL FORMULATION

5.1 Development

Relatively little research has been done to develop a stress-strain-time equation for skeletal muscle. This work has been complicated by the non-uniform cross-sectional areas of many muscles and the fact that the tissue is a composite material composed of connective tissue and muscle cells. General exponential loading curves or the use of discrete elements do not adequately describe this complicated tissue. A constitutive equation will be developed in this research using hereditary integrals.

Y.C. Fung (42) has proposed a general stressstrain-history expression for soft biological tissues of the form

$$\sigma(t) = \int_{0}^{t} G(t - \tau) \frac{d\sigma^{e}[\lambda(\tau)]}{d\lambda} \frac{d\lambda(\tau)}{d\tau} d\tau \qquad (5.1)$$

where σ^e is the elastic stress, λ is the extension ratio and G(t) is a "reduced" relaxation function. Fung found that the elastic stress for rabbit mesentery was

$$\sigma^{e} = D[\lambda - \frac{1}{\lambda^{2}}]e^{b\lambda}$$
 (5.2)

where D and b are constants. Haut and Little (53)

converted the extension ratios to Lagrangian strains using the relationship

$$\varepsilon = \frac{L - L_0}{L_0} = \lambda - 1 \tag{5.3}$$

where L_{0} is the original length and L is the current length. They then rewrote the elastic stress as

$$\sigma^{e} = K[\varepsilon - \varepsilon^{2}]e^{b\varepsilon}. \qquad (5.4)$$

For small strains, (5.4) reduces to

$$\sigma^{e} = K[\varepsilon + (b-1)\varepsilon^{2} + \dots] . \qquad (5.5)$$

They found that the elastic stress for collagen fibers from the rat tail could be expressed as

$$\sigma^{e} = C \varepsilon^{2} . \qquad (5.6)$$

In stress relaxation tests, they determined that the relaxation function could be represented by

$$G(t) = M(1 + \mu \, \ell n \, t)$$
 (5.7)

where μ was the normalized slope of the stress- \mathcal{D}_n (time) curve. Therefore the constitutive equation for collagen fibers was found to be

$$\sigma(t) = E \int_{0}^{t} [1 + \mu \ln(t - \tau)] \epsilon(\tau) \frac{d\epsilon(\tau)}{d\tau} d\tau \qquad (5.8)$$

where E = 2CM.

Preliminary analysis of the response of the anterior gracilis indicated that for strains below 20%,

the experimental curves were linear and relatively independent of strain rate. At higher strains, the curves
possessed second-order characteristics similar to
collagenous tissue. An explanation for this behavior
might be that at lower strains, the muscle cells and tendon
fibers which are in series, carry the load while the
collagenous tissue surrounding the muscle cells is coiled
or slackened. By subtracting the known stress-strain
quasi-static response for collagen from the experimental
curves, the weaker muscle cells were determined to be
linearly elastic throughout this strain region. However
at higher deformations, the collagenous tissue sheath and
the tendon ends dominate the response.

Experimental relaxation tests indicate that very little stress relaxation occurs in Region 1 (below 20% strain). Yet in Region 2 (above 20% strain), the stress relaxes as a linear function of the logarithm of time between one and six minutes after the start of relaxation. The magnitude of the relaxation is slightly dependent upon the strain level but it is not significant enough to change the relaxation function to include strain level as Jenkins and Little (62) did for elastin.

A conceptual model that is consistent with the initial testing results as well as histologic studies is shown in Figure 5.1. The connective tissue sheath which appears in the figure refers to collagenous fibers since they are the primary load-bearing elements.

	Connective Tissue			
Tendon Fibers	Muscle Cells			

Fig. 5.1. Model for skeletal muscle.

The elastic muscle cells are in series with the tendon fibers in Region 1 and the weaker muscle elements dominate the response. At the transition region, the parallel collagenous connective tissue becomes taut and all three elements contribute to the load. However, the connective tissue and tendon carry the majority of the force as the strain level increases. The time-independent connective tissue response in Region 2 will be assumed to be the elastic response of collagenous fibers and will take the form

$$\sigma^{e} = C \varepsilon^{2} . \qquad (5.9)$$

However the initial loading in the tendon and the connective tissue occurs at different times and both the stress and strain values for each of the two elements are different. In addition, the starting time for the relaxation function employed by Haut and Little (53) has been modified to give only non-negative values for the logarithm term. Therefore the reduced relaxation function takes the form:

$$G(t - \tau) = M(1 + \mu \, \varrho_n(t - \tau + 1)) \tag{5.10}$$

where μ has units of $(p_n \text{ minutes})^{-1}$. This change permits

the computation of the logarithm term for small time increments.

An iterative approach was utilized for the development of the composite constitutive equation. A CDC 6500 computer was used to compute stresses and strains in individual elements and the computer program is applicable to any type of strain rate input in either region. It was assumed that over a short time interval, Δt_i , the composite strain increment could be approximated by a linear expression of the form:

$$\Delta \varepsilon_{i} = \beta_{i} \Delta t_{i} \tag{5.11}$$

where β_i is the rate of the input strain. This increment is composed of a strain increment in the tendon

$$\Delta \varepsilon_{i}^{\text{te}} = \beta_{i}^{\text{te}} \Delta t_{i}$$
 (5.12)

as well as an increment in the muscle cells,

$$\Delta \varepsilon_{i}^{m} = \beta_{i}^{m} \Delta t_{i}$$
 (5.13)

where β_{i}^{te} and β_{i}^{m} are the slopes of the strain increments in the tendon and muscle, respectively. The deformation of the connective tissue sheath in parallel with the muscle cells in the higher strain region was found by equating the current lengths of both elements expressed in terms of their strain increments. Furthermore, it was assumed that the total composite deformation in any interval, i, was the sum of the deformations of the tendon and muscle giving

$$\Delta \varepsilon_{i} \ell = \Delta \varepsilon_{i}^{te} \ell^{te} + \Delta \varepsilon_{i}^{m} \ell^{m}$$
 (5.14)

where:

l = total length of the tissue

& te = length of both tendon ends

 ℓ^{m} = length of the muscle cells

$$\ell = \ell^{te} + \ell^{m}$$
.

Using (5.11) and (5.13) this expression may be written as

$$\beta_{i} \ell = \beta_{i}^{te} \ell^{te} + \beta_{i}^{m} \ell^{m}. \qquad (5.15)$$

The equations relating forces take the form

$$A^{te}\sigma^{te} = A^{m}\sigma^{m}$$
 (Region 1)
 $A^{te}\sigma^{te} = A^{m}\sigma^{m} + A^{c}\sigma^{c}$ (Region 2) (5.16a)

where A^{te} , A^{m} and A^{c} are the cross-sectional areas of the elements and σ^{te} , σ^{m} and σ^{c} are the Lagrangian stresses in the elements. Dividing each equation in (5.16a) by A^{te} , a relationship between the stresses may be found. Thus,

$$\sigma^{\text{te}} = A \sigma^{\text{m}}$$
 (Region 1)
 $\sigma^{\text{te}} = A \sigma^{\text{m}} + B \sigma^{\text{c}}$ (Region 2)

where A and B are the percentages of effective area in the muscle and connective tissue, respectively. Knowing the constitutive equations for the tendon, connective tissue and muscle, the total forces in the elements were equated in each time interval and the strain rate, $\beta_{\bf i}^{\bf te}$, was derived. The other slopes, $\beta_{\bf i}^{\bf m}$ and $\beta_{\bf i}^{\bf c}$, as well as all strains and stresses were then found and the composite stress-strain equation generated.

Region 1, Interval 1

Equations (5.6) and (5.7), the expressions for the elastic stress and reduced relaxation function for tendon, may be substituted into the general hereditary integral (equation (5.8)) for interval one, yielding

$$\sigma_{1}^{\text{te}} = E \int_{0}^{t} [1 + \mu \, \partial_{n}(t - \tau + 1)] \varepsilon_{1}(\tau) \, \frac{d\varepsilon_{1}(\tau)}{d\tau} d\tau \qquad (5.17)$$

where E = 2CM.

Setting

$$\epsilon_1^{\text{te}} = \beta_1^{\text{te}} \Delta t_1 \quad \text{for} \quad 0 \le t \le t_1$$
(5.18)

and

$$d\varepsilon_1^{\text{te}}/dt = \beta_1^{\text{te}}$$

and integrating, gives

$$\sigma_1^{\text{te}}(t) = \frac{E(\beta_1^{\text{te}})^2 t^2}{2} + E\mu(\beta_1^{\text{te}})^2 \int_{\Omega}^{t} \tau \, m(t - \tau + 1) \, d\tau. \quad (5.19)$$

The integral in the second term of (5.19) can be evaluated by letting $x = t - \tau + 1$, giving

$$\sigma_1^{\text{te}}(t) = \frac{E(\beta_1^{\text{te}})^2 t^2}{2} + \mu E(\beta_1^{\text{te}})^2 \int_1^{t+1} (t - x + 1) 2\pi x \, dx .$$

At the end of the interval when $t = t_1$,

$$\sigma_1^{\text{te}} = \frac{E(\beta_1^{\text{te}})^2 t_1^2}{2} \cdot S$$
 (5.20)

where

$$S = 1 + \frac{\mu}{t_1^2} \left\{ (t_1 + 1)^2 \ln(t_1 + 1) - \frac{3}{2} (t_1 + 1)^2 + 2(t_1 + 1) - \frac{1}{2} \right\}.$$

The linearly elastic muscle cells have the stressstrain expression

$$\sigma_1^{\rm m}(t) = F \, \varepsilon_1^{\rm m} \tag{5.21}$$

where F is the slope of the curve. From (5.15),

$$\beta_1^m = \frac{1}{\sqrt{m}} \left[\beta_1 \ell - \beta_1^{te} \ell^{te} \right] . \qquad (5.22)$$

Substituting (5.22) into (5.21) yields

$$\sigma_1^{m} = \frac{AF t_1}{\ell^{m}} \left[\beta_1 \ell - \beta_1^{te} \ell^{te}\right]. \tag{5.23}$$

The stresses in (5.20) and (5.23) may be related in (5.16b), giving,

$$\frac{E(\beta_1^{\text{te}})^2 t_1^2}{2} \cdot S = \frac{AF t_1}{\varrho^m} [\beta_1 \ell - \beta_1^{\text{te}} \ell^{\text{te}}].$$

Isolating β_1^{te} gives

$$(\beta_1^{\text{te}})^2 \left[\frac{\text{Et}_1^2}{2}\right] S + \beta_1^{\text{te}} \left[\frac{\text{AF } \ell^{\text{te}}}{\ell^{\text{m}}}\right] - \beta_1 \frac{\text{AF} \ell}{\ell^{\text{m}}} = 0.$$
 (5.24)

Using the quadratic formula, β_1^{te} is

$$\beta_1^{\text{te}} = \frac{1}{\text{ESt}_1} \left\{ -\frac{AF \ell^{\text{te}}}{\ell^{\text{m}}} \pm \sqrt{\left(\frac{AF \ell^{\text{te}}}{\ell^{\text{m}}}\right)^2 + \frac{2E AF \ell S\beta_1 t_1}{\ell^{\text{m}}}} \right\} (5.25a)$$

The tendon and muscle strains can be computed from (5.18) and (5.13) while the strain rate for muscle is derived from (5.15). Therefore,

$$\varepsilon_{1}^{te} = \beta_{1}^{te} t_{1}$$

$$\beta_{1}^{m} = \frac{1}{\ell^{m}} (\beta_{1} \ell - \beta_{1}^{te} \ell^{te})$$

$$\varepsilon_{1}^{m} = \beta_{1}^{m} t_{1}.$$
(5.25b)

The total stress from (5.20), is

$$\sigma_{1} = \sigma_{1}^{\text{te}} = \frac{AF t_{1}}{\ell^{m}} \left[\beta_{1} \ell - \frac{\ell^{\text{te}}}{ESt_{1}} \left\{ -\frac{AF\ell^{\text{te}}}{\ell^{m}} \right\} \right]$$

$$+ \sqrt{\left(\frac{AF\ell^{\text{te}}}{\ell^{m}}\right)^{2} + \frac{2E AF\ell S\beta_{1}t_{1}}{\ell^{m}}}$$
(5.26)

Future Intervals in Region 1

The strains in the composite material, tendon and muscle are:

$$\epsilon(t), \epsilon^{te}(t), \epsilon^{m}(t) = \begin{cases} \beta_{1}^{t}, \beta_{1}^{te}t, \beta_{1}^{m}t & 0 \leq t \leq t_{1} \\ \beta_{2}^{(t-t_{1})} + \epsilon(t_{1}), \beta_{2}^{te}(t-t_{1}) + \epsilon^{te}(t_{1}), t_{1} \leq t \leq t_{2} \\ \vdots & \beta_{2}^{m}(t-t_{1}) + \epsilon^{m}(t_{1}), \vdots & (5.27) \\ \beta_{i}^{t}(t-t_{i-1}) + \epsilon(t_{i-1}), \beta_{i}^{te}(t-t_{i-1}) + \epsilon^{te}(t_{i-1}), & \vdots \\ \beta_{i}^{t}(t-t_{i-1}) + \epsilon^{m}(t_{i-1}) & t_{i-1} \leq t \leq t_{i}. \end{cases}$$

The stress in the tendon in succeeding intervals may be found by substitution of the strain values into (5.17). In the second interval

$$\sigma_{2}^{te}(t) = E(\beta_{1}^{te})^{2} \int_{0}^{t_{1}} \tau[1 + \mu \mathcal{D}(t - \tau + 1)] d\tau$$

$$+ E\beta_{2}^{te} \int_{t_{1}}^{t} [1 + \mu \mathcal{D}(t - \tau + 1)] \qquad (5.28)$$

$$(\beta_{2}^{te}(\tau - t_{1}) + \varepsilon^{te}(t_{1})) d\tau.$$

At the end of the interval, $t = t_2$ and upon integration and letting $\epsilon^{te}(t_1) = \epsilon_1^{te}$, (5.28) becomes

$$\sigma_{2}^{te}(t_{2}) = \frac{E(\beta_{1}^{te})^{2}t_{1}^{2}}{2} + E(\beta_{1}^{te})^{2}\mu \int_{0}^{t_{1}} \tau \, 2\pi(t_{2} - \tau + 1) d\tau$$

$$+ \frac{E(\beta_{2}^{te})^{2}}{2} (t_{2}^{2} - t_{1}^{2}) - E(\beta_{2}^{te})^{2}t_{1}(t_{2} - t_{1})$$

$$+ E(\beta_{2}^{te})\varepsilon_{1}^{te}(t_{2} - t_{1})$$

$$+ E(\beta_{2}^{te})^{2}\mu \int_{0}^{t_{2}} \tau \, 2\pi(t_{2} - \tau + 1) d\tau$$

$$+ E(\beta_{2}^{te})^{2}\mu t_{1} \int_{0}^{t_{2}} \ell\pi(t_{2} - \tau + 1) d\tau$$

$$+ E(\beta_{2}^{te})^{2}\mu t_{1} \int_{0}^{t_{2}} \ell\pi(t_{2} - \tau + 1) d\tau$$

$$+ E(\beta_{2}^{te})^{2}\mu t_{1} \int_{0}^{t_{2}} \ell\pi(t_{2} - \tau + 1) d\tau$$

$$+ E(\beta_{2}^{te})^{2}\mu t_{1} \int_{0}^{t_{2}} \ell\pi(t_{2} - \tau + 1) d\tau$$

The third and fourth terms may be combined to give a term containing $(t_2 - t_1)^2$. Rewriting (5.29) to isolate the stress increment in interval two yields,

$$\sigma_{2}^{\text{te}}(t_{2}) = \sigma_{1}^{\text{te}}(t_{1}) + E(\beta_{1}^{\text{te}})^{2}\mu \int_{0}^{t_{1}} \tau [\partial_{n}(t_{2}-\tau+1) - \partial_{n}(t_{1}-\tau+1)] d\tau$$

$$+ \frac{E(\beta_{2}^{\text{te}})^{2}}{2}(t_{2}-t_{1})^{2} + E\beta_{2}^{\text{te}}\varepsilon_{1}^{\text{te}}(t_{2}-t_{1}) \qquad (5.30)$$

$$+ E(\beta_{2}^{\text{te}})^{2}\mu \int_{0}^{t_{1}} \tau \partial_{n}(t_{2}-\tau+1) d\tau$$

$$- E(\beta_{2}^{\text{te}})^{2}\mu t_{1} \int_{0}^{t_{1}} \partial_{n}(t_{2}-\tau+1) d\tau$$

$$+ E\beta_{2}^{\text{te}}\varepsilon_{1}^{\text{te}}\mu \int_{0}^{t_{2}} \partial_{n}(t_{2}-\tau+1) d\tau .$$

The "tendon" stress in the third interval can be found in a similar way by substituting the appropriate "tendon" strain from (5.27) into (5.17), at $t = t_3$, giving

$$\sigma_{3}^{\text{te}}(t_{3}) = E(\beta_{1}^{\text{te}})^{2} \int_{0}^{t_{1}} \tau[1 + \mu \ln(t_{3} - \tau + 1)] d\tau$$

$$+ E\beta_{2}^{\text{te}} \int_{0}^{t_{2}} [1 + \mu \ln(t_{3} - \tau + 1)] (\beta_{2}^{\text{te}}(\tau - t_{1}) + \epsilon_{1}^{\text{te}}) d\tau$$

$$+ E\beta_{3}^{\text{te}} \int_{t_{2}}^{t_{3}} [1 + \mu \ln(t_{3} - \tau + 1)]$$

$$+ E\beta_{3}^{\text{te}} \int_{t_{2}}^{t_{3}} [1 + \mu \ln(t_{3} - \tau + 1)]$$

$$(\beta_{3}^{\text{te}}(\tau - t_{2}) + \epsilon_{2}^{\text{te}}) d\tau.$$

Upon integration (5.31) becomes

$$\sigma_{3}^{te}(t_{3}) = E(\beta_{1}^{te})^{2} \frac{t_{1}^{2}}{2^{t}} + E(\beta_{1}^{te})^{2} \frac{t_{1}}{\mu_{0}^{f}} \tau_{2n}(t_{3} - \tau + 1) d\tau$$

$$+ \frac{E(\beta_{2}^{te})^{2}}{2} (t_{2}^{2} - t_{1}^{2}) - E(\beta_{2}^{te})^{2} t_{1}(t_{2} - t_{1})$$

$$+ E(\beta_{2}^{te}) \epsilon_{1}^{te}(t_{2} - t_{1})$$

$$+ E(\beta_{2}^{te})^{2} \mu_{1}^{f} \int_{t_{1}}^{t_{2}} \ell_{n}(t_{3} - \tau + 1) d\tau$$

$$- E(\beta_{2}^{te})^{2} \mu_{1}^{f} \int_{t_{1}}^{t_{2}} \ell_{n}(t_{3} - \tau + 1) d\tau$$

$$+ E\beta_{2}^{te} \epsilon_{1}^{te} \mu_{1}^{f} \ell_{n}(t_{3} - \tau + 1) d\tau$$

$$+ \frac{E(\beta_{3}^{te})^{2}}{2} (t_{3}^{2} - t_{2}^{2}) - E(\beta_{3}^{te})^{2} t_{2}(t_{3} - t_{2})$$

$$+ E\beta_{3}^{te} \epsilon_{2}^{te}(t_{3} - t_{2})$$

$$+ E(\beta_{3}^{te})^{2} \mu_{1}^{f} \ell_{n}(t_{3} - \tau + 1) d\tau$$

$$t_{2} t_{3}$$

$$- E(\beta_{3}^{te})^{2} \mu_{2}^{t} \ell_{2}^{f} \ell_{n}(t_{3} - \tau + 1) d\tau$$

$$+ E\beta_{3}^{te} \epsilon_{2}^{te} \mu_{1}^{f} \ell_{n}(t_{3} - \tau + 1) d\tau$$

$$(5.32)$$

The third and fourth terms may again be combined, giving a term containing $(t_2 - t_1)^2$. Also, the ninth and tenth terms may be grouped to give a term in $(t_3 - t_2)^2$. Since $\sigma_3^{\text{te}}(t_3) = \sigma_2^{\text{te}}(t_2) + \Delta \sigma_3^{\text{te}}$ where $\Delta \sigma_3^{\text{te}}$ is the stress increment in the third interval, (5.29) can be used

with (5.32) to give the desired increment. Therefore,

$$\sigma_{3}^{te}(t_{3}) = \sigma_{2}^{te}(t_{2}) + E(\beta_{1}^{te})^{2}\mu \int_{0}^{t_{1}} \tau [2\pi(t_{3}-\tau+1)-2\pi(t_{2}-\tau+1)]d\tau$$

$$+ E(\beta_{2}^{te})^{2}\mu \int_{0}^{t_{2}} \tau [2\pi(t_{3}-\tau+1)-2\pi(t_{2}-\tau+1)]d\tau$$

$$+ E(\beta_{2}^{te})^{2}\mu \int_{0}^{t_{2}} \tau [2\pi(t_{3}-\tau+1)-2\pi(t_{2}-\tau+1)]d\tau$$

$$+ E(\beta_{2}^{te})^{2}\mu \int_{0}^{t_{2}} \tau [2\pi(t_{3}-\tau+1)-2\pi(t_{2}-\tau+1)]d\tau$$

$$+ \frac{E(\beta_{3}^{te})^{2}}{2}(t_{3}-t_{2})^{2} + E(\beta_{3}^{te})^{2}\mu \int_{0}^{t_{3}} \tau [2\pi(t_{3}-\tau+1)]d\tau$$

$$+ E(\beta_{3}^{te})^{2}\mu \int_{0}^{t_{3}} \tau [2\pi(t_{3}-\tau+1)]d\tau$$

The "tendon" stress may now be computed in this ith interval. Using (5.27), the strain may be substituted into (5.17). At the end of the ith interval,

$$\sigma_{i}^{te}(t_{i}) = E \int_{0}^{t_{1}} [1 + \mu \ln(t_{i} - \tau + 1)] (\beta_{1}^{te})^{2} \tau d\tau$$

$$+ E\beta_{2}^{te} \int_{t_{1}}^{t_{2}} [1 + \mu \ln(t_{i} - \tau + 1)] (\beta_{2}^{te}(\tau - t_{1}) + \epsilon_{1}^{te}) d\tau$$

$$+ \dots + E\beta_{i}^{te} \int_{t_{i-1}}^{t_{i}} [1 + \mu \ln(t_{i} - \tau + 1)]$$

$$= [\beta_{i}^{te}(\tau - t_{i-1}) + \epsilon_{i-1}^{te}] d\tau. \qquad (5.34)$$

As before, the stress increment can be separated. Rearranging the order of terms, the general stress becomes

$$\sigma_{i}^{te}(t_{i}) = \sigma_{i-1}^{te}(t_{i-1}) + E(\beta_{i}^{te})^{2} \frac{(t_{i} - t_{i-1})^{2}}{2}$$

$$+ E\beta_{i}^{te} \varepsilon_{i-1}^{te}(t_{i} - t_{i-1})$$

$$+ E(\beta_{i}^{te})^{2}_{\mu} \int_{0}^{t} \tau \mathcal{D}_{n}(t_{i} - \tau + 1) d\tau$$

$$+ E(\beta_{i}^{te})^{2}_{\mu} \int_{0}^{t} \tau \mathcal{D}_{n}(t_{i} - \tau + 1) d\tau$$

$$+ E(\beta_{i}^{te})^{2}_{\mu} \int_{0}^{t} \tau [\mathcal{D}_{n}(t_{i} - \tau + 1) - \mathcal{D}_{n}(t_{i-1} - \tau + 1)] d\tau$$

$$+ E(\beta_{i}^{te})^{2}_{\mu} \int_{0}^{t} \tau [\mathcal{D}_{n}(t_{i} - \tau + 1) - \mathcal{D}_{n}(t_{i-1} - \tau + 1)] d\tau$$

$$+ \int_{j=2}^{j=i-1} E_{\mu} \{(\beta_{j}^{te})^{2} \int_{j-1}^{t_{j}} \tau [\mathcal{D}_{n}(t_{i} - \tau + 1) - \mathcal{D}_{n}(t_{i-1} - \tau + 1)] d\tau$$

$$+ \beta_{i}^{te}(\varepsilon_{j-1}^{te} - \beta_{j}^{te}t_{j-1}) \int_{t_{j-1}}^{t_{j}} [\mathcal{D}_{n}(t_{i} - \tau + 1) - \mathcal{D}_{n}(t_{i-1} - \tau + 1)] d\tau$$

$$- \mathcal{D}_{n}(t_{i-1} - \tau + 1) d\tau \}. \qquad (5.35)$$

The first integral can be evaluated by a change in variables. Letting $x = t_i - \tau + 1$ and $\Delta t_i = t_i - t_{i-1}$,

$$I_{1} = \int_{0}^{t_{i}} \tau \, \ell_{n}(t_{i} - \tau + 1) \, d\tau$$

$$= \int_{0}^{t_{i-1}} (t_{i} - t_{i-1} + 1)$$

$$= \int_{0}^{t_{i-1}} (t_{i} - x + 1) \ell_{n} x \, dx$$

$$= (t_{i} + 1) (1 + \Delta t_{i}) [\ell_{n}(1 + \Delta t_{i}) - 1]$$

$$- \frac{(1 + \Delta t_{i})^{2}}{2} [\ell_{n}(1 + \Delta t_{i}) - \frac{1}{2}] + t_{i} + \frac{3}{4}. \quad (5.36)$$

The second integral in (5.35) may be evaluated by exactly the same change in variables. Thus,

$$I_{2} = \int_{t_{i-1}}^{t_{i}} \ell_{n}(t_{i} - \tau + 1) d\tau = (1 + \Delta t_{i}) \ell_{n}(1 + \Delta t_{i}) - (1 + \Delta t_{i}) + 1.$$
(5.37)

The third integral in (5.35) involves similar variable changes and new limits of integration. Letting $x = t_i - \tau + 1$ in the first term and $x = t_{i-1} - \tau + 1$ in the last term, the third integral, following a grouping of terms, yields

$$I_{3} = \int_{0}^{t_{1}} \tau [\mathcal{D}_{n}(t_{i} - \tau + 1) - \mathcal{D}_{n}(t_{i-1} - \tau + 1)] d\tau$$

$$= \int_{t_{i}+t_{1}+1}^{t_{i}+1} (t_{i} - x + 1) \mathcal{D}_{n} x dx - \int_{t_{i-1}-t_{1}+1}^{t_{i-1}+1} (t_{i-1} - x + 1) \mathcal{D}_{n} x dx$$

$$= \frac{(t_{i}+1)^{2}}{2} \mathcal{D}_{n}(t_{i}+1) - \frac{3}{4} (t_{i}+1)^{2}$$

$$- (t_{i}+1)(t_{i} - t_{1}+1)[\mathcal{D}_{n}(t_{i} - t_{1}+1) - 1]$$

$$+ \frac{(t_{i}-t_{1}+1)^{2}}{2} \mathcal{D}_{n}(t_{i} - t_{1}+1) - \frac{1}{2}$$

$$- \frac{(t_{i-1}+1)^{2}}{2} \mathcal{D}_{n}(t_{i-1}+1)$$

$$+ \frac{3}{4}(t_{i-1}+1)^{2} + (t_{i-1}+1)(t_{i-1}-t_{1}+1)$$

$$[\mathcal{D}_{n}(t_{i-1}-t_{1}+1) - 1]$$

$$- \frac{(t_{i-1}-t_{1}+1)^{2}}{2} \mathcal{D}_{n}(t_{i-1}-t_{1}+1) - \frac{1}{2} \cdot (5.38)$$

The fourth integral in (5.35) also may be handled by variable changes. If $x = t_i - \tau + 1$ in the first term and $x = t_{i-1} - \tau + 1$ in the second term, the integral becomes

$$\begin{split} &\mathbf{I}_{4} = \int_{\mathbf{t}_{j-1}}^{\mathbf{t}_{j}} \mathbf{T}[\partial n(\mathbf{t}_{i} - \mathbf{\tau} + 1) - \partial n(\mathbf{t}_{i-1} - \mathbf{\tau} + 1)] \, d\mathbf{\tau} \\ &= \int_{\mathbf{t}_{i}}^{\mathbf{t}_{i}-\mathbf{t}_{j}+1} (\mathbf{t}_{i} - \mathbf{x} + 1) \partial n \, \mathbf{x} \, d\mathbf{x} \\ &= \int_{\mathbf{t}_{i}-\mathbf{t}_{j}+1}^{\mathbf{t}_{i}-\mathbf{t}_{j}+1} (\mathbf{t}_{i-1} - \mathbf{x} + 1) \partial n \, \mathbf{x} \, d\mathbf{x} \\ &= (\mathbf{t}_{i} + 1) (\mathbf{t}_{i} - \mathbf{t}_{j-1} + 1) [\partial n(\mathbf{t}_{i} - \mathbf{t}_{j-1} + 1) - 1] \\ &- \frac{(\mathbf{t}_{i} - \mathbf{t}_{j-1} + 1)^{2}}{2} [\partial n(\mathbf{t}_{i} - \mathbf{t}_{j-1} + 1) - \frac{1}{2}] \\ &- (\mathbf{t}_{i} + 1) (\mathbf{t}_{i} - \mathbf{t}_{j} + 1) [\partial n(\mathbf{t}_{i} - \mathbf{t}_{j} + 1) - 1] \\ &+ \frac{(\mathbf{t}_{i} - \mathbf{t}_{j} + 1)^{2}}{2} [\partial n(\mathbf{t}_{i} - \mathbf{t}_{j} + 1) [\partial n(\mathbf{t}_{i-1} - \mathbf{t}_{j-1} + 1) - 1] \\ &+ \frac{(\mathbf{t}_{i} - \mathbf{t}_{j-1} + 1)^{2}}{2} [\partial n(\mathbf{t}_{i-1} - \mathbf{t}_{j-1} + 1) - \frac{1}{2}] \\ &+ (\mathbf{t}_{i-1} + 1) (\mathbf{t}_{i-1} - \mathbf{t}_{j} + 1) [\partial n(\mathbf{t}_{i-1} - \mathbf{t}_{j} + 1) - \frac{1}{2}] \\ &+ (\mathbf{t}_{i-1} + 1) (\mathbf{t}_{i-1} - \mathbf{t}_{j} + 1) [\partial n(\mathbf{t}_{i-1} - \mathbf{t}_{j} + 1) - \frac{1}{2}] \\ &- \frac{(\mathbf{t}_{i-1} - \mathbf{t}_{j} + 1)^{2}}{2} [\partial n(\mathbf{t}_{i-1} - \mathbf{t}_{j} + 1) - \frac{1}{2}] \\ &- \frac{(\mathbf{t}_{i-1} - \mathbf{t}_{j} + 1)^{2}}{2} [\partial n(\mathbf{t}_{i-1} - \mathbf{t}_{j} + 1) - \frac{1}{2}] \\ &- \frac{(\mathbf{t}_{i-1} - \mathbf{t}_{j} + 1)^{2}}{2} [\partial n(\mathbf{t}_{i-1} - \mathbf{t}_{j} + 1) - \frac{1}{2}] \\ &- \frac{(\mathbf{t}_{i-1} - \mathbf{t}_{j} + 1)^{2}}{2} [\partial n(\mathbf{t}_{i-1} - \mathbf{t}_{j} + 1) - \frac{1}{2}] \\ &- \frac{(\mathbf{t}_{i-1} - \mathbf{t}_{j} + 1)^{2}}{2} [\partial n(\mathbf{t}_{i-1} - \mathbf{t}_{j} + 1) - \frac{1}{2}] \\ &- \frac{(\mathbf{t}_{i-1} - \mathbf{t}_{j} + 1)^{2}}{2} [\partial n(\mathbf{t}_{i-1} - \mathbf{t}_{j} + 1) - \frac{1}{2}] \\ &- \frac{(\mathbf{t}_{i-1} - \mathbf{t}_{j} + 1)^{2}}{2} [\partial n(\mathbf{t}_{i-1} - \mathbf{t}_{j} + 1) - \frac{1}{2}] \\ &- \frac{(\mathbf{t}_{i-1} - \mathbf{t}_{j} + 1)^{2}}{2} [\partial n(\mathbf{t}_{i-1} - \mathbf{t}_{j} + 1) - \frac{1}{2}] \\ &- \frac{(\mathbf{t}_{i-1} - \mathbf{t}_{i} + 1)^{2}}{2} [\partial n(\mathbf{t}_{i-1} - \mathbf{t}_{i} + 1) - \frac{1}{2}] \\ &- \frac{(\mathbf{t}_{i-1} - \mathbf{t}_{i} + 1)^{2}}{2} [\partial n(\mathbf{t}_{i-1} - \mathbf{t}_{i} + 1) - \frac{1}{2}] \\ &- \frac{(\mathbf{t}_{i-1} - \mathbf{t}_{i} + 1)^{2}}{2} [\partial n(\mathbf{t}_{i-1} - \mathbf{t}_{i} + 1) - \frac{1}{2}] \\ &- \frac{(\mathbf{t}_{i-1} - \mathbf{t}_{i} + 1)^{2}}{2} [\partial n(\mathbf{t}_{i-1} - \mathbf{t}_{i} + 1) - \frac{1}{2}] \\ &- \frac{(\mathbf{t}_{i-1} - \mathbf{t}_{i} + 1)^{2}}{2} [\partial n(\mathbf{t}_{i-1} - \mathbf{t}_{i} + 1) - \frac{1}{2}] \\ &- \frac{$$

The final integral in (5.35) is handled in exactly the same fashion using identical variable changes as in

the previous integrals. The fifth integral takes the form

$$I_{5} = \int_{t_{j-1}}^{t_{j}} [\ln(t_{i} - \tau + 1) - \ln(t_{i-1} - \tau + 1)] d\tau$$

$$= (t_{i} - t_{j-1} + 1) [\ln(t_{i} - t_{j-1} + 1) - 1]$$

$$- (t_{i} - t_{j} + 1) [\ln(t_{i} - t_{j} + 1) - 1]$$

$$- (t_{i-1} - t_{j-1} + 1) [\ln(t_{i-1} - t_{j-1} + 1) - 1]$$

$$+ (t_{i-1} - t_{j} + 1) [\ln(t_{i-1} - t_{j} + 1) - 1] . \tag{5.40}$$

Equation (5.35) may be expressed explicitly in terms of these integrals or the latter may be simply presented in terms of the symbols I_1 to I_5 . Choosing the second approach, in any interval, i, for i greater than one, the tendon stress is

$$\sigma_{i}^{te} = \sigma_{i-1}^{te} + \frac{E(\beta_{i}^{te})^{2}}{2} (\Delta t_{i})^{2} + E\beta_{i}^{te} \varepsilon_{i-1}^{te} \Delta t_{i}$$

$$+ E(\beta_{i}^{te})^{2} \mu [I_{1} - t_{i-1}^{I_{2}}] + E\beta_{i}^{te} \varepsilon_{i-1}^{te} \mu I_{2}$$

$$+ E(\beta_{1}^{te})^{2} \mu I_{3} + \sum_{j=2}^{j=i-1} E\mu [(\beta_{j}^{te})^{2} I_{4}$$

$$+ (\beta_{j}^{te} \varepsilon_{j-1}^{te} - (\beta_{j}^{te})^{2} t_{j-1}) I_{5}] . \qquad (5.41)$$

The elastic stress in the muscle cells is

$$\sigma_{\mathbf{i}}^{\mathbf{m}} = \mathbf{F} \varepsilon_{\mathbf{i}}^{\mathbf{m}} = \mathbf{F} \varepsilon_{\mathbf{i}-1}^{\mathbf{m}} + \mathbf{F} \Delta \varepsilon_{\mathbf{i}}^{\mathbf{m}}$$
,

and using (5.15) and $\sigma_{i-1}^{m} = F \epsilon_{i-1}^{m}$, yields

$$\sigma_{i}^{m} = \sigma_{i-1}^{m} + \frac{F\Delta t_{i}}{\rho_{m}} (\beta_{i} \ell - \beta_{i}^{te} \ell^{te}). \qquad (5.42)$$

Substituting (5.41) and (5.42) into (5.16b) gives

$$(\beta_{i}^{te})^{2} \{ \frac{E}{2} (\Delta t_{i})^{2} + E\mu [I_{1} - t_{i-1}I_{2}] \}$$

$$+ \beta_{i}^{te} \{ E\epsilon_{i-1}^{te} \Delta t_{i} + E\epsilon_{i-1}^{te} \mu I_{2} + \frac{AF\Delta t_{i}\ell^{te}}{m} \}$$

$$+ [E(\beta_{1}^{te})^{2} \mu I_{3} + \sum_{j=2}^{j=i-1} E\mu [(\beta_{j}^{te})^{2}I_{4}]$$

$$+ (\beta_{j}^{te} \epsilon_{j-1}^{te} - (\beta_{j}^{te})^{2}t_{j-1})I_{5}] - \frac{\beta_{i}\Delta t_{i}AF\ell}{\sigma^{m}}] = 0.$$
 (5.43)

Solving for $\beta_{\,\, i}^{\,\, te}$ by the use of the quadratic formula and dividing both the numerator and denominator by $\Delta t_{\,\, i}$ gives

$$\beta_{i}^{te} = \frac{1}{E\Delta t_{i}(1 + \frac{2\mu}{(\Delta t_{i})^{2}}[I_{1} - t_{i-1}I_{2}])} \{-[E\epsilon_{i-1}^{te}(1 + \frac{\mu I_{2}}{\Delta t_{i}}) + \frac{AF\ell^{te}}{\ell^{m}}]$$

$$\pm \sqrt{\left[E\epsilon_{i-1}^{te}(1+\frac{\mu I_{2}}{\Delta t_{i}})+\frac{AF\ell^{te}}{\ell^{m}}\right]^{2}-2E(1+\frac{2\mu}{(\Delta t_{i})^{2}}\left[I_{1}-t_{i-1}I_{2}\right])P_{i}}}$$
(5.44)

where

$$P_{i} = E(\beta_{1}^{te})^{2} \mu I_{3} + \sum_{j=2}^{j=i-1} E\mu \left[(\beta_{j}^{te})^{2} I_{4} \right]$$

$$+ (\beta_{j}^{te} \varepsilon_{j-1}^{te} - (\beta_{j}^{te})^{2} t_{j-1}) I_{5} - \frac{\beta_{i}^{\Delta t} i^{AF\ell}}{\ell^{m}}.$$

The strain rates, strain increments and strains can be found by use of the relations

$$\beta_{i}^{m} = \frac{1}{\rho^{m}} \left(\beta_{i} \ell - \beta_{i}^{te} \ell^{te} \right), \qquad (5.45)$$

$$\Delta \varepsilon_{i}^{te} = \beta_{i}^{te} \Delta t_{i}$$
, $\varepsilon_{i}^{te} = \varepsilon_{i-1}^{te} + \Delta \varepsilon_{i}^{te}$, (5.46)

$$\Delta \varepsilon_{i}^{m} = \beta_{i}^{m} \Delta t_{i}, \quad \varepsilon_{i}^{m} = \varepsilon_{i-1}^{m} + \Delta \varepsilon_{i}^{m}.$$
 (5.47)

The stresses in the tendon and muscle can be found by substituting (5.44) into (5.41) and (5.42), respectively.

Region 2 Interval 1

At approximately 20% strain, the collagenous fibers which reside in the epi-, peri- and endoysium surrounding the muscle cells straighten and begin to assume a share of the load. The constitutive equation for this collagenous component is the same as the equation for the tendon. The effect of the connective tissue is only modified by its cross-sectional area.

The governing equations for stress and strain are similar to Region 1. A balance of forces of the three components gives equation (5.16a) and following division by the original cross-sectional area, equation (5.16b) results. A balance of deflections for the elements gives (5.14) and substitution of strain rates yields (5.15) for this region. It is assumed that the lengths of the muscle and connective tissue components are equal throughout Region 2. At the transition region, an expression which

relates the lengths of the muscle and connective tissue takes the form

$$\ell^{c} = (1 + \bar{\epsilon}^{m}) \ell^{m} \tag{5.48}$$

where ℓ^c = initial length of the connective tissue $\bar{\epsilon}^m$ = strain in the muscle at the transition region. Equating the lengths of the muscle and connective tissue throughout the region yields

$$(1 + \varepsilon^{\mathbf{c}}) \ell^{\mathbf{c}} = (1 + \varepsilon^{\mathbf{m}}) \ell^{\mathbf{m}} . \tag{5.49}$$

Substituting (5.48) into (5.49) and isolating ϵ^{C} , the connective tissue strain becomes

$$\varepsilon^{c} = \frac{\varepsilon^{m} - \overline{\varepsilon}^{m}}{1 + \overline{\varepsilon}^{m}} . \tag{5.50}$$

An increment in strain is

$$\Delta \varepsilon^{\mathbf{C}} = \frac{\Delta \varepsilon^{\mathbf{m}}}{1 + \overline{\varepsilon}^{\mathbf{m}}} = \frac{\ell^{\mathbf{m}} \Delta \varepsilon^{\mathbf{m}}}{\ell^{\mathbf{C}}}.$$
 (5.51)

Substituting $\Delta \epsilon^m = \frac{\Delta t}{\ell^m} (\beta \ell - \beta^{te} \beta^{te})$ into (5.51) gives an expression in terms of the "tendon" strain rate,

$$\Delta \varepsilon^{\mathbf{c}} = \frac{\Delta t}{\ell^{\mathbf{c}}} (\beta \ell - \beta^{\mathbf{te}} \ell^{\mathbf{te}}) . \qquad (5.52)$$

In the first interval of the second region which is designated as interval KT, the "connective tissue" stress has the same form as the "tendon" stress in the first interval of Region 1. Therefore, with S defined as before in (5.20),

$$\sigma_{KT}^{c}(t) = \frac{E(\Delta \varepsilon_{KT}^{c})^{2}}{2} S. \qquad (5.53)$$

Substituting (5.52) into (5.53) and expanding yields

$$\sigma_{KT}^{c}(t) = \frac{E(\Delta t_{KT})^{2}}{2(\ell^{c})^{2}} [(\beta_{KT})^{2}\ell^{2} - 2\beta_{KT}\ell^{\beta}_{KT}^{te} \ell^{te} + (\beta_{KT}^{te})^{2}(\ell^{te})^{2}]S \qquad (5.54)$$

Substituting (5.41) and (5.42) (with i = KT) and (5.54) into (5.16b) and grouping terms around β_{KT}^{te} gives

$$(\beta_{KT}^{te})^{2} \{ \frac{E}{2} (\Delta t_{KT})^{2} [1 + \frac{2\mu}{(\Delta t_{KT})^{2}} (I_{1} - t_{NT} I_{2})] - \frac{BE(\Delta t_{KT})^{2} (\ell^{te})^{2} S}{2(\ell^{c})^{2}} \}$$

+
$$\beta_{KT}^{te} \{ E \epsilon_{NT}^{te} \Delta t_{KT} [1 + \frac{\mu}{\Delta t_{KT}} I_2] \}$$

$$+ \frac{B\beta_{KT}ES\ell\ell^{te}(\Delta t_{KT})^{2}}{(\ell^{c})^{2}} + \frac{AF\Delta t_{KT}\ell^{te}}{\ell^{m}}$$

$$+ \{E(\beta_{1}^{te})^{2}\mu I_{3} + \sum_{j=2}^{j=NT} E\mu[(\beta_{j}^{te})^{2}I_{4} + I_{5}(\beta_{j}^{te}\epsilon_{j-1}^{te} - (\beta_{j}^{te})^{2}t_{j-1})]$$

$$- (\beta_{KT})^{2}\ell^{2} \frac{BE(\Delta t_{KT})^{2}S}{2(\ell^{c})^{2}} - \frac{AF\beta_{KT}\Delta t_{KT}\ell}{\ell^{m}} \} = 0$$
(5.55)

where NT = KT - 1.

Let

$$Y_{KT} = 1 + \frac{2\mu}{(\Delta t_{KT})^2} (I_1 - t_{NT} I_2),$$
 (5.56)

$$TA_{KT} = E \epsilon_{NT}^{te} (1 + \frac{\mu}{\Delta t_{KT}} I_2) + \frac{B\beta_{KT}^{ESll}^{te} \Delta t_{KT}}{(\ell^c)^2} + \frac{AFl^{te}}{\ell^m} \quad (5.57)$$

and

$$QS_{j} = E_{\mu} [(\beta_{j}^{te})^{2}I_{4} + (\beta_{j}^{te} \epsilon_{j-1}^{te} - (\beta_{j}^{te})^{2}t_{j-1})]. \qquad (5.58)$$

Dividing both sides of (5.55) by $\Delta t_{\mbox{KT}}$ and using the quadratic formula, the strain rate in the tendon in interval KT becomes

$$\beta_{KT}^{te} = \frac{1}{E_{\Delta}t_{KT}(Y_{KT} - \frac{B(\ell^{te})^{2}S}{(\ell^{c})^{2}})} \left\{ -TA_{KT} + \sqrt{(TA_{KT})^{2} - 2E(Y_{KT} - \frac{B(\ell^{te})^{2}S}{(\ell^{c})^{2}})(E(\beta_{1}^{te})^{2}\mu_{1}^{j=NT})^{j=NT}} \right\}$$

$$-(\beta_{KT})^{2}\ell^{2} \frac{BE(\Delta t_{KT})^{2}(S)}{2(\ell^{c})^{2}} \frac{AF\beta_{KT}\Delta t_{KT}\ell}{\ell^{m}} \right\}.$$
(5.59)

The strain rates in the connective tissue and muscle become

$$\beta_{KT}^{c} = \frac{1}{\ell^{c}} \left[\beta_{KT}^{\ell} - \beta_{KT}^{te} \ell^{te} \right],$$

$$\beta_{KT}^{m} = \frac{1}{\ell^{m}} \left[\beta_{KT}^{\ell} - \beta_{KT}^{te} \ell^{te} \right].$$
(5.60)

The strain increments and total strains in all the elements are

$$\Delta \varepsilon_{KT}^{te} = \beta_{KT}^{te} \Delta t_{KT}, \quad \varepsilon_{KT}^{te} = \varepsilon_{NT}^{te} + \Delta \varepsilon_{KT}^{te},$$

$$\Delta \varepsilon_{KT}^{c} = \beta_{KT}^{c} \Delta t_{KT}, \quad \varepsilon_{KT}^{c} = \Delta \varepsilon_{KT}^{c},$$

$$\Delta \varepsilon_{KT}^{n} = \beta_{KT}^{m} \Delta t_{KT}, \quad \varepsilon_{KT}^{m} = \varepsilon_{NT}^{m} + \Delta \varepsilon_{KT}^{c}.$$
(5.61)

The stress increments and total stresses in the tendon, muscle and connective tissue can be determined by substituting (5.59) into (5.41), (5.42) and (5.54), respectively.

Future Intervals in Region 2

The stress equation for the connective tissue resembles that of the tendon in that the effects of stress in the previous intervals accumulate. The tendon and muscle stresses are again (5.41) and (5.42). Letting $\ell = j + NT$, the connective tissue stress is

$$\sigma_{i}^{c} = \sigma_{i-1}^{c} + \frac{E(\beta_{i}^{c})^{2}(\Delta t_{i})^{2}}{2} [1 + \frac{2\mu}{(\Delta t_{i})^{2}} (\overline{I}_{1} - t_{k-1} \overline{I}_{2})]$$

$$+ E\beta_{i}^{c} \Delta t_{i} \varepsilon_{i-1}^{c} (1 + \frac{\mu}{\Delta t_{i}} \overline{I}_{2}) + E(\beta_{KT}^{c})^{2} \mu \overline{I}_{3}$$

$$+ \frac{j=k-1}{\sum_{j=2}^{c} E\mu[(\beta_{k}^{c})^{2} \overline{I}_{4} + \overline{I}_{5}(\beta_{k}^{c} \varepsilon_{k-1}^{c} - (\beta_{k}^{c})^{2} t_{j-1})]$$
(5.62)

where $\overline{\mathbf{I}}$ are integrals evaluated when $\mathbf{t} = \mathbf{t}_k = \mathbf{t}_{i-NT}$. Since $\Delta \varepsilon_{\mathbf{i}}^{\mathbf{c}} = \frac{\Delta \mathbf{t}_{\mathbf{i}}}{\ell^{\mathbf{c}}} [\beta_{\mathbf{i}} \ell - \beta_{\mathbf{i}}^{\mathbf{t}} \ell^{\mathbf{t}}]$, (5.62) becomes $\sigma_{\mathbf{i}}^{\mathbf{c}} = \sigma_{\mathbf{i}-1}^{\mathbf{c}} + \frac{E(\Delta \mathbf{t}_{\mathbf{i}})^2}{2(\ell^{\mathbf{c}})^2} [(\beta_{\mathbf{i}})^2 \ell^2 - 2\beta_{\mathbf{i}} \ell \beta_{\mathbf{i}}^{\mathbf{t}} \ell^{\mathbf{t}} \ell^{\mathbf{t}} + (\beta_{\mathbf{i}}^{\mathbf{t}})^2 (\ell^{\mathbf{t}})^2]$ $\cdot [1 + \frac{2\mu}{(\Delta \mathbf{t}_{\mathbf{i}})^2} (\overline{\mathbf{I}}_{\mathbf{1}} - \mathbf{t}_{k-1} \overline{\mathbf{I}}_{\mathbf{2}})]$ $+ \frac{E\varepsilon_{\mathbf{i}-1}^{\mathbf{c}} \Delta \mathbf{t}_{\mathbf{i}}}{\ell^{\mathbf{c}}} [\beta_{\mathbf{i}} \ell - \beta_{\mathbf{i}}^{\mathbf{t}} \ell^{\mathbf{t}}] (1 + \frac{\mu}{\Delta \mathbf{t}_{\mathbf{i}}} \overline{\mathbf{I}}_{\mathbf{2}}) + E(\beta_{\mathbf{KT}}^{\mathbf{c}})^2 \mu \overline{\mathbf{I}}_{\mathbf{3}}$ $+ \frac{\mathbf{j} = \mathbf{k} - 1}{\ell^{\mathbf{c}}} E\mu[(\beta_{\ell}^{\mathbf{c}})^2 \overline{\mathbf{I}}_{\mathbf{4}} + \overline{\mathbf{I}}_{\mathbf{5}}(\beta_{\ell}^{\mathbf{c}} \ell_{\ell-1} - (\beta_{\ell}^{\mathbf{c}})^2 \mathbf{t}_{\mathbf{j}-1})] . \tag{5.63}$ Let Y_i and QS_j be defined as in (5.56) and (5.58) and let

$$QT_{j} = E\mu[(\beta_{\ell}^{c})^{2}\overline{I}_{4} + \overline{I}_{5}(\beta_{\ell}^{c}\varepsilon_{\ell-1}^{c} - (\beta_{\ell}^{c})^{2}t_{j-1})]. \quad (5.64)$$

Substituting (5.41), (5.42) and (5.63) into equation (5.16b) and collecting terms of powers of β_i^{te} yields

$$(\beta_{i}^{te})^{2} \frac{E(\Delta t_{i})^{2}}{2} (Y_{i} - \frac{B(\ell^{te})^{2}}{(\ell^{c})^{2}} Y_{k})$$

$$+ \beta_{i}^{te} \{E_{\varepsilon}^{te}_{i-1} \Delta t_{i} (1 + \frac{\mu}{\Delta t_{i}} I_{2}) + \frac{BE\ell^{te} \Delta t_{i}}{\ell^{c}} [\frac{\beta_{i}^{\Delta t_{i}\ell}}{\ell^{c}} Y_{k} + \varepsilon_{i-1}^{c} (1 + \frac{\mu}{\Delta t_{i}} \overline{I}_{2})] + \frac{AF\Delta t_{i}\ell^{te}}{\ell^{m}} \} + \{(\beta_{1}^{te})^{2} E_{\mu} I_{3} + \frac{j=i-1}{\Sigma} [QS_{j} - \frac{BE(\beta_{i})^{2}\ell^{2}(\Delta t_{i})^{2}}{2(\ell^{c})^{2}} Y_{k} - \frac{AF\beta_{i}^{\Delta t_{i}\ell}}{\ell^{m}} - \frac{BE\varepsilon_{i-1}^{c} \Delta t_{i}\beta_{i}\ell}{\ell^{c}} [1 + \frac{\mu\overline{I}_{2}}{\Delta t_{i}}] - BE(\beta_{KT}^{c})^{2} \mu\overline{I}_{3} - B\sum_{j=2}^{j=k-1} QT_{j} \} = 0.$$

$$(5.65)$$

Dividing both sides of (5.65) by Δt_i and applying the quadratic formula gives

$$\beta_{i}^{te} = \frac{1}{E\Delta t_{i}[Y_{i} - \frac{B(\ell^{te})^{2}}{(\ell^{c})^{2}}Y_{k}]}$$

$$+ \sqrt{(TA_{i})^{2} - 2E(Y_{i} - \frac{B(\ell^{te})^{2}}{(\ell^{c})^{2}}Y_{k}) \cdot P_{i}}$$
(5.66)

where

$$TA_{i} = E \varepsilon_{i-1}^{te} (1 + \frac{\mu I_{2}}{\Delta t_{i}}) + \frac{BE \ell^{te}}{\ell^{c}} \left[\frac{\beta_{i} \ell^{t}}{\ell^{c}} Y_{k} + \varepsilon_{i-1}^{c} (1 + \frac{\mu}{\Delta t_{i}} \overline{I}_{2}) \right] + \frac{AF \ell^{te}}{\ell^{m}}$$

$$(5.67a)$$

and

$$P_{i} = (\beta_{1}^{te})^{2} E_{\mu} I_{3} + \sum_{j=2}^{j=i-1} QS_{j} - \frac{BE(\beta_{i})^{2} (\Delta t_{i})^{2} L^{2}}{2(L^{c})^{2}} Y_{i}$$

$$- \frac{AF\beta_{i}^{\Delta} t_{i}^{\ell}}{L^{m}} - \frac{BE\epsilon_{i-1}^{c} \beta_{i}^{\Delta} t_{i}^{\ell} (1 + \frac{\mu}{\Delta t_{i}} \overline{I}_{2})}{L^{c}}$$

$$- BE(\beta_{KT}^{c})^{2} \mu I_{3} - B \sum_{j=2}^{j=k-1} QT_{j}. \qquad (5.67b)$$

Letting i replace KT, the strain rates, strain increments and total strains can be found from (5.60) and (5.61) by letting

$$\varepsilon_{i}^{c} = \varepsilon_{i-1}^{c} + \Delta \varepsilon_{i}^{c} . \qquad (5.68)$$

Stress increments and total stresses are obtained by substituting (5.66) into (5.41), (5.42) and (5.63).

5.2 Application to Various Passive Tests

This generalized approach for handling a composite material permits any form of strain-rate input, β_i , to be analyzed. The gracilis was subjected to three types of experimental tests: relaxation, constant strain rate loading and unloading, and sinusoidal loading.

5.2a. Relaxation Test

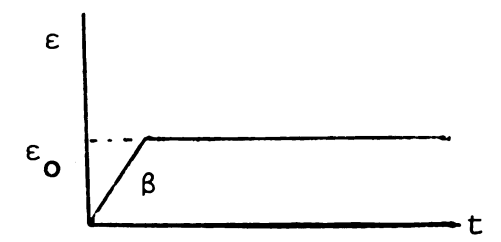


Figure 5.2. Experimental stress relaxation test

In the stress relaxation test, the specimen was deformed at a constant strain rate, $\beta_{\mbox{\scriptsize i}}$, to a predetermined strain level such that

$$\varepsilon_{i} = \beta_{i} t_{i}. \tag{5.69}$$

When a constant β_i is substituted into the expressions for β_i^{te} in the intervals of both regions, all strains and stresses may be obtained for the deformation phase of the test. At a prescribed strain level when relaxation is to begin, β_i is set equal to zero in the β_i^{te} expression and the stresses in all components as well as the total stress are known in succeeding time intervals.

5.2b. Constant Strain Rate Loading Test

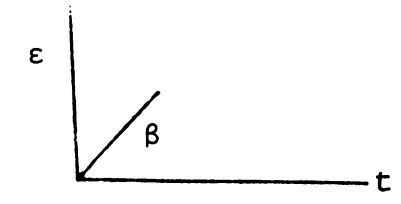


Figure 5.3. Constant strain rate test

In this test, the deformation is exactly the same as the initial part of the constant strain rate

portion for the stress relaxation test. Therefore,

$$\varepsilon_{i} = \beta_{i} t_{i}. \tag{5.70}$$

5.2c. Constant Strain Rate Loading and Unloading Test

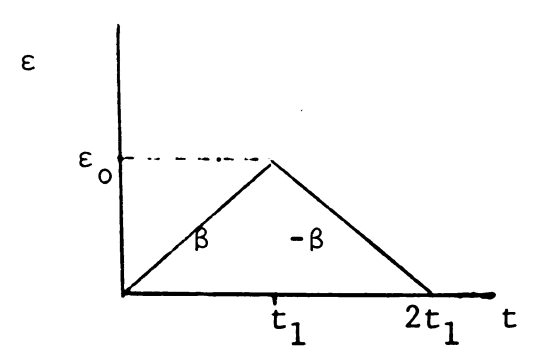


Figure 5.4. Constant strain rate loading and unloading test

In this test, the deformation is again applied at a constant strain rate through succeeding time intervals until the desired strain level is achieved. The strain rate is then reversed and deformation proceeds at a rate, $-\beta$. Therefore,

$$\varepsilon_{i} = \begin{cases} \beta_{i}^{t} & 0 \leq t \leq t_{1} \\ -\beta_{i}^{t} + 2\beta_{i}^{t}_{1} & t_{1} \leq t \leq 2t_{1}. \end{cases}$$
 (5.71)

5.2d. Sinusoidal Loading Test



Figure 5.5. Sinusoidal strain input test

In this test, the strain is given by

$$\varepsilon_{i} = \frac{\varepsilon_{o}}{2} (1 - \cos \omega_{i} t_{i})$$
 (5.72)

where ϵ_0 is the amplitude and ω_i is the frequency of oscillation. The strain rate or slope in any interval, i, is given by

$$\beta_{i} = \frac{d\varepsilon_{i}}{dt} = \omega_{i} \frac{\varepsilon_{0}}{2} (\sin \omega_{i} t) . \qquad (5.73)$$

When (5.73) is substituted into the expressions in Regions 1 and 2, the strains and stresses are obtained.

At lower strain levels, the constant strain-rate phase of the relaxation test was used to determine the slope of the stress-strain curve for muscle cells. At higher strains, the total curve also displayed the general relation-ship between the stress and the square of the strain for the collagenous tendon and connective tissue sheath elements. The relaxation phase of the stress relaxation test and the last three strain-rate inputs served as a check on the validity of the model in predicting the stress response to quasi-static and dynamic loading.

5.3 Active Tests

From numerous experimental tetanic stimulation tests which were performed on the anterior gracilis muscle, the shape of the curve has been found to be sinusoidal and its peak is displaced by a value of approximately 25% strain

from the length of initial passive loading. The tetanic force can be expressed in terms of stress by division by the original cross-sectional area, A_0 , and the length corresponding to a particular force level can be written in terms of strain, ϵ , when referred to the initial passive length.

Since the force of stimulation is generated within the muscle cells, a force balance in Region 1 yields

$$\overline{A} \ \overline{\sigma} = A^{te} \sigma^{te} = A^{m} \sigma^{m} + A^{m} \sigma^{stim}$$
or
$$\sigma^{te} = A(\sigma^{m} + \sigma^{stim})$$
(5.74)

where $A^m \sigma^{\text{stim}}$ is the tetanic force at a particular strain level, \overline{A} is the total cross-sectional area of the muscle, $\overline{\sigma}$ is the total stress in the muscle and A is the ratio, A^m/A^{te} . In Region 2, the force balance takes the form

$$\overline{A} \overline{\sigma} = A^{te} \sigma^{te} = A^{m} \sigma^{m} + A^{c} \sigma^{c} + A^{m} \sigma^{stim}$$
or
$$\sigma^{te} = A(\sigma^{m} + \sigma^{stim}) + B\sigma^{c}.$$
(5.75)

The tetanic stress, σ^{stim} , has the general form

$$\sigma^{\text{stim}} = K_1 \frac{P_0}{A^m} \sin(K_2(\epsilon + K_3))$$
 (5.76)

where P_o is the peak tetanic force at the active "resting length,"

 ϵ is the total strain when referred to the passive length

and K_1 , K_2 and K_3 are constants.

Following a determination of the passive stress for a prescribed strain-rate input, the total stress can be found by a simple addition of the active and passive stresses at certain strain levels. Equations (5.74) and (5.76) are used in Region 1 while equations (5.75) and (5.76) must be utilized in the second region.

CHAPTER VI

PRESENTATION AND DISCUSSION OF RESULTS

6.1 Presentation

6.1a. Results of Tests on Unstimulated Anterior Gracilis
Muscle

The experimental stress-strain curves for constant strain-rate deformation at various strain rates are shown in Figure 6.1. The unstimulated anterior gracilis muscle was found to exhibit sensitivity to the rate of applied deformation at strain levels above 20%, while a linear region relatively independent of strain rate, existed below this strain. A general incremental constitutive equation for skeletal muscle incorporating the response of both muscle cells and connective tissue was developed in Chapter V for both regions and was used to compare with the experimental results.

Micro-anatomy studies indicated that an anatomic model could be formed by arranging muscle cells and their collagenous connective tissue sheaths in parallel and placing both these elements in series with the collagenous tendon ends. The constitutive equation for collagenous fibers was previously determined by Haut and Little (53) and took the form:

$$\sigma(t) = E \int_{0}^{t} [1 + \mu \ln(t - \tau)] \varepsilon(\tau) \frac{d\varepsilon(\tau)}{d\tau} d\tau \qquad (5.8)$$

where $\sigma(t)$ was the stress in the collagen bundles at any time, t, μ was the normalized slope of the stress- \ln (time) curve, E was the "elastic" modulus, ϵ was the strain in the fiber bundles and τ was a variable of integration. The magnitudes of E and μ were found from preliminary stress relaxation tests by Haut and Little to be 23×10^6 dynes/cm. 2 and -0.23 (\ln min.) $^{-1}$, respectively. The general form of the stress-strain relationship for muscle cells in this study was derived by subtracting the experimental muscle response in preliminary constant strain-rate loading tests from the "elastic" response of collagenous tissue (neglecting the $[1 + \mu \ln(t - \tau)]$ term) at various strain levels. The muscle cells were found to have a linear constitutive equation of the form

$$\sigma^{m} = F \epsilon^{m} \tag{5.21}$$

where σ^{m} and ε^{m} were the stress and strain in the muscle cells, respectively, and F was determined to be 7.5×10^4 dynes/cm. ². The constitutive equations for muscle cells and collagenous tissue were then mathematically combined using the anatomic model to analyze portions of the experimental stress-strain curves for constant strain-rate loading of the muscle. Two regions in the curves were observed. In Region 1, corresponding to strains below 20%,

the muscle cells and tendon were assumed to act in series while the connective tissue sheaths were slackened. At higher strains, the tendon and the connective tissue sheaths effectively carried the load.

In order to match theory with experiment, the three material parameters, E, μ and F had to be properly chosen. It was found from later inspection of Haut and Little's mathematical development that E was in error by a factor of two, thus increasing the constant to 46×10^6 dynes/cm. $^2.$ Also stress relaxation tests were conducted by Haut and Little at only three strain levels and some variation existed in their choice of the viscous parameter, $\mu.$ Though the functional form of the constitutive equation for collagen was included in the mathematical model for muscle, modifications were necessary in the magnitudes of the material parameters.

Computations using the incremental constitutive equations for muscle were achieved by programming the appropriate equations on the computer. The ratios of tendon length to total muscle length $(1^{te}/1)$ and muscle cell length to total muscle length $(1^m/1)$ were first set at 0.06 and 0.94, respectively, where the muscle length, 1, was known for each experimental test. The ratio of the collagenous tissue cross-sectional area to total cross-sectional area and muscle cell area to total area were also kept constant at 0.04 and 0.96, respectively. Each of the parameters, E, μ and F were then varied separately to obtain the best fit of the

theoretical to experimental stress-strain curves for constant strain-rate loading and the stress-time curves for stress relaxation. Values of the parameters, E and μ , were determined to be 35 × 10⁶ dynes/cm.² and -0.35 (ln min.)⁻¹, respectively, while F was found to be 7.5 × 10⁴ dynes/cm.². The latter value remained unchanged from preliminary tests because the muscle cells, assumed to be in series with the tendon ends at lower strain levels, were the weaker component and dominated the response.

In Figures 6.2-6.6, experimental stress-strain curves (as generated by the X-Y plotter) for constant strainrate loading of the muscle are compared with theoretical stress-strain curves. Each experimental curve is the mean of a number of tests and one standard deviation from the mean is shown for different strain levels. Equation 5.26 was used to generate the theoretical stress in the first interval of Region 1 for a strain increment of two percent and for future intervals in this region (corresponding to further strain increments of two percent), equations 5.36-5.41 and 5.44 were employed to construct the theoretical curves. For the first strain increment in Region 2, the use of equation 5.59 coupled with equations 5.36-5.41 resulted in the theoretical stresses. For future strain intervals in Region 2, equations 5.36-5.41 and 5.66 provided the composite stresses for the theoretical curve. In all intervals, β_i was the value of the strain rate for each test. The theoretical stresses and

strains in the tendon, muscle cells and connective tissue sheath components were also computed. The choice of $F = 7.5 \times 10^4$ dynes/cm. 2 for a material parameter resulted in good agreement between theory and experiment for Region 1 in Figures 6.2-6.6. In the second region, good agreement was again evident up to 40% to 45% composite strain for the various strain rates. At this level where the theoretical and experimental curves deviated, the computer output for the theoretical model indicated that the tendon, connective tissue sheath and muscle cells had undergone strains of 3 to 4%, 10% to 15% and 30% to 40%, respectively. The contrast in these theoretical strain values was due to differences in the initial lengths of the model components. Though the ratios of muscle cell and tendon lengths to total muscle length were determined by experimental methods (see Section 4.4a), the collagenous fibers in the connective tissue sheaths were assumed to not deform until 20% strain was reached in the composite tissue.

A comparison of experimental and theoretical stress relaxation tests appears in Figures 6.7-6.11 for various peak strains and strain rates. The initial portion of the experimental stress-time curves was generated by constant strain-rate deformation to prescribed strain levels. The stresses were then monitored over time at that strain in the second part of the graphs. The theoretical stresses in loading were determined from the same equations as the

previous constant strain-rate tests with β_i again representing the strain rate in any interval, i. Time was monitored in the computer program during each interval in Regions 1 and 2 and stress-time curves were then constructed. The theoretical relaxation portions were generated using the equations from Region 1 when peak strains were less than 20% and from Region 2 for peak strains above 20%. As expected the theoretical and experimental curves were quite similar during the loading phase for different strain rates. theoretical equations predicted smaller stresses than the observed experimental stresses for strains of 45% or more as seen in Figure 6.7. For peak strains of 20% or less (e.g. Figure 6.10), the total theoretical stress relaxation was much smaller than the experimental results, producing stresstime curves of quite different shape. For peak strains in Region 2, the shapes of the theoretical and experimental relaxation curves were similar (see Figures 6.8 and 6.9) though theoretical stresses declined somewhat faster than the experimental values. Quite good agreement between the relaxation curves is observed for Figures 6.7 and 6.11 if the peak theoretical and experimental stresses are first aligned. In general, the choice of the material parameters resulted in a good comparison for both phases of the stress relaxation tests.

The incremental theoretical equations were then utilized to predict the response of the anterior gracilis

muscle to a single cycle of constant strain-rate deformation. Single experimental stress-strain curves are shown in Figures 6.12-6.15 for different strain rates and the theoretical curves are shown for comparison. The experimental curves, which would appear on an X-Y recorder, were composed of a loading portion similar to the constant strain-rate deformation curves in Figures 6.2-6.6 and an unloading phase, developed by recording the force during unloading at the same strain rate. The theoretical curves were constructed for the intervals during loading by the use of the same equations for Regions 1 and 2 (with β_i being the positive strain rate in each interval). Unloading in Region 2 and then in the intervals of Region 1 was accomplished by changing the sign of β_i . For the lower strain rates (Figures 6.12-6.13) experimental and theoretical loading curves compared quite well up to 35% to 40% strain. Above this strain level, the theoretical equations predicted lower stress levels as before. In Figure 6.12, for a strain rate of 7.0%/min., both unloading curves were quite close and showed complete unloading at approximately 12-15% strain. The areas of the theoretical and experimental closed curves (or hysteresis loops) were approximately equal in Figure 6.12 but the theoretical equations predicted a smaller area for 15.5%/min. strain rate (Figure 6.13). At still higher strain rates (Figures 6.14-6.15), the experimental stresses in loading far exceeded the theoretical predictions for strain levels above 35%.

areas of the theoretical hysteresis loops continued to decrease with respect to the experimental loops for increasing strain rates and the experimental unloading curves crossed the strain axis at strains approaching 20%.

The final test of the validity of the theoretical equations to predict experimental tests on the unstimulated gracilis muscle is shown in Figures 6.16-6.20. The muscle was subjected to positive sinusoidally-varying strains and the force was recorded against time on the Sanborn Recorder. The stress response of the tissue is seen for various frequencies of oscillation and peak strain levels. Stress has been plotted as a function of the number of cycles of strain input, n, and only the peak stresses or envelopes of the sinusoidally-shaped stress-time curves are shown. The same equations have been used as in previous tests to generate the theoretical stresses in the intervals of Regions 1 and 2. However the strain rate, β_i , which was constantly changing, was defined by equation 5.73. Only the peak theoretical stresses were taken from the computer output for each cycle. Figure 6.16 reveals that the theoretical and experimental curves possessed similar shapes for a low frequency of oscillation (3.0 Rad./min.) and for a moderately small peak strain level (23.0%). As the frequency was increased (Figure 6.17), the experimental peak stresses exceeded the theoretical values though the curves were parallel following five cycles. The theoretical equations were also unable to

was subjected to peak sinusoidal strains of more than 40%, the effects of frequency of oscillation became quite important. For a frequency of 4.0 Rad./min. (Figure 6.18), little or no experimental stress decay or fatigue occurred compared to that predicted by theory. When the frequency was increased (Figures 6.19 and 6.20) peak stresses became only half those obtained experimentally. However, the theoretical and experimental curves remained parallel after a few cycles of oscillation. Best agreement in the sinusoidal tests was observed for frequencies below 20-30 Rad./min. and for peak strains under 40-45%.

6.1b. Results of Tests on Fully Stimulated Anterior Gracilis Muscle

The anterior gracilis muscle was given supramaximal stimuli at prescribed frequencies, current intensities and stimulus durations to generate tetanic forces. A plot of the mean of eight experimental tests displaying tetanic force (gm. force) and total muscle length (cm.) is shown in Figure 6.21. One standard deviation from the mean of the tetanic curves is given for different muscle lengths and a force-length curve for unstimulated muscle is shown for comparison. The tetanic curve has a sinusoidal shape and the force peaks at a muscle length of approximately 2.75 cm. The maximum or peak tetanic force at this length is about 21.6 gm. force. It is seen that tetanic forces are

generated in the muscle below the gauge length (length at which first passive force is recorded). The force in the unstimulated muscle is less than one-sixth the tetanic force even at a length of 3.3 cm.

The experimental tetanic force values for each test were divided by the cross-sectional area of the muscle at zero passive strain (gauge length) to develop a "tetanic stress" which was plotted against the passive strain. This curve as well as the theoretical tetanic curve are displayed in Figure 6.22.

To match theory and experiment the theoretical tetanic stress was found to be related to the sine of the passive strain and was shown in Chapter V to take the form,

$$\sigma^{\text{stim}} = K_1 \frac{P_0}{A^m} \sin(K_2(\epsilon + K_3))$$
 (5.76)

where P_0 was the peak tetanic force (gm. force), A^m was the cross-sectional area of the muscle (cm.²), ϵ was the passive strain (cm./cm.) in the whole muscle and K_1 , K_2 and K_3 were constants. The tetanic force was found to be 21.6 gm. while the cross-sectional area was approximately 0.015 cm.². The constant, K_1 , which had a value of 980 was used to convert grams force to dynes. The constants, K_2 and K_3 , were found to be 144 and 0.375, respectively, and were selected to give the best agreement between the theoretical and experimental curves. The maximum stress, corresponding to the maximum value of the sine function at

25% strain was thus determined to be 1.41×10^6 dynes/cm.². Above 25% strain, the experimental passive stress can be seen to contribute to the total response.

6.2 Discussion

6.2a. Experimental Passive Tests

The passive experimental results of this study show similar tendencies with those of other researchers. first indication of passive force for constant strain-rate loading of the anterior gracilis muscle occurred at 2.12 cm. or at 78% of the resting length. Bahler et al. (10, 11) confirmed that this length was about 2.1 cm. or 80% of the resting length for rat anterior gracilis muscles of approximately the same weight. Rosenblueth et al. (76) found similar gauge length to resting length percentages of 77%, 78% and 83% for tests on frog sartorius, cat soleus and cat gastrocnemius muscles, respectively. Geffen (45) and Parmley et al. (70) arrived at similar percentages of 74-78% for experiments on the rat gastrocnemius and cat papillary muscles, respectively. Aubert et al. (6), Hill (see Geffen (45)), Rack and Westbury (73) and Walker and Thomas (82) discovered that the gauge length to resting length percentages exceeded 90% while Schottelius and Senay (77), using rat gastrocnemius muscles, determined that the passive tension first occurred at 3% above the resting length. Only Hartree and Hill (see Geffen (45)) and Sonneblick et al. (80) concluded that the passive length was less than or equal to 70% of the resting length.

The linear region in the experimental passive constant strain-rate deformation tests (Figure 6.1) resembles the "rubber-like" region described by Abbott (3) and the linear regions in the force-length curves displayed by Bahler (7) and Rosenblueth et al. (76). Hill (59) also noted the somewhat linear region for loading to 20%-25% passive strain but stated that the resting tension increased exponentially with length in this interval. Sonnenblick et al. (80) showed that no linear region existed up to 20% strain for tensile tests on human papillary cardiac muscles. Unlike the anterior gracilis muscle which attained stress levels of 15,000-16,000 dynes/cm. 2 at 20% strain, the stress in the resting papillary muscle at 20% strain was found to be 0.4 gm./mm. 2 (approximately 40,000 dynes/cm. 2).

The unstimulated response of the anterior gracilis muscle at higher strain levels (Figure 6.1) agrees with the results of Abbott (3) who claimed that the "normal" elasticity which existed in this region was a combination of the response of the collagenous tissue and the resting tension in the muscle cells. As described by Abbott (3), Hill and Weiss, Fogh and Buchthal claimed that the muscle was much stiffer at the longer lengths and that the supporting collagenous tissue carried most of the load. Hill (59) also determined that a normal curvature was evident in the loading curves above 25% strain for frog sartorius muscles. The stress which was found to be approximately 50,000-

60,000 dynes/cm. 2 at 40% strain (see Figure 6.1) differed from the stresses quoted by Sonnenblick et al. (80) of over 200,000 dynes/cm. 2 at the same strain level. However, Bahler's (7) force-length curve for rat anterior gracilis muscles revealed that at higher strains, the forces were less than those observed in this study at even 5-6% strain/min. Though no family of experimental loading curves was found in the literature which revealed the rate sensitivity of skeletal muscle, Fung (40) did show that the force in rabbit papillary muscle increased with increasing rates of deformation.

A limited amount of work has been done that can be compared with the other passive experimental tests in this study. The experimental stress relaxation tests (Figures 6.7-6.11) which were analyzed over a time period of 10-15 minutes show some similarities with the research of Abbott and Lowy (1) who investigated stress decay following stretch at various deformation rates. In both studies the peak stress before relaxation was larger for the higher strain rates. However the total amount of relaxation was not determined by Abbott and Lowy since they only monitored the stress decay for 4-6 seconds. Utilizing triceps surae muscles from the rat, Walker and Thomas (82) displayed stress relaxation curves induced by slow and quick stretches of the muscles to peak strains under 21%. Walker and Thomas found, as in this research, that 1) stress relaxation

was rapid during the first minute while only a small amount occurred in the next four minutes and 2) peak stress was larger for the more rapid stretch. The rates of extension were not given for comparison with this study and the peak stresses at 3% strain (180,000 dynes/cm. 2 and 90,000 dynes/cm. 2 for quick and slow stretch, respectively) were much larger than observed in this research.

Fung (40) displayed the effects of one cycle of loading of rabbit papillary muscles for various rates of deformation and the resulting force-displacement curves generally resemble the results shown in Figures 6.12-6.15. However, Fung found that even when the rate of muscle extension was increased by 100 times, the area of the hysteresis loops either remained constant or decreased. Hoffman et al. (60) showed one hysteresis loop for cyclic loading of cardiac papillary muscles but the area of the loop was quite small compared to the results of this study and no attempt was made to explore the rate sensitivity of the tissue.

A number of authors have also investigated the effects of repetitive displacement oscillation of passive skeletal muscle as was shown in Figures 6.16-6.20. Gasser and Hill (44) revealed that a minimum amount of fatigue occurred following continued cyclic oscillation of the frog sartorius muscle and little stress decay occurred following 15-30 cycles in this research. Though the initial stresses

are seen to increase with increasing frequency between 3.0 Rad./min. and 75.0 Rad./min. (Figures 6.16-6.20), Rack (72) found that the peak force in cat soleus muscle remained constant during in vivo sinusoidal stretching at frequencies between 94 and 4300 Rad./min. However, the oscillations were made between lengths which were below the resting length and from this study, this length region corresponded to strains below 25%. Since the anterior gracilis muscle was found to be relatively insensitive to strain rate in this region, minimal stress fatigue would be expected.

6.2b. Experimental Active Tests

Isometric tetanic tension versus length curves similar to Figure 6.21 have been displayed by various authors (7, 10, 11, 26, 27). Bahler (7) and Bahler, Fales and Zierler (10, 11) obtained different peak tetanic tensions for fully stimulated rat anterior gracilis muscle. Unlike the peak tetanic tension of 21.6 grams force found in this study, Bahler (7) showed that peak values of 32 gm. were attained for 140-165 gm. rats at a resting length of approximately 2.7 cm. while Bahler et al. (10) found that peak tetanic tensions of 35 gm. occurred for rats of similar size. However in another study on Wistar rats by Bahler et al. (11), the peak tetanic tension and resting length were determined to be 24 gm. and 2.6 cm., respectively. In all the studies by Bahler et al. (7, 10, 11) the temperature was maintained at 17.5°C. as opposed to 25°C. in this research.

The peak isometric tetanic stresses in this study of 1.41×10^6 dynes/cm. 2 match the results of Bahler et al. (11) who determined that a peak stress of 1.31×10^6 dynes/cm. 2 could be generated by tetanized isometric anterior gracilis muscles from Wistar rats. The results of this study compare with Casella's (22) findings for the frog semitendinosus muscles at 20° C. (1.45 × 10^6 dynes/cm. 2) but a discrepancy exists at the same temperature for the frog anterior tibial muscle (2.45 × 10^6 dynes/cm. 2). The findings of Close and Hoh (26) that the peak isometric tetanic stresses at 25° C. for the rat extensor digitorum longus and soleus muscles were 2.35×10^6 dynes/cm. 2 and 1.76×10^6 dynes/cm. 2 , respectively, were somewhat higher than the value from this study.

6.2c. Theoretical Passive Modeling

The theoretical equations for passive skeletal muscle in this study are not easily compared with the discrete models previously proposed. Hill's (56) series element which was present during muscle contraction represented the tendon ends and myofilaments while the parallel element, corresponding to the connective tissue sheaths and sarcolemmas, modeled the response of unstimulated muscle (see Figure 3.1). The mathematical model advanced in this research for passive anterior gracilis muscle differs from Hill's parallel nonlinear elastic element because it accounts for the muscle's rate sensitivity and includes the

mechanical response of the tendon ends and muscle cells as well. The cardiac models of Sonnenblick (79) and Hoffman et al. (60) which suggest that the parallel and series elements should be placed in series and discrete viscous elements should be added, are closer representations of passive muscle. The viscoelastic passive model proposed by Glantz (46) which contains exponential springs in series and in parallel with a linear damper is still just another simplification of the continuous quasi-linear integral approach employed in this study.

The theoretical stress-strain curves for the anterior gracilis muscle (Figures 6.2-6.6) are not unlike the theoretical tension-extension curves which Hill and Hartree (54) proposed for amphibian skeletal muscle. Hill and Hartree revealed that greater passive tensions were observed for faster rates of extension indicating that viscoelastic effects were present in unstimulated muscle.

The theoretical stress-strain relations which have been developed previously for unstimulated skeletal muscle (69), heart muscle (40) and biological fibers (16, 42, 53, 64) all differ in some degree with the equations presented in Chapter V. Nubar's (69) development was based upon relating the longitudinal strain in muscle fibers to the perpendicular distance of these fibers from the muscle's central axis (assuming a pennate-shaped or non-uniform muscle cross-section). Nubar included three elastic

coefficients in his equations but no viscous behavior was discussed. Fung (40) determined that exponential relationships existed between stress and muscle extension for the parallel and series elements in Hill's model (Figure 3.1). The muscle length was then expressed in terms of the contractile myofilament lengths. However no attempt was made in this research to include the myofilament response and Fung's equations completely neglected the time-dependent characteristics of muscle. Unlike Fung (42) who developed an exponential relationship between stress and extension ratio and included strain history, Blatz et al. (16) found that the stress in biological fibers (including skeletal muscle) was better related to a power law of the extension ratio but with no time effects. The viscoelastic equations which appear in this study are based upon Fung's work (42) but Fung has not analyzed skeletal muscle and Blatz et al. have not separated the responses of the anatomic elements in muscle tissue. King and Lawton's (64) stress-strain equation for elastomers such as muscle tissue bears the least resemblance to the equations in Chapter V in that the stress in the muscle was related to the temperature of the material as well as to the number and lengths of the molecular chains within the muscle fibers.

Fung's quasi-linear viscoelastic hereditary integral was utilized by Haut and Little (53) to generate the viscoelastic integral for collagen (Equation 5.8). Only the

functional form of the hereditary integral was employed in Chapter V to represent the response of the tendon ends and collagenous connective tissue sheath. The values for the material parameters, E and μ , were changed to account for discrepancies in Haut and Little's analysis and to establish a better fit of the theoretical model to the data for constant strain-rate loading and stress relaxation The limit of the applicability of Haut and Little's model to predict collagenous response was noted to be 3-4% strain and relatively large differences occurred above 8-10% strain. In the development of the skeletal muscle model, a tabulation was kept in the computer program of the strains in the collagenous tendon, collagenous tissue sheath and muscle cells for all composite strain levels. noted that at 40% composite strain where the theoretical loading curves deviated from the experimental values, the strains in the tendon were determined to be 3-4% while the connective tissue sheath strains were 10-15%. Therefore, the validity of the skeletal muscle mathematical model presented here is substantiated by Haut and Little's documentation of strain limits for collagen fibers.

6.2d. Theoretical Active Modeling

The empirical expression relating the isometric tetanic stress and the passive strain was found to be sinusoidal in nature (Equation 5.76) and the graph of this equation in Figure 6.22 matches the experimental results

for passive strains up to 50%. However Bahler (7) found that a quadratic expression of the form:

$$P(1) = 0.99 - 0.055(1-1_0) - 4.48(1-1_0)^2$$

- where P(1) was the isometric tetanic force expressed as a fraction of P_0 , the peak isometric tension
 - 1 was the length of the muscle expressed as a fraction of 1_0 , the muscle length at which peak isometric tension occurred

produced good agreement between theory and experiment over the physiological length range. Bahler's equation does not account for the muscle cross-sectional area and therefore makes the comparison of different muscles very difficult. Nubar's (69) stress-strain equation for passive skeletal muscle also contained additional terms which accounted for the contractile force developed by stimulated muscle. The form of the terms, which differed greatly from Equation 5.76, was a polynomial in strain containing the same three elastic coefficients as in the passive model. It was not possible to compare the equations since no values were assigned to the material parameters.

6.2e. Implications

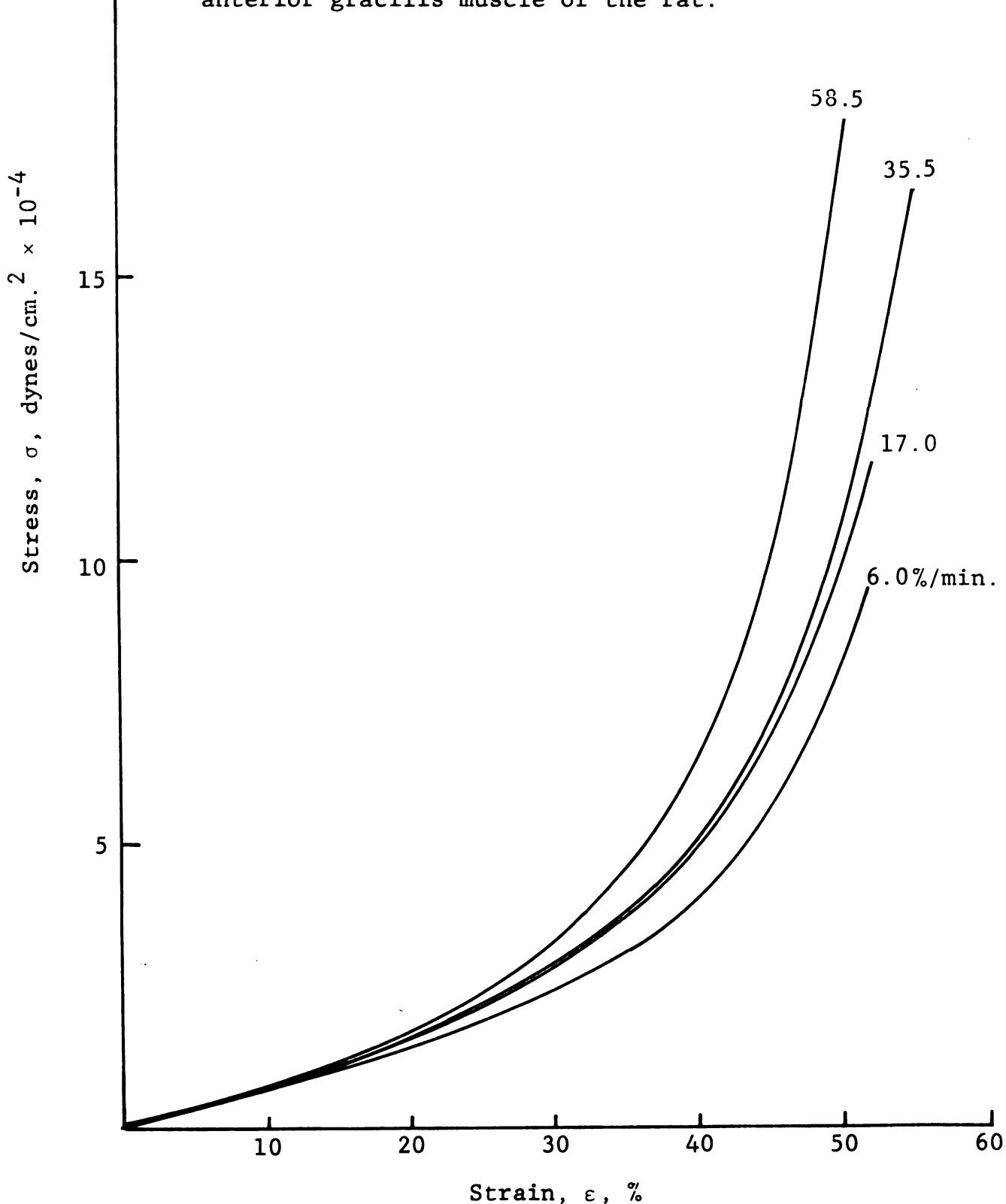
The histologic studies were performed to develop the anatomic model in Figure 5.1 and to generate the ratios of muscle cell and connective tissue cross-sectional areas to total cross-sectional areas. The paraffin technique which

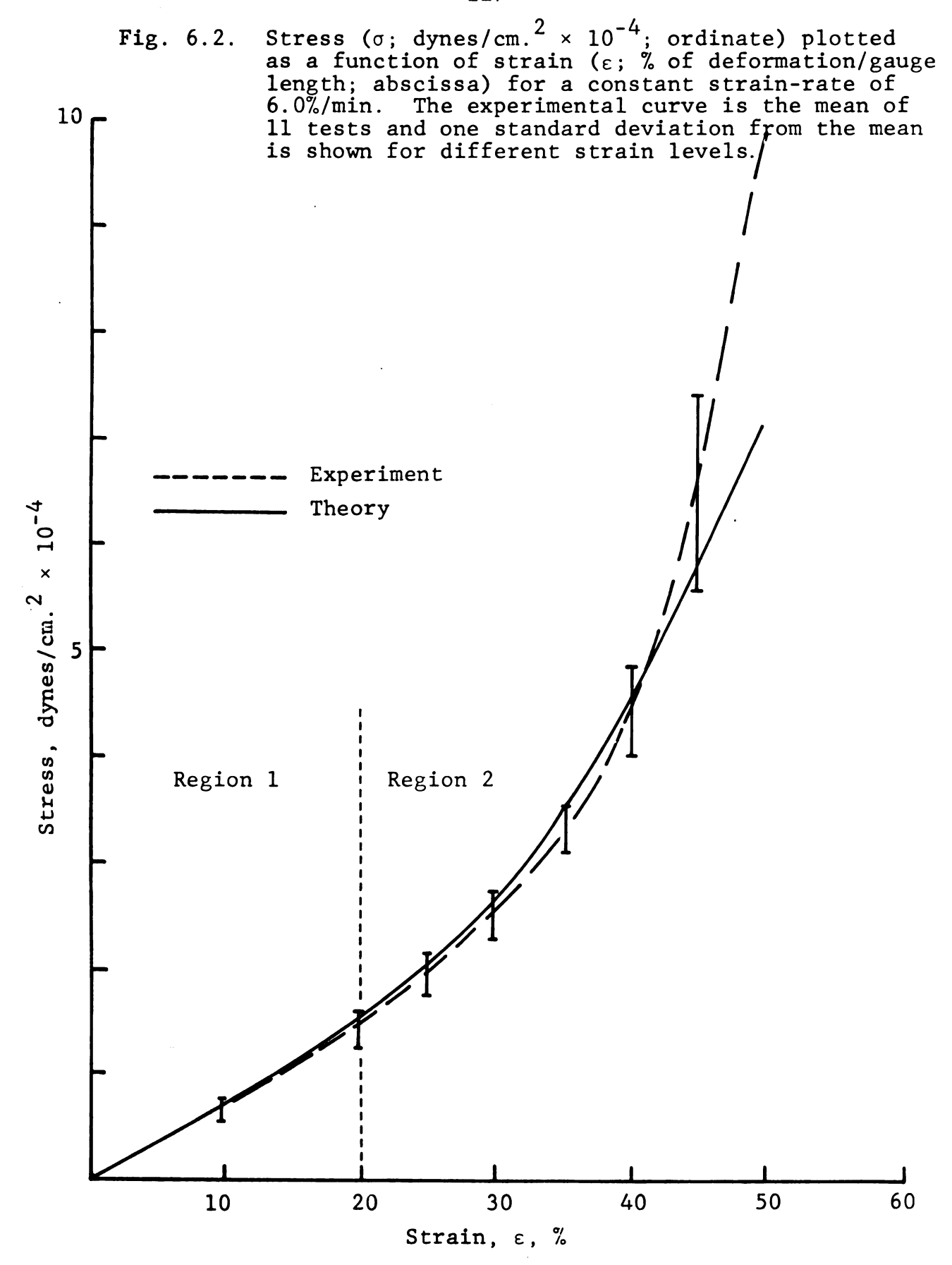
was utilized could be used for muscles which varied in crosssectional area along their lengths. Hematoxylin and eosin
stain would be useful for observing the general shape and
organization of normal or diseased muscle cells and Gomori's
trichrome stain could be used to reveal the locations and
amounts of the collagenous connective tissue. The enlarger
could also be used to give an accurate picture of the muscle
in longitudinal and cross-sectional views.

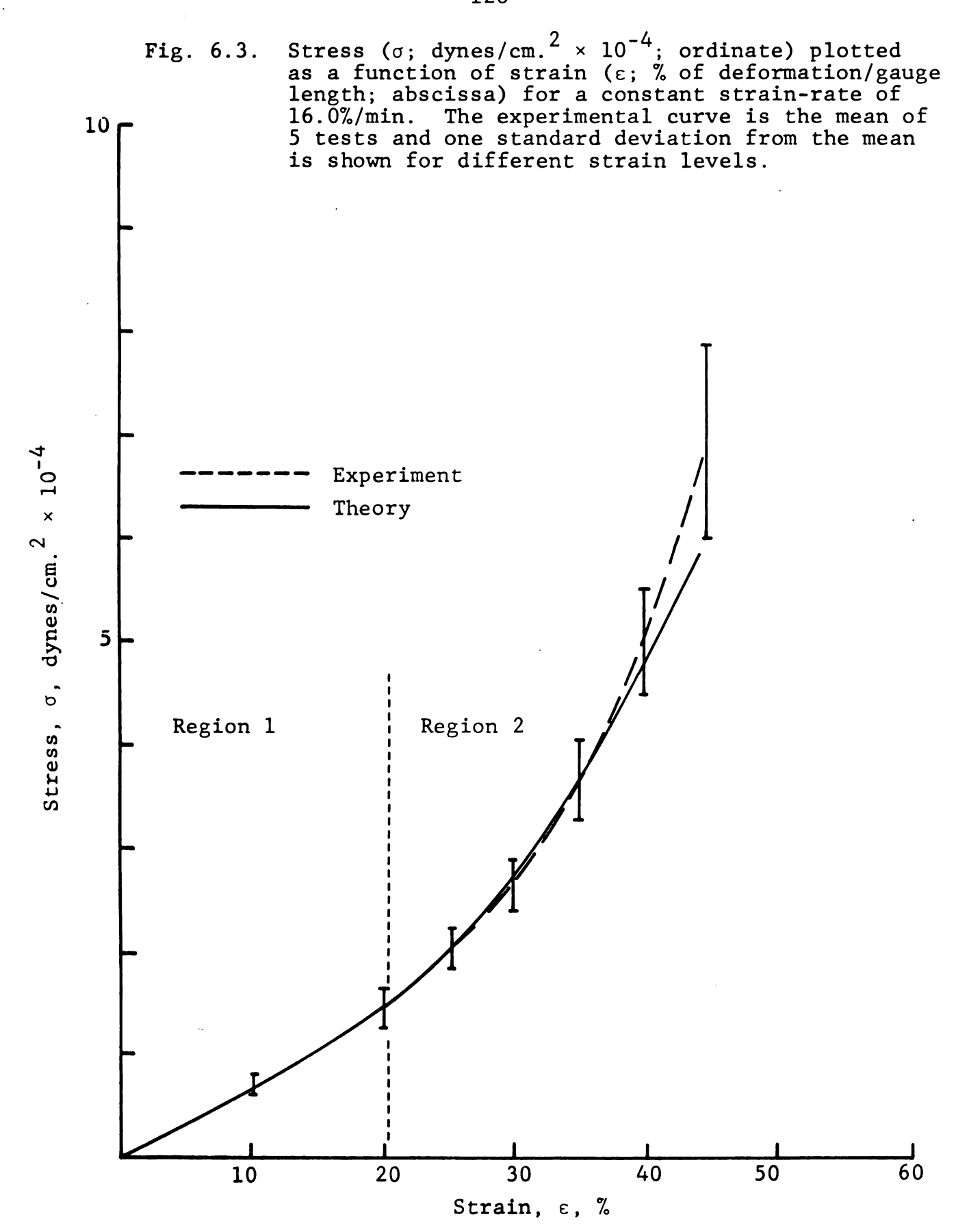
The physiological tests were employed to determine the parameters of stimulation (pulse frequency, current intensity and pulse duration) and also to establish the variation of isometric tetanic tension with muscle length. The results of the physiological tests indicate that indirect stimulation with predetermined stimulus parameters yields tetanic forces in the muscle cells. The choice of a mammalian muscle with a thickness of less than one millimeter enables in vitro tests to be conducted giving reproducible tetanic tensions at various muscle lengths for over two hours after surgery. Future in vitro tests should be performed to establish the effects of temperature upon the twitch and tetanic tensions of the anterior gracilis and other mammalian muscles. In vivo tests should also be run on skeletal muscles of various sizes and fiber types to determine what differences occur as a result of removing the muscle from the body and providing indirect stimulation.

The mathematical expressions in Chapter V adequately predict the response of passive and fully tetanized anterior gracilis muscle from the Sprague Dawley rat at 25°C. Once modifications are made in the equations to account for temperature, fiber orientation and muscle fiber types, insight can be gained into the anatomic and physiological changes which occur in diseased muscle such as in the various forms of muscular dystrophy. The theoretical expressions which are developed will also provide material parameters for the design of prosthetic materials and devices which simulate the action of unstimulated and contracted skeletal muscle.

Fig. 6.1. Stress (σ ; dynes/cm. $^2 \times 10^{-4}$; ordinate) plotted as a function of strain (ϵ ; % of deformation/gauge length; abscissa) for different strain-rates (%/min.) shown for each curve. The curves are the results of experimental tests on the unstimulated anterior gracilis muscle of the rat.

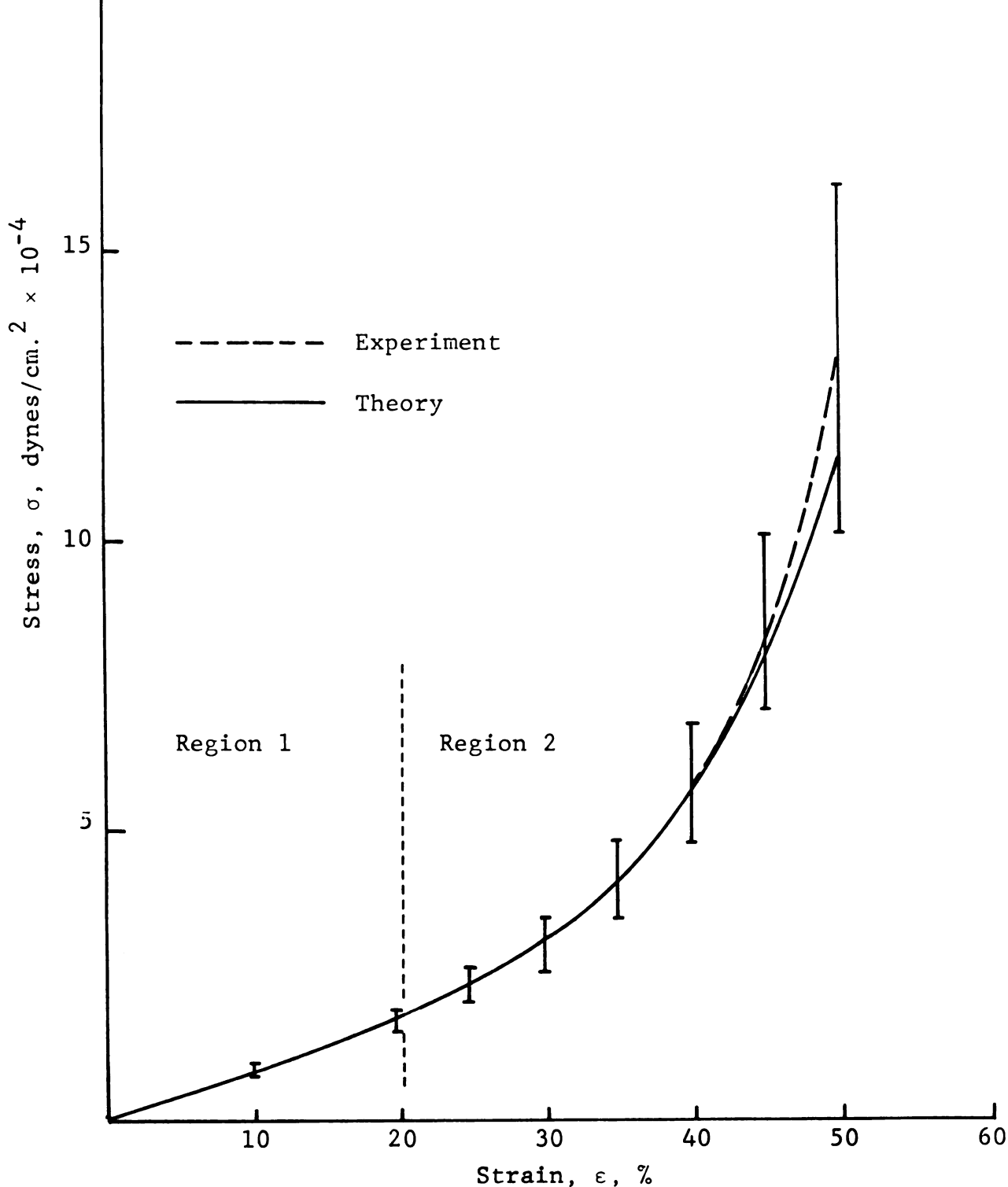


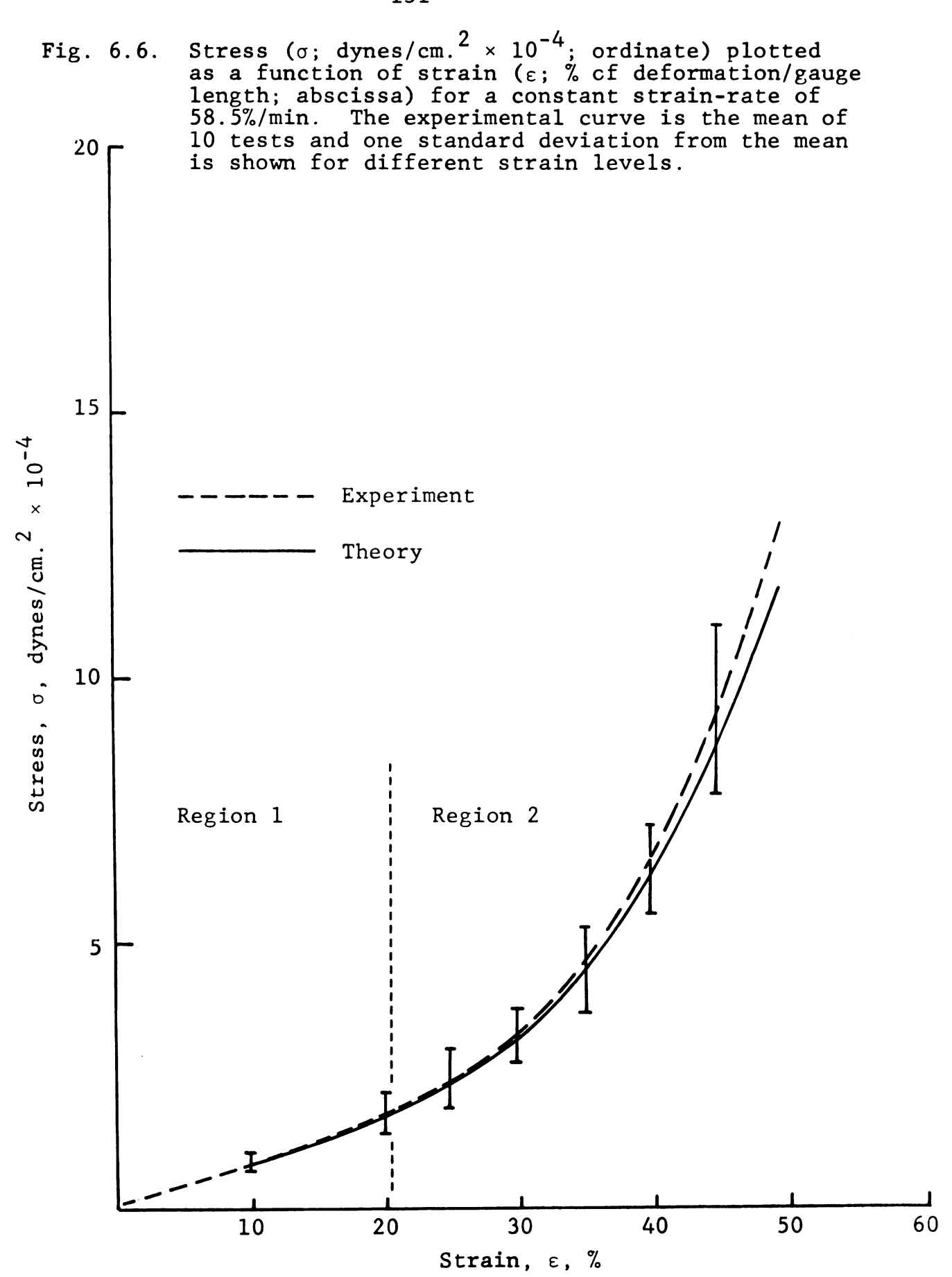


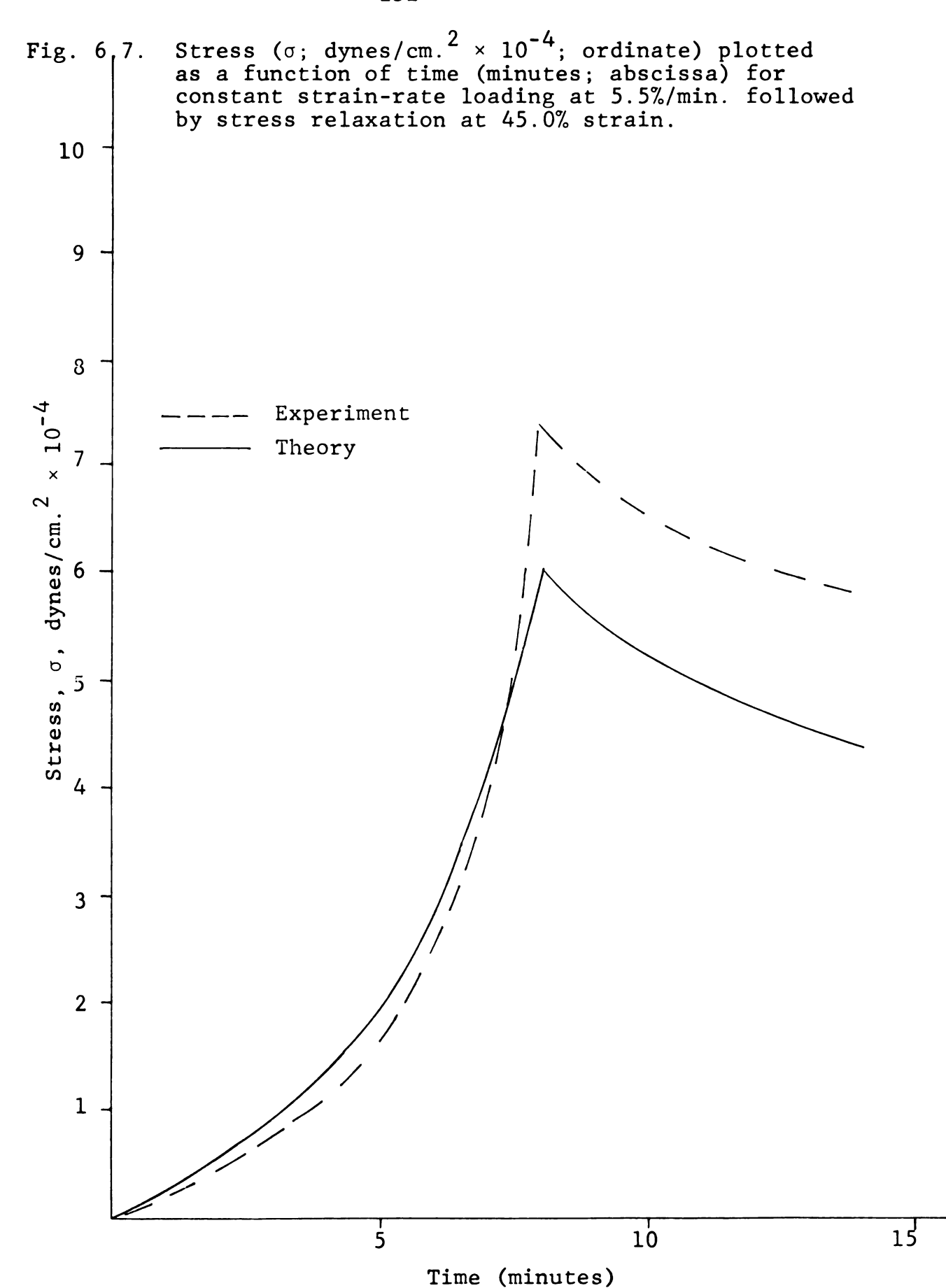


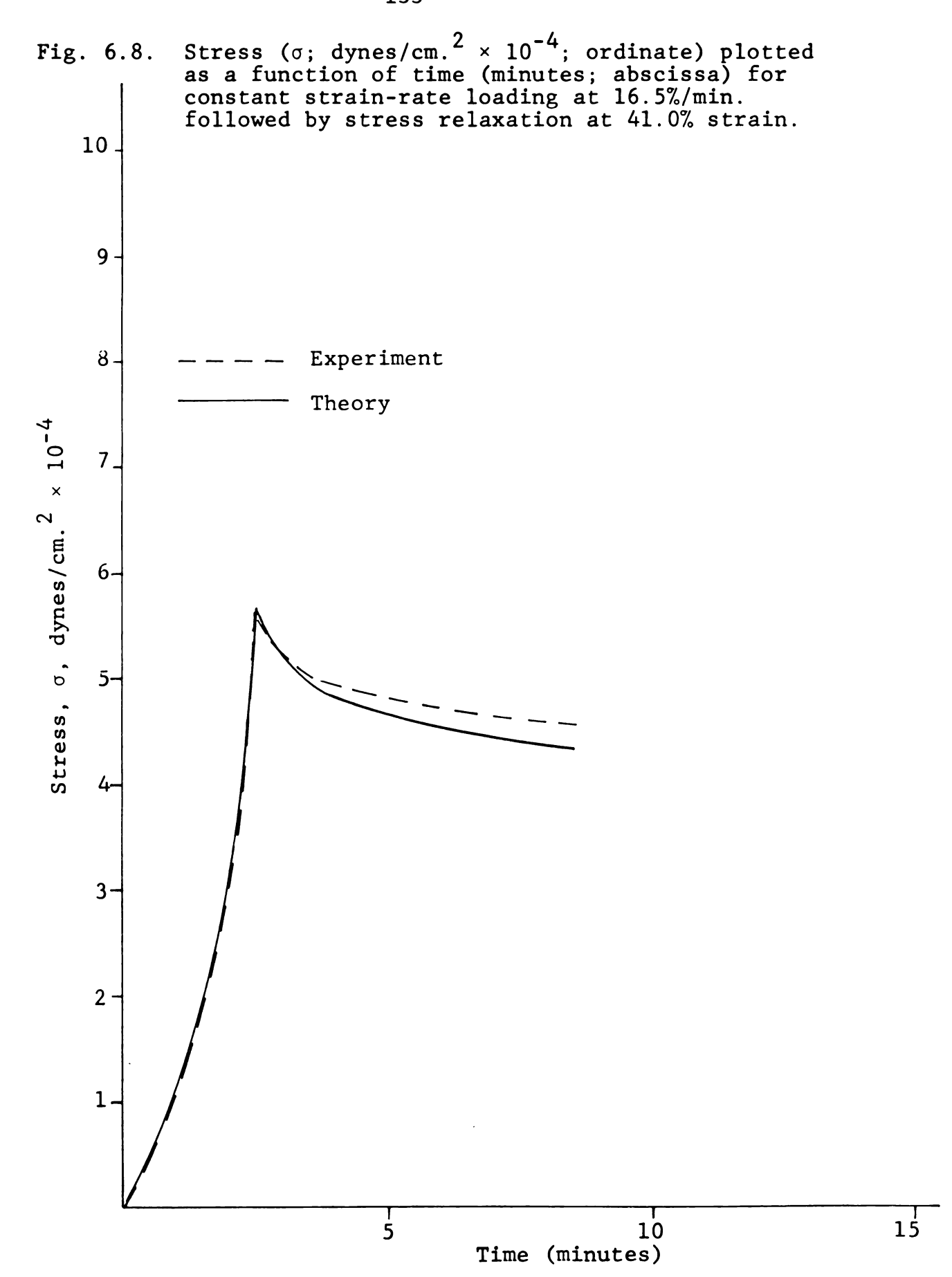
Stress (σ ; dynes/cm.² × 10⁻⁴; ordinate) plotted as a function of strain (ϵ ; % of deformation/gauge length; abscissa) for a constant strain-rate of Fig. 6.4. 35.0%/min. The experimental curve is the mean 20 of 10 tests and one standard deviation from the mean is shown for different strain levels. 15 Stress, σ , dynes/cm² × 10^{-4} Experiment Theory 10 Region 1 Region 2 5 10 50 20 30 40 Strain, ε, %

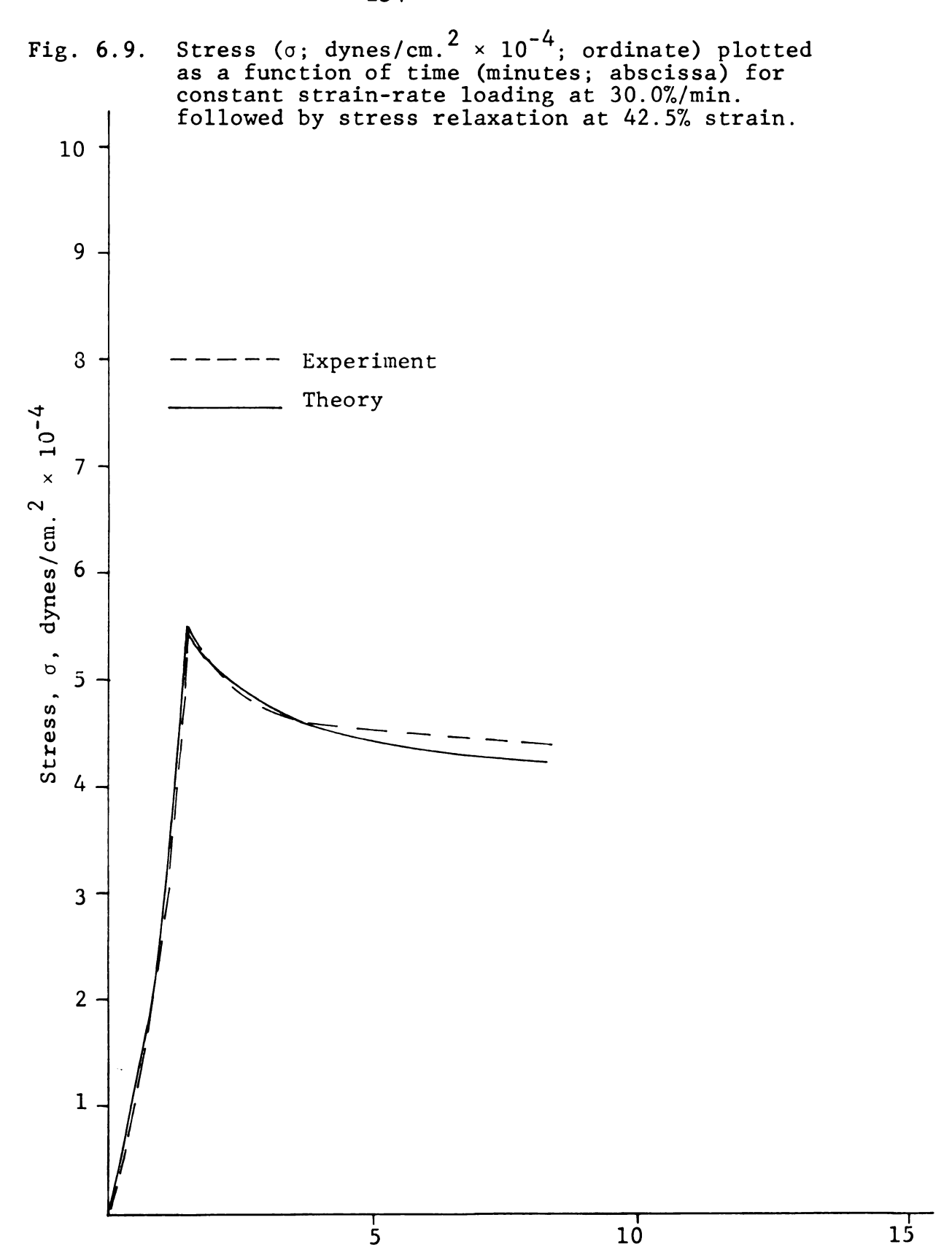
Fig. 6.5. Stress (σ ; dynes/cm. $^2 \times 10^{-4}$; ordinate) plotted as a function of strain (ϵ ; % of deformation/gauge length; abscissa) for a constant strain-rate of 46.5%/min. The experimental curve is the mean of 4 tests and one standard deviation from the mean is shown for different strain levels.



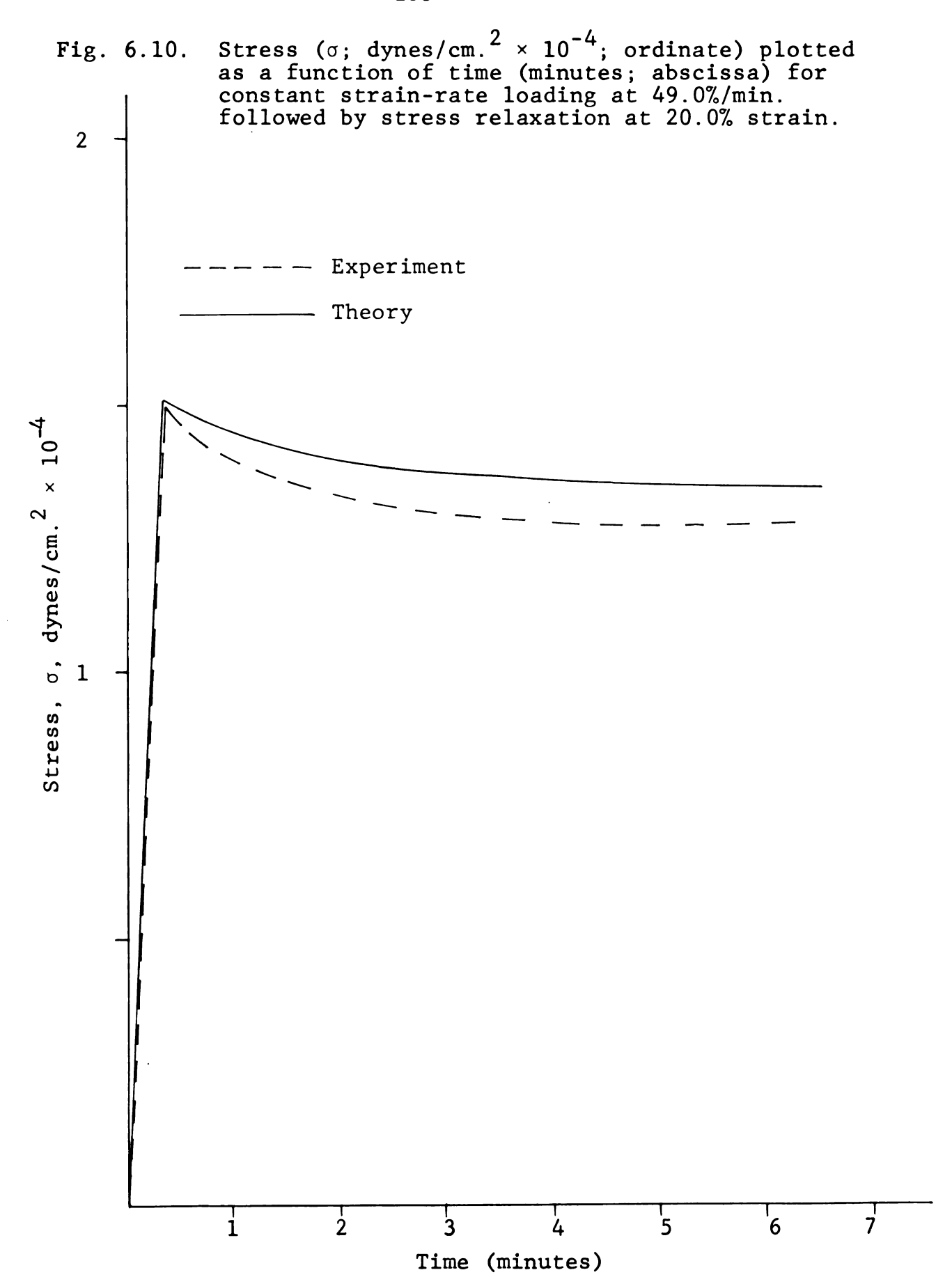








Time (minutes)



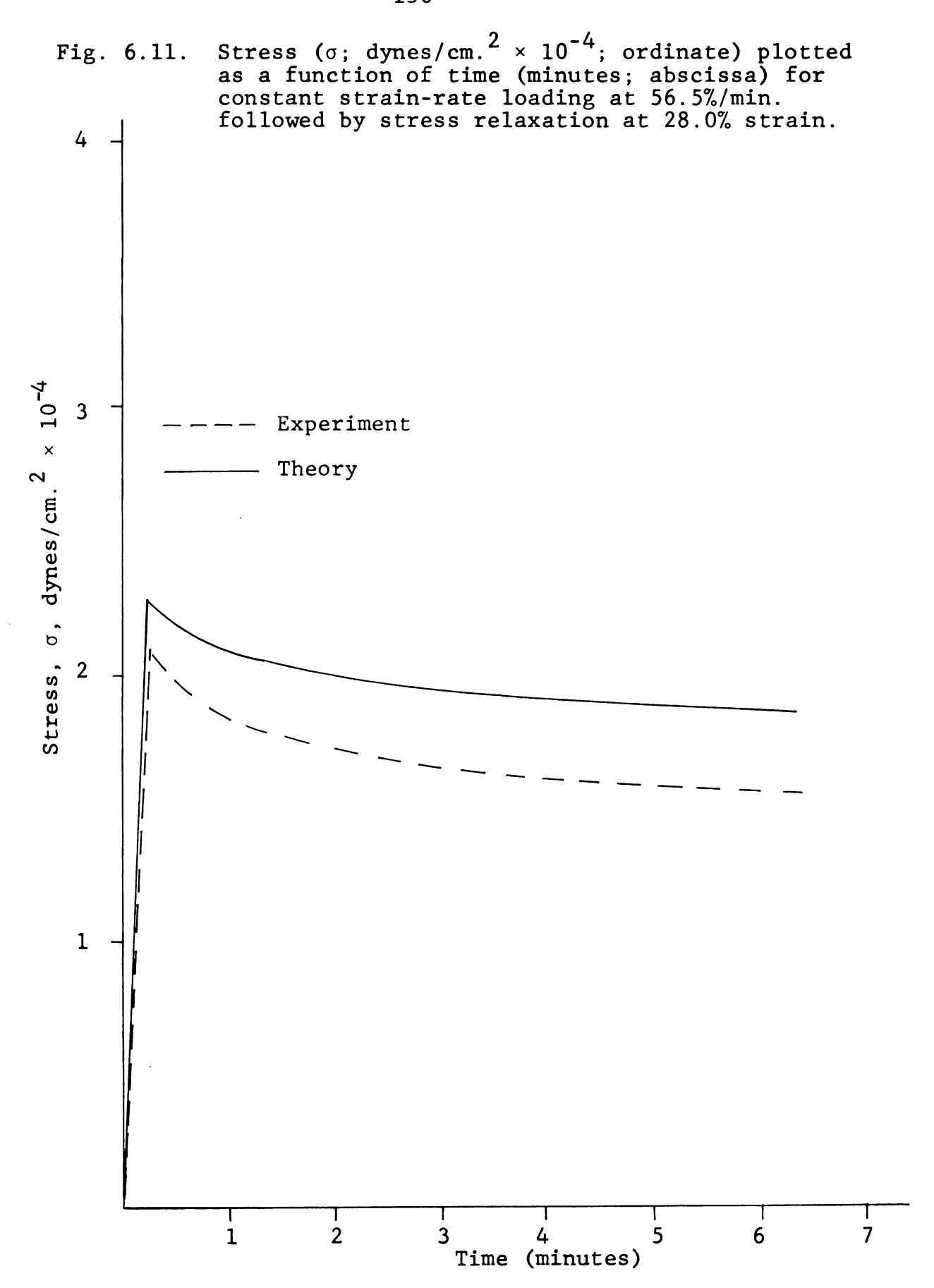
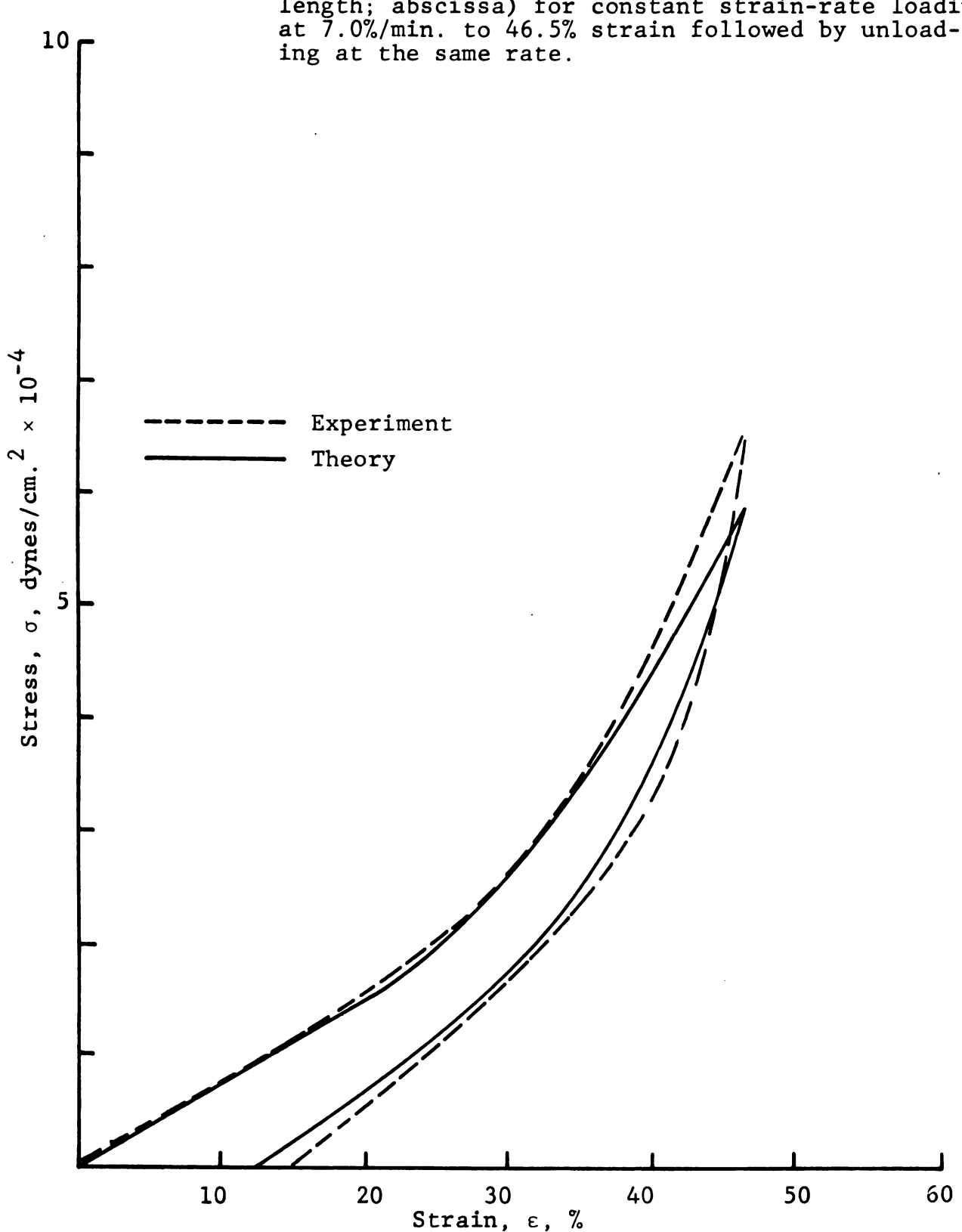


Fig. 6.12. Stress (σ ; dynes/cm. $^2 \times 10^{-4}$; ordinate) plotted as a function of strain (ϵ ; % of deformation/gauge length; abscissa) for constant strain-rate loading at 7.0%/min. to 46.5% strain followed by unloading at the same rate.



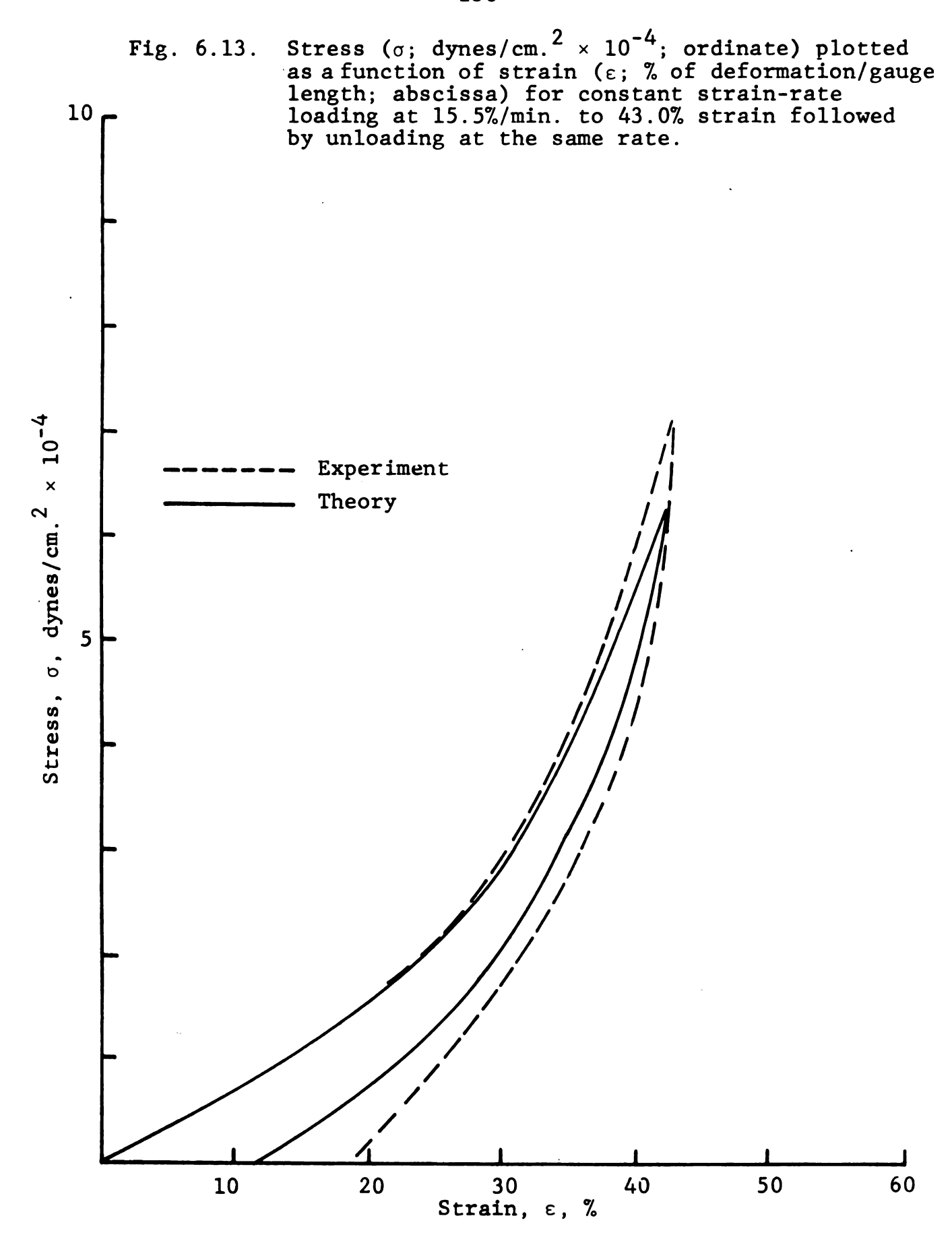


Fig. 6.14. Stress (σ ; dynes/cm. $^2 \times 10^{-4}$; ordinate) plotted as a function of strain (ε ; % of deformation/gauge length; abscissa) for constant strain-rate loading at 35.0%/min. to 46.5% strain followed by unloading at the same rate.

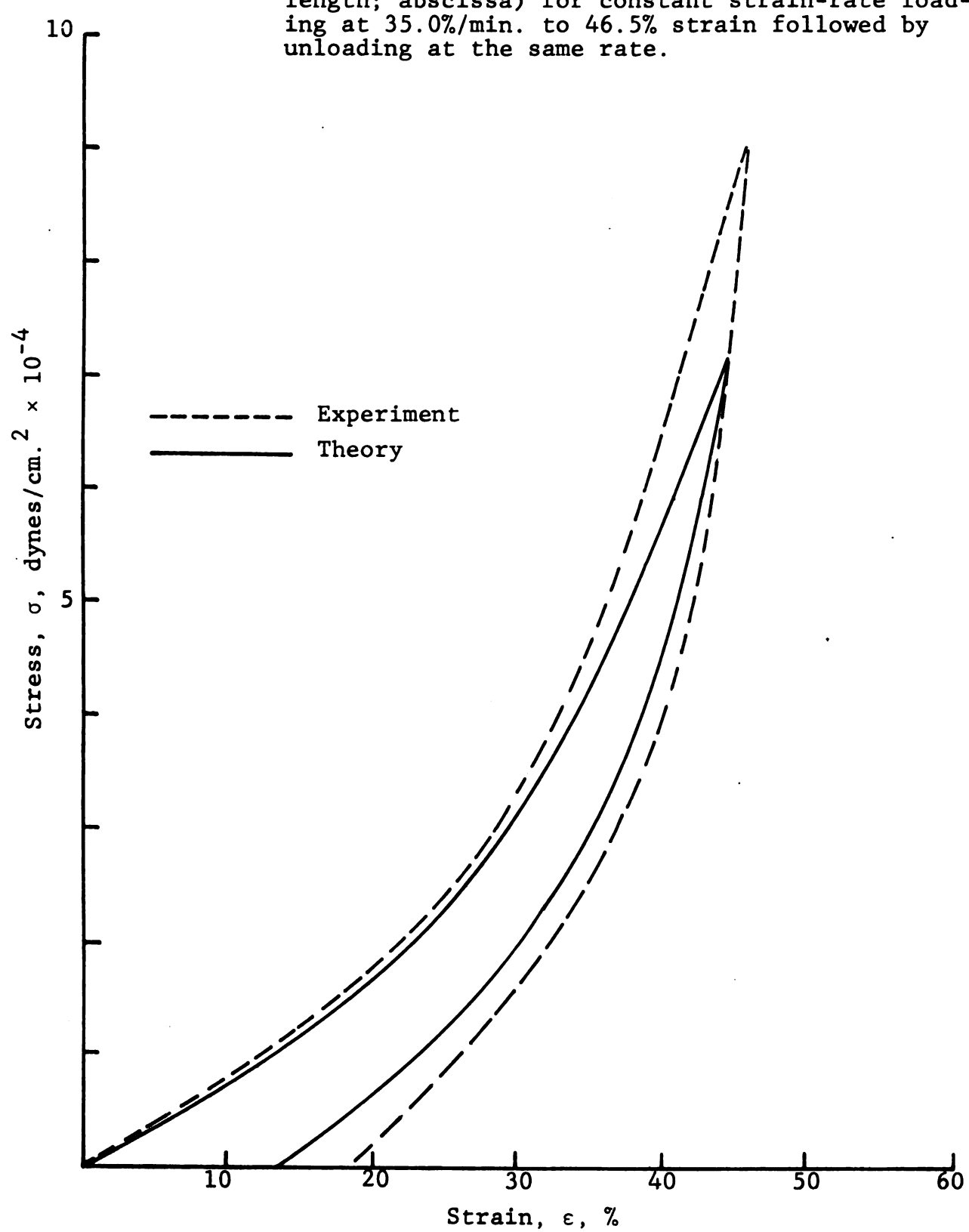


Fig. 6.15. Stress (σ ; dynes/cm. $^2 \times 10^{-4}$; ordinate) plotted as a function of strain (ε ; % of deformation/gauge length; abscissa) for constant strain-rate loading at 65.5%/min. to 48.0% strain followed by unloading at the same rate.

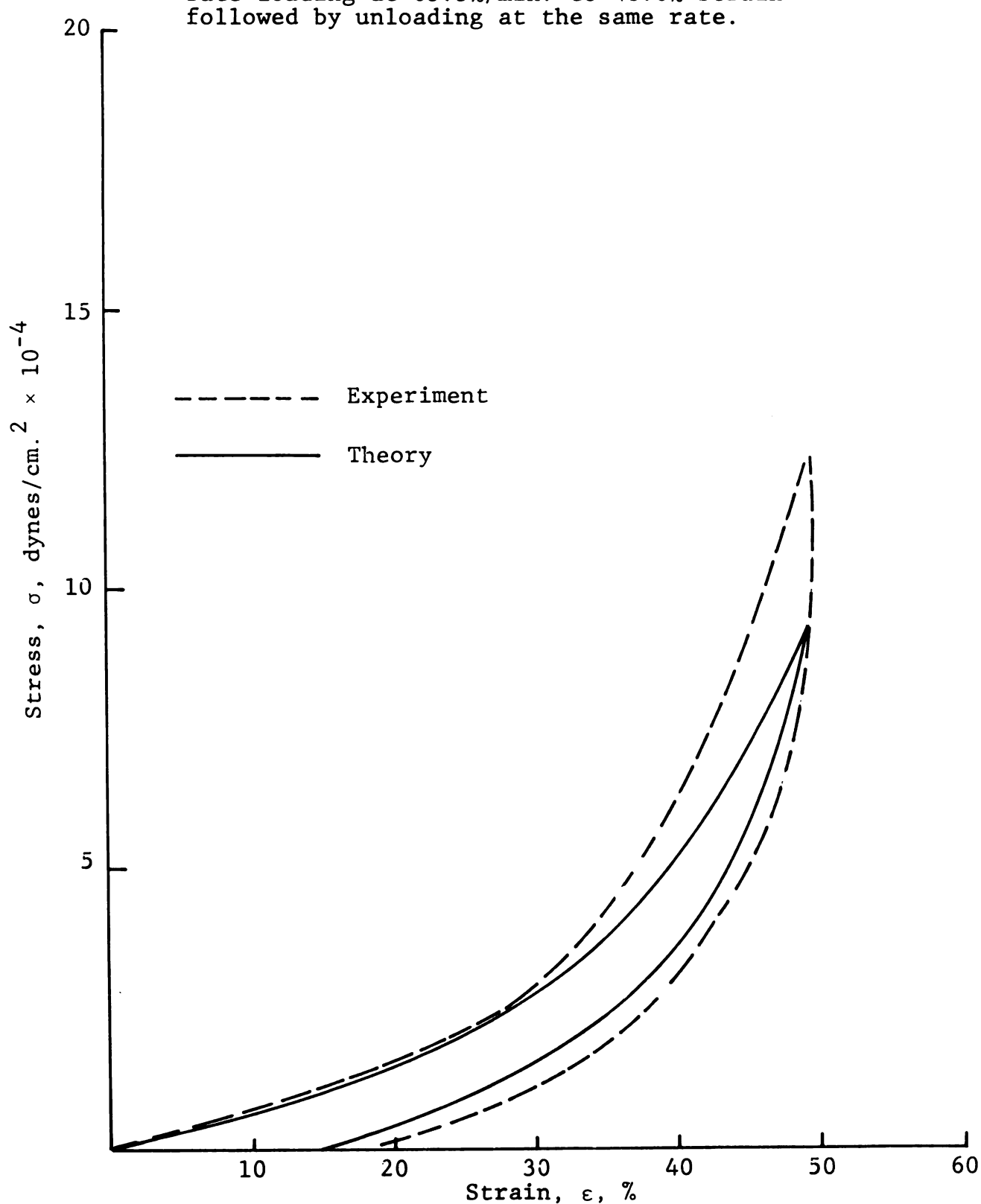


Fig. 6.16. Peak stress (σ_p ; dynes/cm. $^2 \times 10^{-4}$; ordinate) plotted as a pfunction of cycle number (n; abscissa) for positive sinusoidally-varying strains. The frequency of oscillation is 3.0 Rad./min. and the peak strain level is 23.0%. Only the envelopes of the stress cycle number curve are shown.

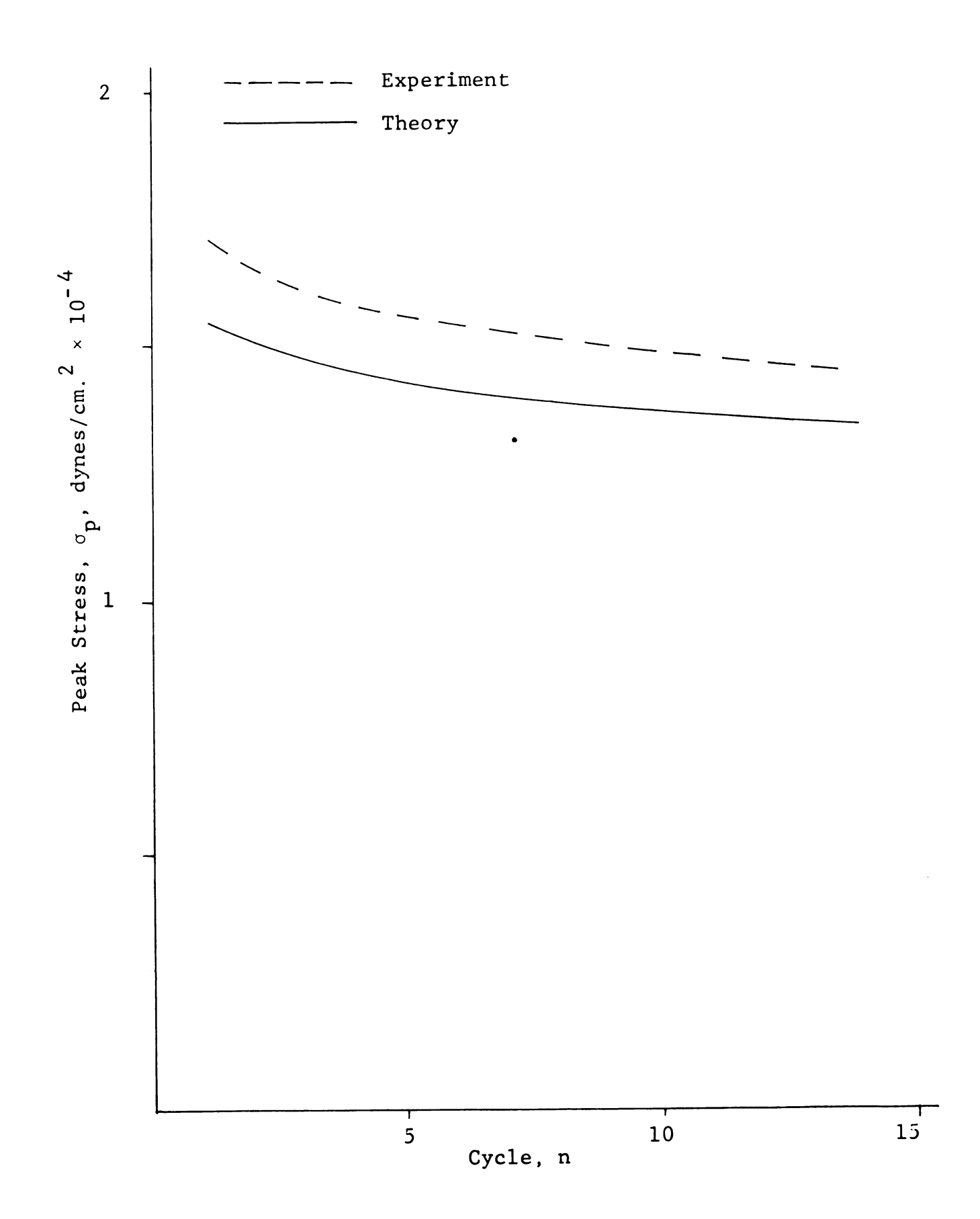


Fig. 6.17. Peak stress (σ_p ; dynes/cm. $^2 \times 10^{-4}$; ordinate) plotted as a pfunction of cycle number (n; abscissa) for positive sinusoidally-varying strains. The frequency of oscillation is 47.0 Rad./min. and the peak strain level is 28.5%. Only the envelopes of the stress-cycle number curve are shown.

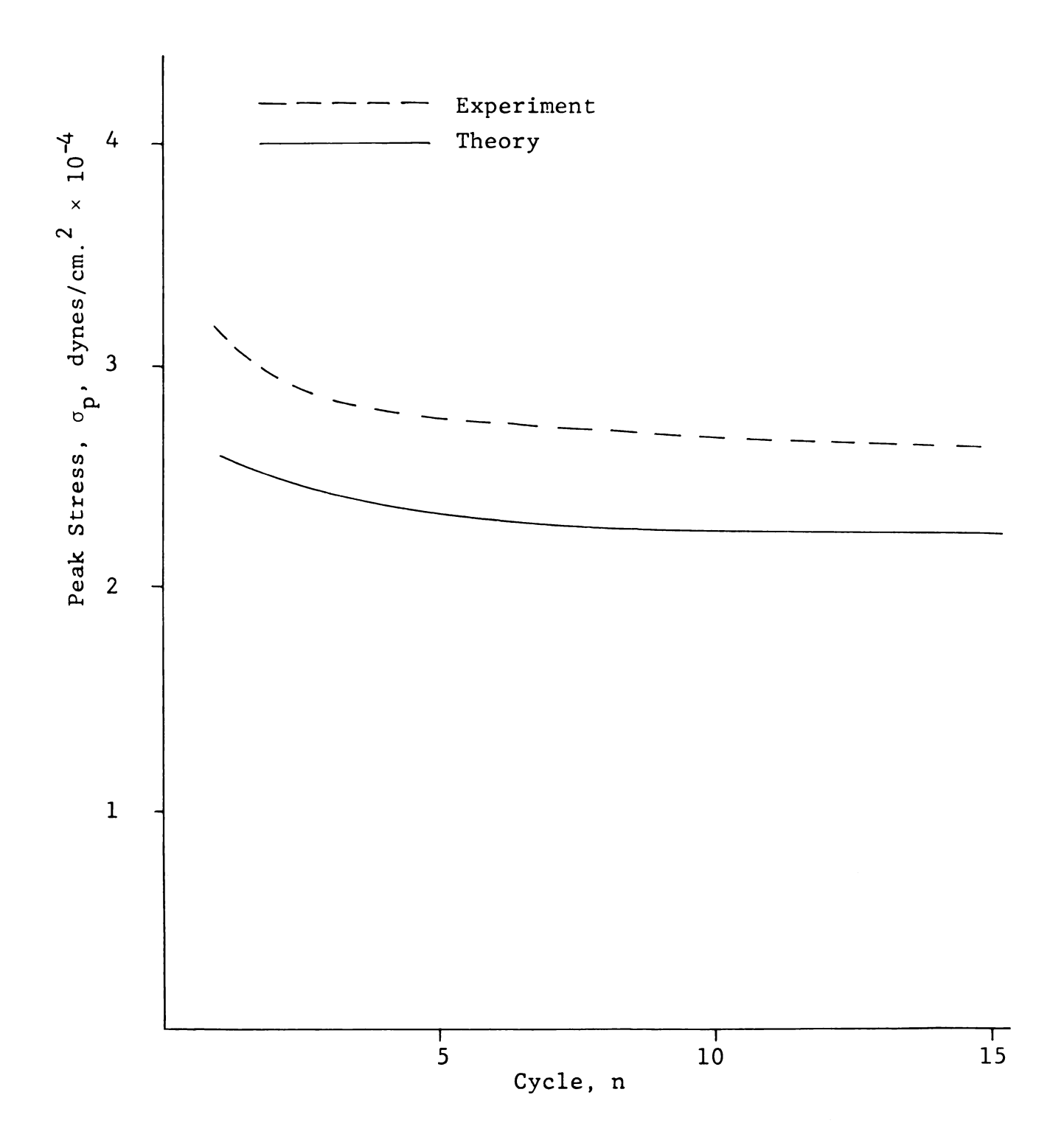
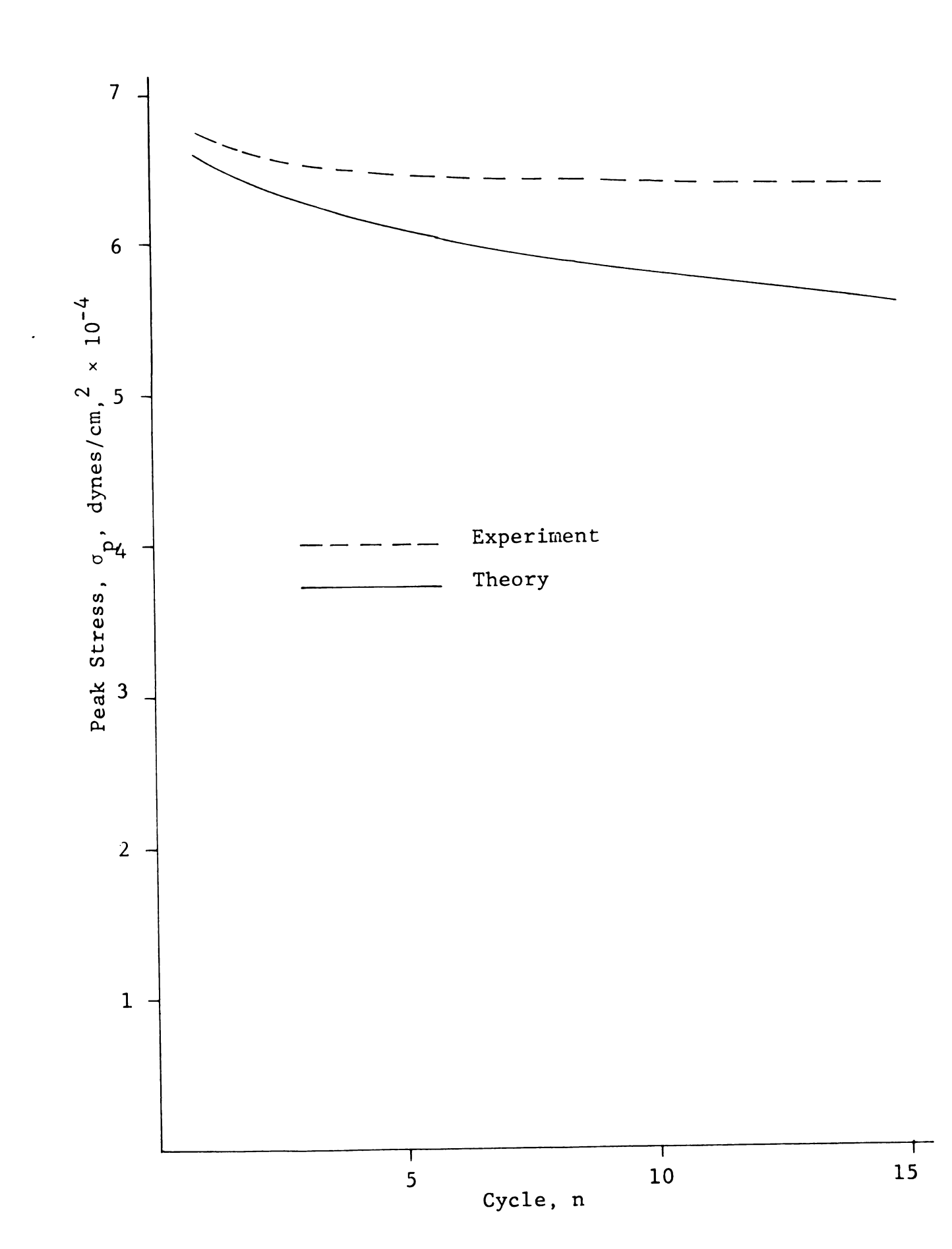
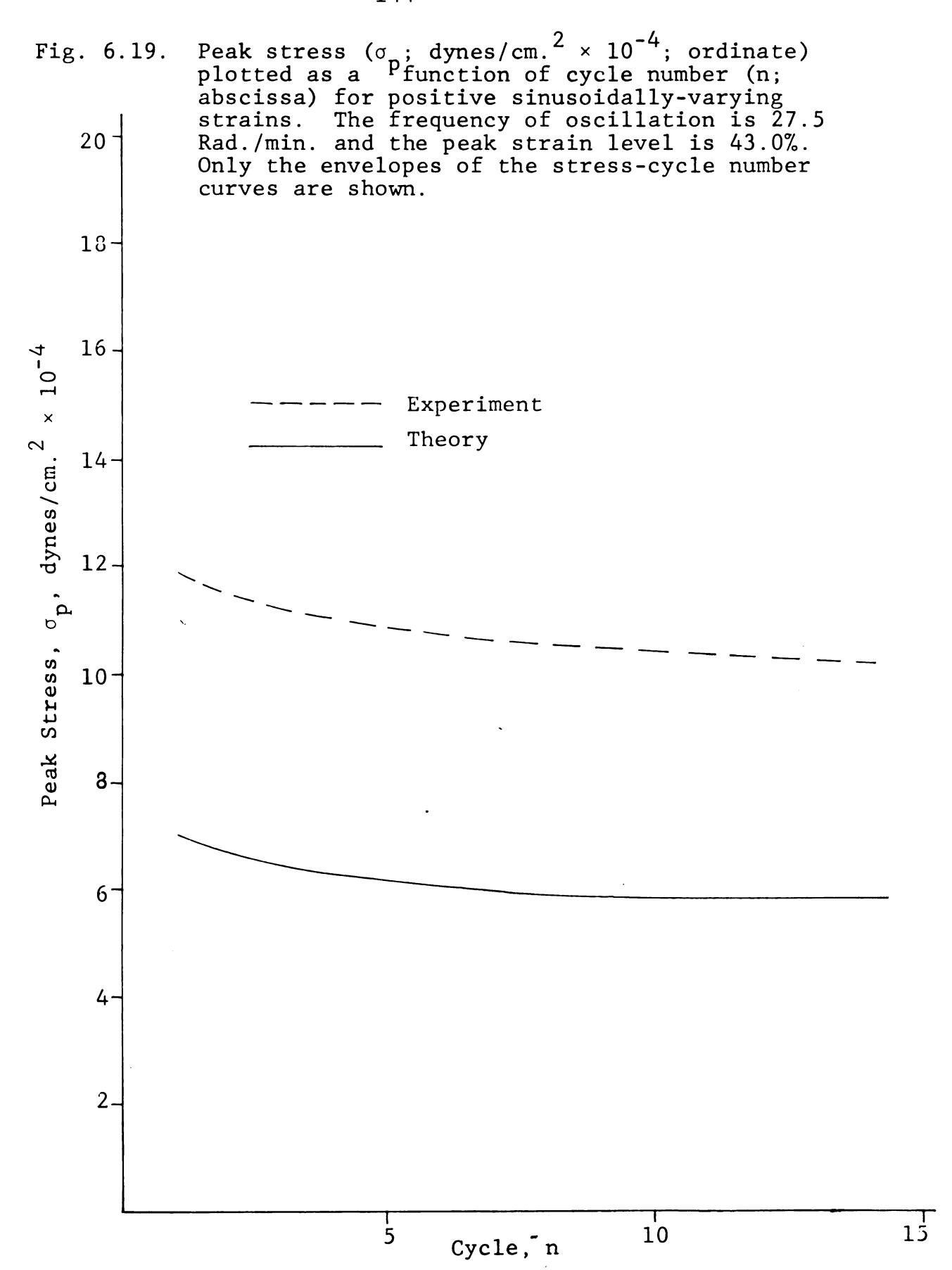


Fig. 6.18. Peak stress (σ_p ; dynes/cm. $^2 \times 10^{-4}$; ordinate) plotted as a function of cycle number (n; abscissa) for positive sinusoidally-varying strains. The frequency of oscillation is 4.0 Rad./min. and the peak strain level is 44.5%. Only the envelopes of the stress-cycle number curve are shown.





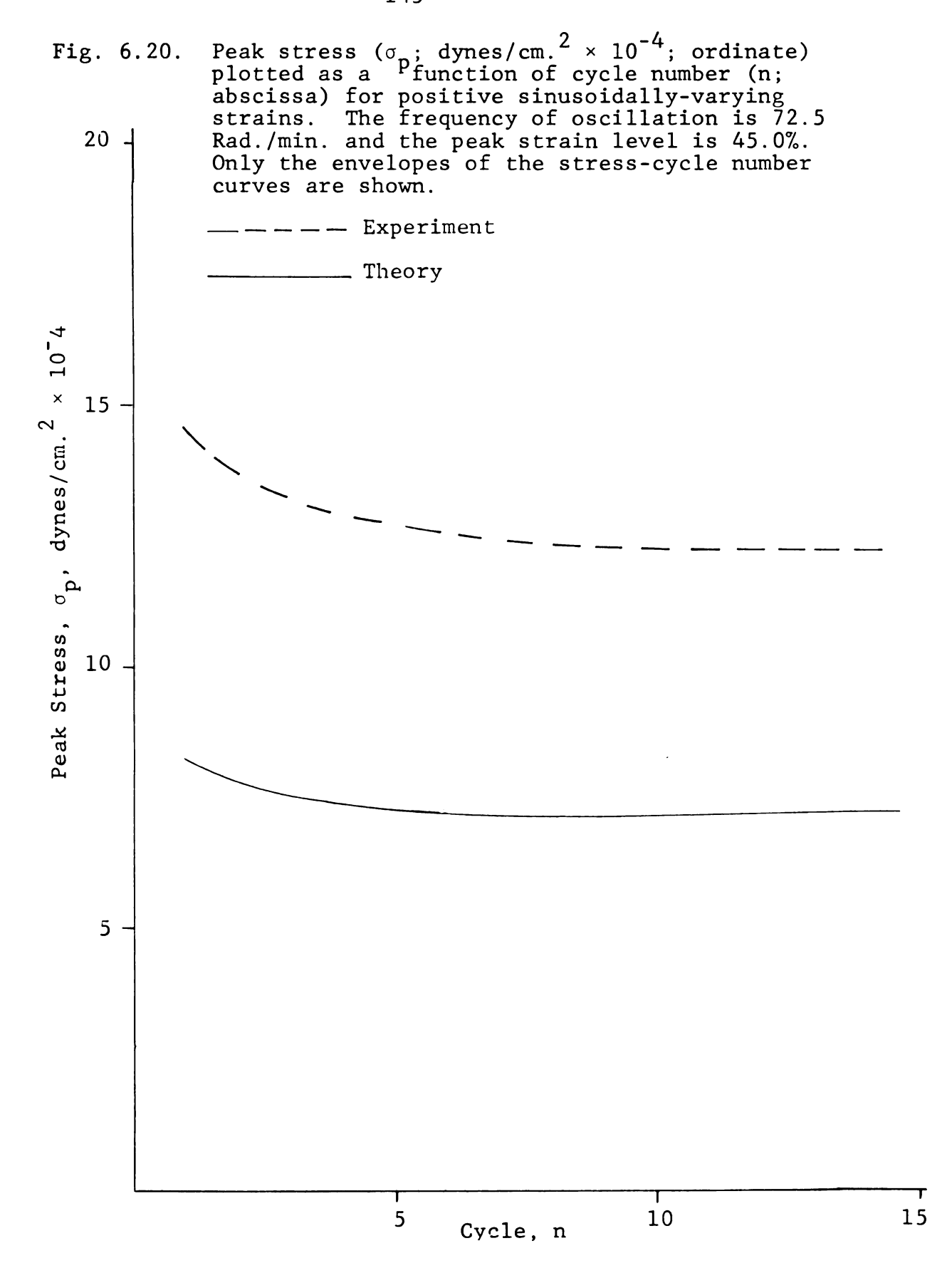


Fig. 6.21. Force (F; grams force; ordinate) plotted as a function of muscle length (cm.; abscissa) for tetanized and unstimulated (passive) muscle. The experimental tetanic curve, constructed point-by-point, is the mean of 8 tests and one standard deviation from the mean is shown for different muscle lengths. The passive experimental curve is shown for comparison.

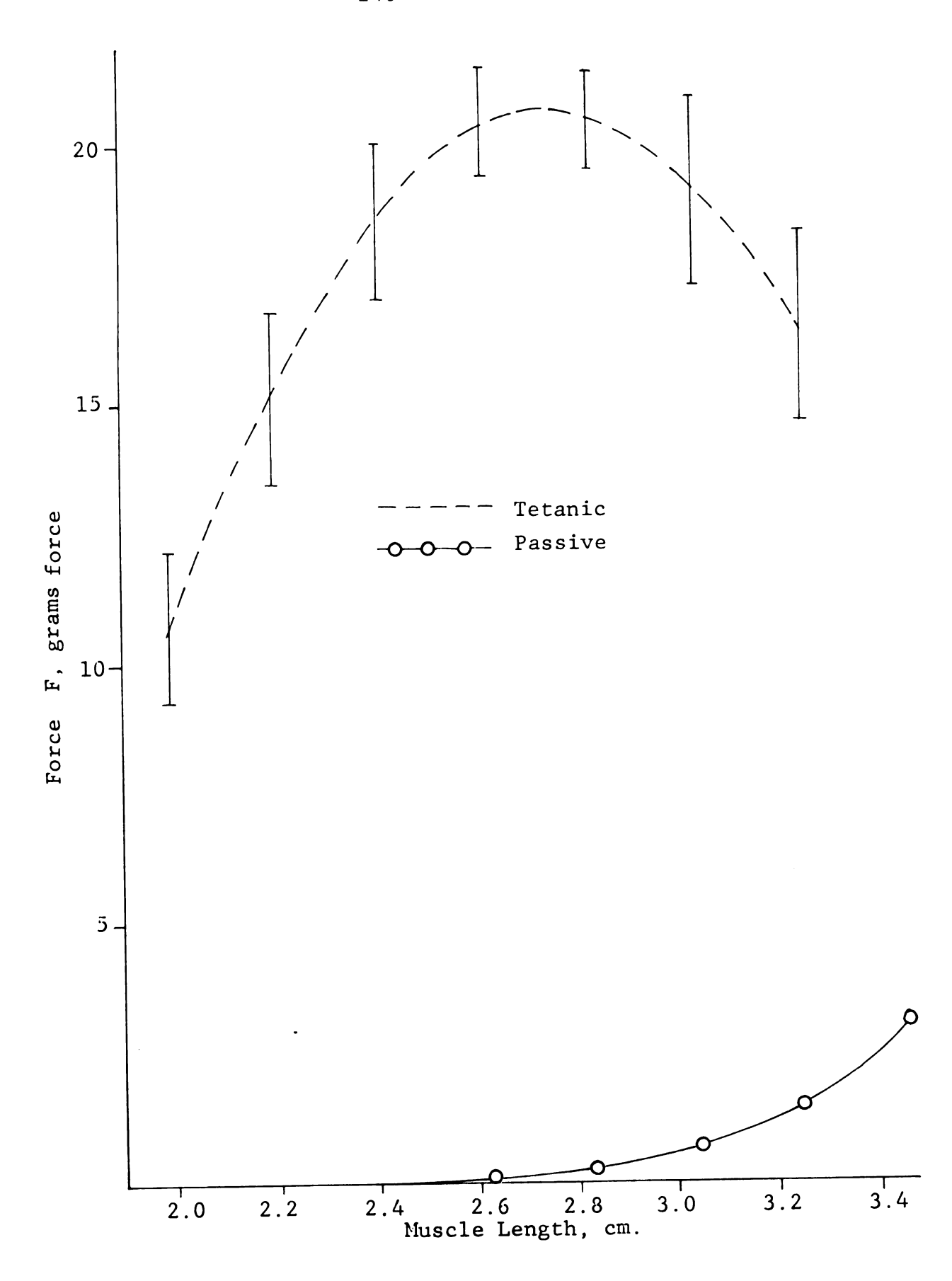
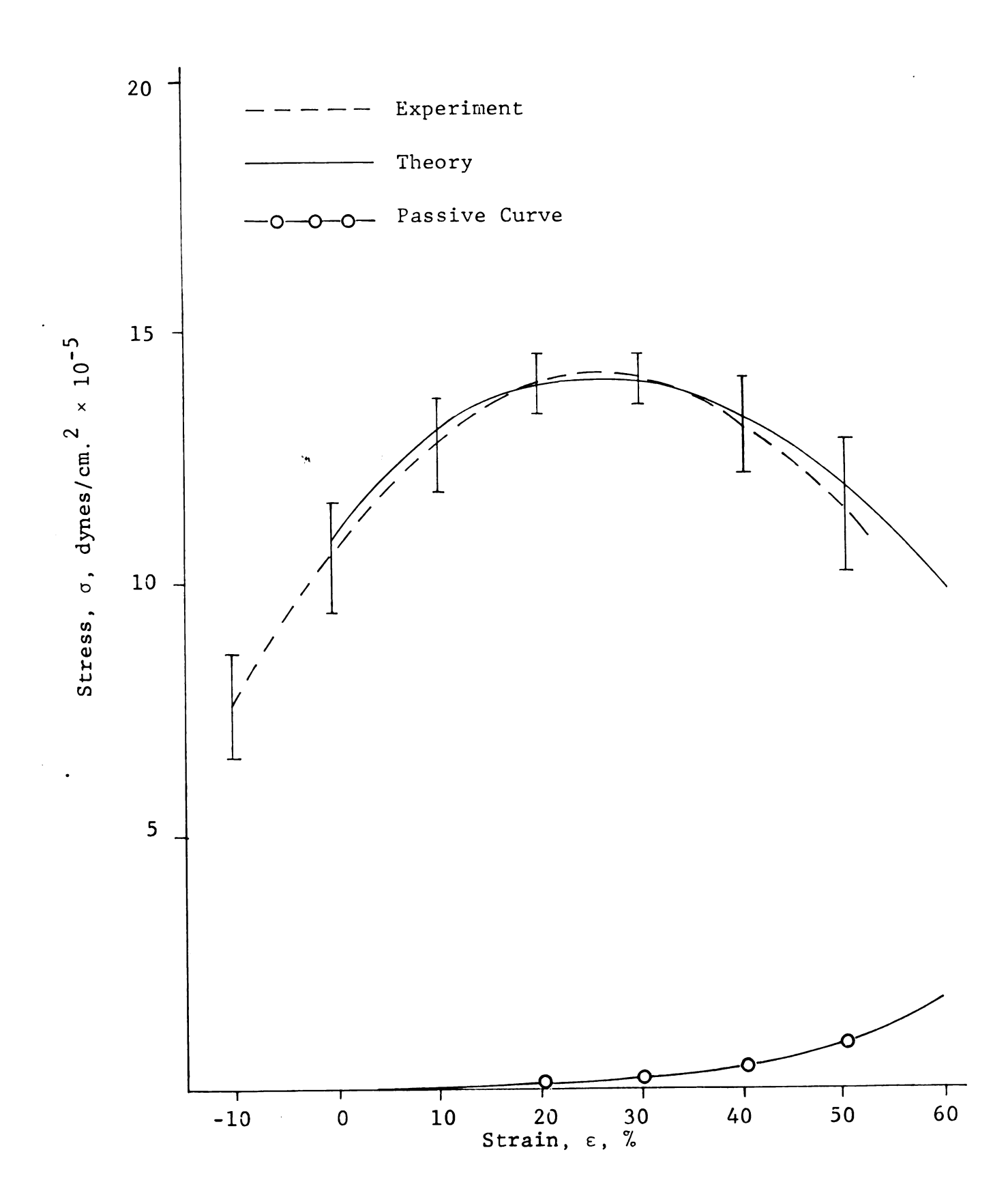


Fig. 6.22. Stress (σ ; dynes/cm. $^2 \times 10^{-5}$; ordinate) plotted as a function of strain (ε ; % of deformation/ gauge length; abscissa) for tetanized and unstimulated (passive) muscle. The experimental tetanic curve is the mean of 8 tests and one standard deviation from the mean is shown for different strain levels. The passive experimental curve is shown for comparison.



CHAPTER VII

CONCLUSIONS

A uniaxial composite constitutive equation was formulated for the anterior gracilis muscle under unstimulated, in vitro conditions and an empirical expression was obtained for the tetanic response of the tissue throughout the passive strain region. From histologic studies on the anterior gracilis muscle, an anatomic model was developed as shown in Figure 5.1. This model and the known response of collagenous tissue were used to derive the constitutive equation for muscle cells. The constitutive equations were then combined using an incremental approach to compute the theoretical stresses and strains in the individual components and the composite tissue.

The anterior gracilis muscle was suitable for testing from both engineering and physiological viewpoints. The uniform cross-sectional area permitted the formulation of the theoretical equations and the determination of experimental stresses. The use of a very thin muscle enabled more muscle fibers to be nourished through passive diffusion.

Histologic studies of cross-sections of the tissue provided ratios of muscle cells to connective tissue and

optical measurements which were made of the muscle in the bath established the ratios of tendon length and muscle cell length to total muscle length. These ratios represented constants in the theoretical equations.

The theoretical equations for the composite tissue were subjected to four passive tests. 1) Constant strainrate tests (Figures 6.2-6.6) showed close agreement between experiment and theory for various strain rates up to 40% composite strain. The experimental linear region at low strain levels was predicted by the equations and the curvature predicted by the equations at higher strain levels was observed in the experimental behavior. 2) Stress relaxation tests (Figures 6.7-6.11) indicated that the general shape of the theoretical curves during the loading and relaxation phases resembled experimental curves though the peak experimental stress levels were not always predicted in theory. For lower peak strain levels, relaxation was often smaller for the theoretical curves and at higher peak strains, good agreement was obtained if the curves were first aligned following the loading phase. 3) Cyclic tests (Figures 6.12-6.15) on anterior gracilis muscle revealed that theoretical hysteresis loops were smaller than experimental loops and greater deviations were observed at higher strain rates and for larger composite strains. Upon unloading, the theoretical curves returned to zero load at larger strain levels than were

observed in the experimental curves. 4) The sinusoidal tests (Figures 6.16-6.20) showed the least agreement between theory and experiment. For peak composite strains above 45%, initial experimental peak stresses were sometimes twice those generated by theory. In addition, less stress decline or fatigue was usually evident in the theoretical results for various strain rates. If the initial peak stresses for experiment and theory were similar, the curves patterned each other quite well for 15-30 cycles. The best agreement was seen for frequencies of oscillation below 20 radians per minute.

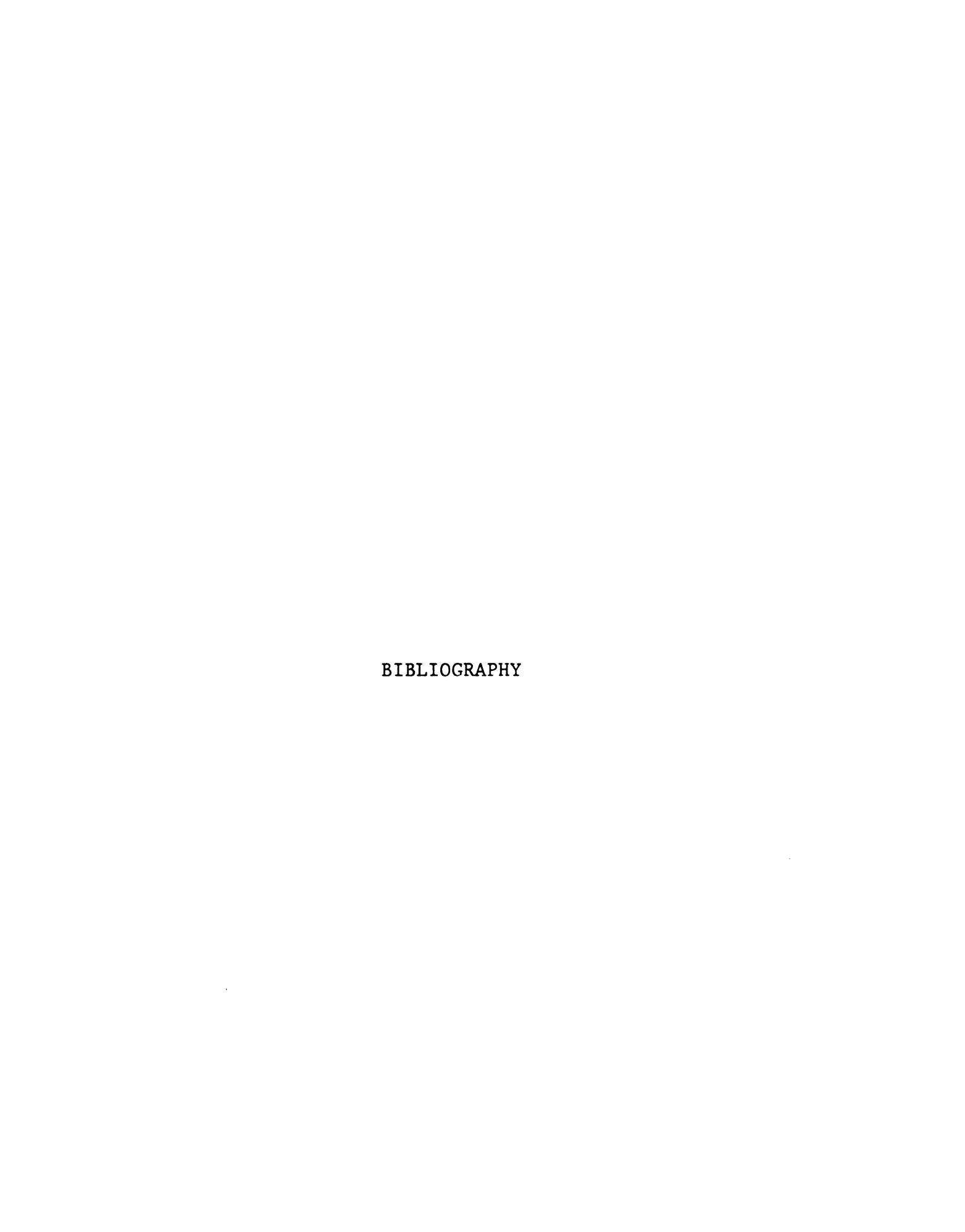
The theoretical equations that have been developed for unstimulated muscle have adequately predicted the experimental results for various passive tests. However, above 40-45% strain in the composite tissue, the theoretical curves did not achieve the stress levels of the experimental The theoretical strains for the tissue components were monitored and a composite strain level of 45% corresponded to only 3-5% strain in the tendon and 10-15% strain in the connective tissue sheath. Haut and Little (53) developed the constitutive equation for collagen fibers assuming small strains of no more than 3-4% and larger strains caused irreversible effects in the fibers. fore, for theory to match experiment in passive tests on composite muscle tissue above 45% strain, the constitutive equation for collagen fibers would have to be changed to account for irreversible effects.

1
1
!
;
ı
1
,

The tetanic tests (Figures 6.21 and 6.22) were made using predetermined parameters of stimulation. The choice of a sinusoidal relationship between the generated active stress and the passive strain provided good agreement for 20-25% strain above and below the resting length. Possibly a quadratic expression would follow the experimental curves as well and provide better agreement at the extremes of the tetanic curve. However, the maximum tetanic stress was found to be approximately 1.41×10^6 dynes/cm. which resembles stress values previously reported in the literature (11, 22, 26, 56, 59). The peak tetanic force for the anterior gracilis in the Wistar rat was found by Bahler (7) to be about 32 gm. while the peak tetanic force in this study was only found to be 21.6 gm. Possibly the variation in the species of rat and differences in the percentages of fiber types accounted for the discrepancy in the tension. tetanic stresses must first be obtained for the fast-twitch and slow-twitch fibers before an attempt can be made to compare the findings or show how these forces are distributed in the heterogeneous muscle. However the reproducibility in the tetanic tension values in this study for two to three hours indicated that the muscle was not undergoing significant deterioration.

Future tests that are performed on skeletal muscle might focus upon the variation of parameters such as temperature, pH, and the content of the nutrient bath. It

would be informative to conduct experiments on in vivo muscle to determine values of tetanic tension. The muscle could be tested for longer time periods in the living animal because the blood supply would be intact and direct stimulation could be employed. However a method would have to be developed to accurately determine changes in muscle length during the unstimulated tests.



BIBLIOGRAPHY

- 1. Abbott, B.C. and Lowy, J. "Stress Relaxation in Muscle," Proceedings of the Royal Society of London, Ser. B., Vol. 146, 1957, pp. 281-288.
- 2. Abbott, B.C. and Wilkie, D.R. "The Relationship between Velocity of Shortening and the Tension-Length Curve of Skeletal Muscle," Journal of Physiology (London), Vol. 120, 1953, pp. 214-223.
- 3. Abbott, B.C. "Muscle Mechanics," <u>Biomechanics</u>: <u>Its</u>
 <u>Foundations and Objectives</u>, Y.C.B. Fung, N. Perrone
 and M. Anliker, eds. New Jersey: Prentice-Hall,
 1972, pp. 209-215.
- 4. Abramowitz, M. and Segun, I.A. <u>Handbook of Mathematical Functions</u>, New York: <u>Dover Publications</u>, Inc., 1964.
- 5. Apter, J.A. and Graessley, W.W. "A Physical Model for Muscular Behavior," <u>Biophysical Journal</u>, Vol. 10, 1970, pp. 539-555.
- 6. Aubert, X., Roquet, M.L. and Van der Elst, J. "The Tension-Length Diagram of the Frog's Sartorius Muscle," Archives Internationales de Physiologie et de Biochimie, Vol. 59, 1951, pp. 239-241.
- 7. Bahler, A.S. "A Quantitative Investigation into the Dynamics of an <u>In Vitro</u> Mammalian Muscle." Unpublished Ph.D. dissertation, The Johns Hopkins University, 1966.
- 8. Bahler, A.S. "The Series Elastic Element of Mammalian Skeletal Muscle," American Journal of Physiology, Vol. 213, 1967, pp. 1560-1564.
- 9. Bahler, A.S. "Modeling of Mammalian Skeletal Muscle," <u>IEEE Transactions on Bio-Medical Engineering</u>, Vol. <u>BME-15, No. 4, 1968, pp. 249-257.</u>
- 10. Bahler, A.S., Fales, J.T. and Zierler, K.L. "The Active State of Mammalian Skeletal Muscle," <u>Journal of General Physiology</u>, Vol. 50, 1967, pp. 2239-2253.

- 11. Bahler, A.S., Fales, J.T. and Zierler, K.L. "The Dynamic Properties of Mammalian Skeletal Muscle," Journal of Clinical Physiology, Vol. 51, 1968, pp. 369-384.
- 12. Barany, M. and Close, R.I. "The Transformation of Myosin in Cross-innervated Rat Muscles," J. Physiol. (London), Vol. 213, 1971, pp. 455-474.
- 13. Barnard, R.J., Edgerton, V.R. and Peter, J.B. "Effect of Exercise on Skeletal Muscle. I. Biochemical and Histochemical Properties," J. of Applied Physiol., Vol. 28, 1970, pp. 762-766.
- 14. Barnard, R.J., Edgerton, V.R. and Peter, J.B. "Effect of Exercise on Skeletal Muscle. II. Contractile Properties," J. of Applied Physiol., Vol. 28, 1970, pp. 767-770.
- 15. Barnard, R.J., Edgerton, V.R., Furukawa, T. and Peter, J.B. "Histochemical, Biochemical and Contractile Properties of Red, White and Intermediate Fibers," Amer. J. Physiol., Vol. 220, 1971, pp. 410-414.
- 16. Blatz, P.L., Chu, B.M. and Wayland, H. "On the Mechanical Behavior of Elastic Animal Tissue," <u>Trans. Soc. Rheology</u>, Vol. 13, 1969, pp. 83-102.
- 17. Bloom, W. and Fawcett, D.W. A Textbook of Histology, Philadelphia: W.B. Saunders Co., Ninth Edition, 1968.
- 18. Buchthal, F., Kaiser, E. and Rosenfalck, P. "The Rheology of the Cross-striated Muscle Fiber with Particular Reference to Isotonic Conditions," <u>Dan. Biol. Medd.</u>, Vol. 21, 1951, pp. 1-318.
- 19. Buchthal, F. and Rosenfalck, P. "Elastic Properties of Striated Muscle," <u>Tissue Elasticity</u>, J.W. Remington, ed. Washington, D.C.: Amer. Physiol. Society, 1957, pp. 73-93.
- 20. Buller, A.J., Eccles, J.C. and Eccles, R.M. "Interactions between Motoneurons and Muscles in Respect of the Characteristic Speeds of their Responses," J. Physiol. (London), Vol. 150, 1960, pp. 417-439.
- 21. Carlson, F.D. "Kinematic Studies on Mechanical Properties of Muscle," <u>Tissue Elasticity</u>, J.W. Remington, ed. Washington, D.C.: Amer. Physiol. Society, 1957, pp. 55-72.

- 22. Casella, C. "Tensile Force in Total Striated Muscle, Isolated Fiber and Sarcolemma," Acta Physiol. Scandinav., Vol. 21, 1951, pp. 380-401.
- 23. Close, R.I. "Dynamic Properties of Fast and Slow Skeletal Muscles of Mammals," Exploratory Concepts in Muscular Dystrophy and Related Disorders, A. Milhorat, ed. Amsterdam: Exerpta Medica Foundation, 1967, pp. 142-149.
- 24. Close, R.I. "Neural Influences on Physiological Properties of Fast and Slow Limb Muscles,"

 Contractility of Muscle Cells and Related Processes,
 J. Podolsky, ed. Englewood Cliffs, N.J.: Prentice Hall, 1971, pp. 175-188.
- 25. Close, R.I. "Dynamic Properties of Mammalian Skeletal Muscles," <u>Physiological Reviews</u>, Vol. 52, 1972, pp. 129-197.
- 26. Close, R.I. and Hoh, J.F.Y. "Influence of Temperature on Isometric Contractions of Rat Skeletal Muscles," <u>Nature</u>, Vol. 217, 1968, pp. 1179-1180.
- 27. Cullingham, P.J., Lind, A.R. and Morton, R.J. "The Maximal Isometric Tetanic Tensions Developed by Mammalian Muscle, In Situ, at Different Temperatures," Quar. J. of Exptal. Physiology, Vol. 45, 1960, pp. 142-156.
- 28. DeFiore, M.S.H. Atlas of Human Histology, Philadelphia: Lea and Febringer, Third Edition, 1967.
- 29. Dreizen, P. and Gershman, L.C. "Relationship of Structure to Function in Myosin. II. Salt Denaturation and Recombination Experiments," <u>Biochemistry</u>, Vol. 9, 1970, pp. 1688-1693.
- 30. Ebashi, S., Endo, M. and Ohtsuki, I. "Control of Muscle Contraction," Quart. Rev. Biophys., Vol. 2, 1969, pp. 351-384.
- 31. Eccles, J.C., Eccles, R.M. and Lundberg, A. "The Action Potentials of the Alpha Motoneurons Supplying Fast and Slow Muscles," J. Physiol. (London), Vol. 142, 1958, pp. 275-291.
- 32. Eccles, J.C., Eccles, R.M. and Kozak, W. "Further Investigations on the Influence of Motoneurones on the Speed of Muscle Contraction," J. Physiol. (London), Vol. 163, 1962, pp. 324-339.

- 33. Eccles, J.C. "The Effects of Nerve Cross-Union on Muscular Contraction," Exploratory Concepts in Muscular Dystrophy and Related Disorders, A Milhorat, ed. Amsterdam: Exerpta Med. Foundation, 1967, pp. 151-160.
- 34. Edgerton, V.R., Gerchman, L. and Carrow, R. "Histochemical Changes in Rat Skeletal Muscle after Exercise," Exptl. Neurol., Vol. 24, 1969, pp. 110-123.
- 35. Elliott, D.H. and Crawford, G.N.C. "The Thickness and Collagen Content of Tendon Relative to the Cross-Sectional Area of Muscle During Growth," Proc. Roy. Soc. (London), Ser. B., Vol. 162, 1965, pp. 198-202.
- 36. Evans, C.L. and Hill, A.V. "The Relation of Length to Tension Development and Heat Production on Contraction in Muscle," J. of Physiology, Vol. 49, 1914-15, pp. 10-16.
- 37. Fenn, W.O. and Marsh, B.S. "Muscular Force at Different Speeds of Shortening," J. of Physiol. (London), Vol. 85, 1935, pp. 277-297.
- 38. Fex, S. "'Trophic' Influence of Implanted Fast Nerve on Innervated Slow Muscle," Physiol. Bohemoslavaca, Vol. 18, 1969, pp. 205-208.
- 39. Fung, Y.C.B. "Elasticity of Soft Tissues in Simple Elongation," Amer. J. Physiology, Vol. 213, 1967, pp. 1532-1544.
- 40. Fung, Y.C.B. "Mathematical Representation of Mechanical Properties of Heart Muscle," J. Biomechanics, Vol. 3, 1970, pp. 381-404.
- 41. Fung, Y.C. "Comparison of Different Models of the Heart Muscle," J. Biomechanics, Vol. 4, 1971, pp. 289-295.
- 42. Fung, Y.C. "Stress-Strain-History Relations of Soft Tissues in Simple Elongation," Biomechanics: Its Foundations and Objectives, Y.C. Fung, N. Perrone and M. Anliker, eds. New Jersey: Prentice-Hall, 1972, pp. 181-208.
- 43. Ganong, W.F. Review of Medical Physiology, Los Altos, Calif.: Lange Medical Publications, Fifth Edition, 1971.
- 44. Gasser, H.S. and Hill, A.V. "The Dynamics of Muscular Contraction," Proc. Royal Soc., Series B, Vol. 96, 1924, pp. 398-437.

- 45. Geffen, L.B. "Optimum Length for Contraction of Rat Circulated Limb Muscles," Archives Internationales de Physiologie et de Biochimie, Vol. 72, 1964, pp. 825-834.
- 46. Glantz, S.A. "A Constitutive Equation for the Passive Properties of Muscle," J. Biomechanics, Vol. 7, 1974, pp. 137-145.
- 47. Goldspink, G. and Rowe, R.W.D. "Studies on Postembryonic Growth and Development of Skeletal Muscle. II. Some Physiological and Structural Changes that are Associated with Growth and Development of Skeletal Muscle Fibers," Proc. Roy. Irish Acad., Sect. B, Vol. 66, 1968, pp. 85-99.
- 48. Goldspink, G. "The Proliferation of Myofibrils During Muscle Fiber Growth," J. Cell Science, Vol. 6, 1970, pp. 593-604.
- 49. Greene, E.C. Anatomy of the Rat, Philadelphia: The American Philosophical Society, 1935.
- 50. Ham, A.W. Histology, Philadelphia: J.B. Lippincott Co., Sixth Edition, 1969.
- 51. Hanson, J. and Huxley, H.E. "The Molecular Basis of Contraction in Cross-Striated Muscles," The Structure and Function of Muscle, Vol. 1, G.H. Bourne, ed. New York: Academic Press, Inc., 1960, pp. 183-227.
- 52. Haut, R.C. "A Constitutive Equation for Collagen Fibers." Unpublished Ph.D. dissertation, Michigan State University, 1971.
- 53. Haut, R.C. and Little, R.W. "A Constitutive Equation for Collagen Fibers," J. <u>Biomechanics</u>, Vol. 5, 1972, pp. 423-430.
- 54. Hill, A.V. and Hartree, W. "The Thermo-elastic Properties of Muscle," <u>Philosophical Transactions of the Royal Society of London</u>, Series B., Vol. 210, 1920, pp. 153-173.
- 55. Hill, A.V. "The Maximum Work and Mechanical Efficiency of Human Muscles and Their Most Economical Speed,"

 J. of Physiology, Vol. 56, 1922, pp. 19-41.
- 56. Hill, A.V. "The Heat of Shortening and the Dynamic Constants of Muscle," Proc. of the Royal Society, Series B, Vol. 126, 1938, pp. 136-195.

- 57. Hill, A.V. "The Abrupt Transition from Rest to Activity in Muscle," Proc. Royal Soc., Series B, Vol. 136, 1949, pp. 399-420.
- 58. Hill, A.V. "The Series Elastic Component of Muscle," <u>Proc. Royal</u> <u>Soc.</u>, Series B, Vol. 137, 1950, pp. <u>273-280</u>.
- 59. Hill, A.V. "The Mechanics of Active Muscle," Proc. Royal Soc., Series B, Vol. 141, 1953, pp. 104-117.
- 60. Hoffman, B.F., Bassett, A.L. and Bartelstone, H.J.
 "Some Mechanical Properties of Isolated Mammalian
 Cardiac Muscle," <u>Circulation</u> <u>Research</u>, Vol. 23,
 1968, pp. 219-312.
- 61. Jenkins, R.B. "A Constitutive Equation for Parallel-Fibered Elastic Tissue." Unpublished Ph.D. dissertation, Michigan State University, 1973.
- 62. Jenkins, R.B. and Little, R.W. "A Constitutive Equation for Parallel-Fibered Elastic Tissue," J. Biomechanics, Vol. 7, 1974, pp. 397-402.
- 63. Jewell, B.R. and Wilkie, D.R. "An Analysis of the Mechanical Components in Frog's Striated Muscle,"

 J. of Physiology, Vol. 143, 1958, pp. 515-540.
- 64. King, A.L. and Lawton, R.W. "Elasticity of Body Tissues," Medical Physics, Vol. II, O. Glasser, ed. Chicago: Year Book Publishing Inc., 1950, pp. 303-316.
- 65. Leeson, T.S. and Leeson, C.R. <u>Histology</u>, Philadelphia: W.B. Saunders Co., Second Edition, 1970.
- 66. Levin, A. and Wyman, J. "The Viscous Elastic Properties of Muscle," Proc. Royal Soc., Series B, Vol. 101, 1927, pp. 218-243.
- 67. Luna, L.G. (ed.) Manual of Histologic Staining Methods of the Armed Forces Institute of Pathology, New York: McGraw Hill Book Co., Third Edition, 1968.
- 68. Muir, A.R. "The Growth of Muscle and the Differentiation into Fibre Types," Scoliosis and Muscle, P.A. Zorab, ed. Philadelphia: J.B. Lippincott Co., 1974, pp. 14-23.
- 69. Nubar, Y. "Stress-Strain Relationships in Skeletal Muscle," Annals of the New York Academy of Sciences, Vol. 93, 1962, pp. 857-876.

- 70. Parmley, W.W., Brutsaert, D.L. and Sonnenblick, E.H. "Effects of Altered Loading on Contractile Events in Isolated Cat Papillary Muscle," Circulation Research, Vol. 24, 1969, pp. 521-532.
- 71. Peter, J.B. "Skeletal Muscle: Diversity and Mutability of its Histochemical, Electron Microscopic, Biochemical, and Physiologic Properties," The Striated Muscle, C.M. Pearson and F.K. Mostofi, eds. Baltimore: The Williams and Wilkins Co., 1973, pp. 1-18.
- 72. Rack, P.M.H. "The Behavior of a Mammalian Muscle during Sinusoidal Stretching," J. of Physiology, Vol. 183, 1966, pp. 1-14.
- 73. Rack, P.M.H. and Westbury, D.R. "The Effects of Length and Stimulus Rate on Tension in the Isometric Cat Soleus Muscle," J. of Physiology, Vol. 204, 1969, pp. 443-460.
- 74. Rhodin, J.A.G. <u>Histology</u>, <u>A Text and Atlas</u>, New York: Oxford University Press, 1974.
- 75. Rosenblueth, A., Alanis, J. and Rubio, R. "A Comparative Study of the Isometric and Isotonic Contractions of Striated Muscles," Archives Internationales de Physiologie et de Biochimie, Vol. 66, 1958, pp. 330-352.
- 76. Rosenblueth, A., Alanis, J. and Rubio, R. "The Influence of Initial Load and Length on the Amplitude of Muscular Contraction," Archives Internationales de Physiologie et de Biochimie, Vol. 66, 1958, pp. 354-372.
- 77. Schottelius, B.A. and Senay, L.C., Jr. "Effect of Stimulation-Length Sequence on Shape of Length-Tension Diagram," Amer. J. of Physiol., Vol. 186, 1956, pp. 127-130.
- 78. Somylo, A.P. and Somylo, A.V. "Vascular Smooth Muscle.
 I. Normal Structure, Pathology, Biochemistry and
 Biophysics," <u>Pharmacological</u> <u>Reviews</u>, Vol. 20, 1968,
 pp. 197-272.
- 79. Sonnenblick, E.H. "Series Elastic and Contractile Elements in Heart Muscle: Changes in Muscle Length," Amer. J. Physiol., Vol. 207, 1964, pp. 1330-1338.

- 80. Sonnenblick, E.H., Braunwald, E. and Morrow, A.G.
 "The Contractile Properties of Human Heart Muscle:
 Studies on Myocardial Mechanics of Surgically Excised
 Papillary Muscles," J. of Clinical Investigation,
 Vol. 44, 1965, pp. 966-977.
- 81. Tuttle, W.W. and Schottelius, B.A. <u>Textbook of Physiology</u>, St. Louis: C.V. Mosby Co., 1969.
- 82. Walker, S.M. and Thomas, A.G. "Changes in Twitch Tension Induced by Quick Stretch and Stress Relaxation," Amer. J. Physiol., Vol. 198, 1960, pp. 523-527.
- 83. Walker, W.F., Jr. <u>Dissection of the Rat, Laboratory Studies in Biology</u>, Series 840 and 841, San Francisco: W.H. Freeman and Co., 1970.
- 84. Weibel, E.R. and Elias, H. "Introduction to Stereologic Techniques," Quantitative Methods in Morphology, E.R. Weibel and H. Elias, eds. Berlin: Springer-Verlag, 1967, pp. 89-98.
- 85. Wilkie, D.R. "Measurement of the Series Elastic Component at Various Times During a Single Muscle Twitch," J. Physiol. (London), Vol. 134, 1956, pp. 527-530.



APPENDIX A

METHOD FOR NEURAL STIMULATION OF THE IN VITRO ANTERIOR GRACILIS MUSCLE

Principle:

In order to generate contractile muscle force, the in vitro anterior gracilis muscle can be stimulated by a variety of methods including direct electrical stimulation of the nerve trunk segment.

Equipment:

A suction electrode was designed with the assistance of Drs. Pax and Drewes of the Physiology Department. A drawing of the electrode appears in Figure A.1. Glass tubing (I.D. 0.305 cm., O.D. 0.487 cm.) was heated and bent at a 90° angle and one end of the tubing was drawn into a tip following heating. Polyethylene tubing (Intramedic PE 200, Clay Adams, Inc., Parsippany, N.J.) with an inside diameter of 0.140 cm. and an outside diameter of 0.190 cm. was also heated, drawn into a tip and secured on the glass tip. A polyethylene tube (I.D. 0.340 cm., O.D. 0.605 cm.) was attached to the other end of the glass tubing and one end of a polyethylene Y tube (I.D. 0.305 cm., O.D. 0.509 cm.) was inserted into the straight polyethylene tubing. The other arms of the Y tube were connected to polyethylene

tubing (I.D. 0.340 cm., 0.D. 0.605 cm.). One of these tubes was attached to a disposable syringe (Plastipak Luer-Lok Tip 5 cc., Becton, Dickinson and Co., Rutherford, N.J.) while the other tube was secured to a metal terminal. The terminal was then connected to a male plug and platinum needle electrode (Grass Model E-2, Grass Instruments Co., Ouincy. Mass.) and the lead from the electrode was attached to the positive terminal of the Grass Stimulator. chloride, plated silver wire (exactly like that used for indirect muscle stimulation) was soldered to the metal terminal and was passed down the tubing to the tip of the glass tube. A second segment of plated silver wire was wrapped around the polyethylene tip, secured along the tubing, attached to another needle electrode and the needle electrode lead, in turn, was connected to the negative side of the Grass Stimulator. This second wire served as a ground lead in the chamber bath.

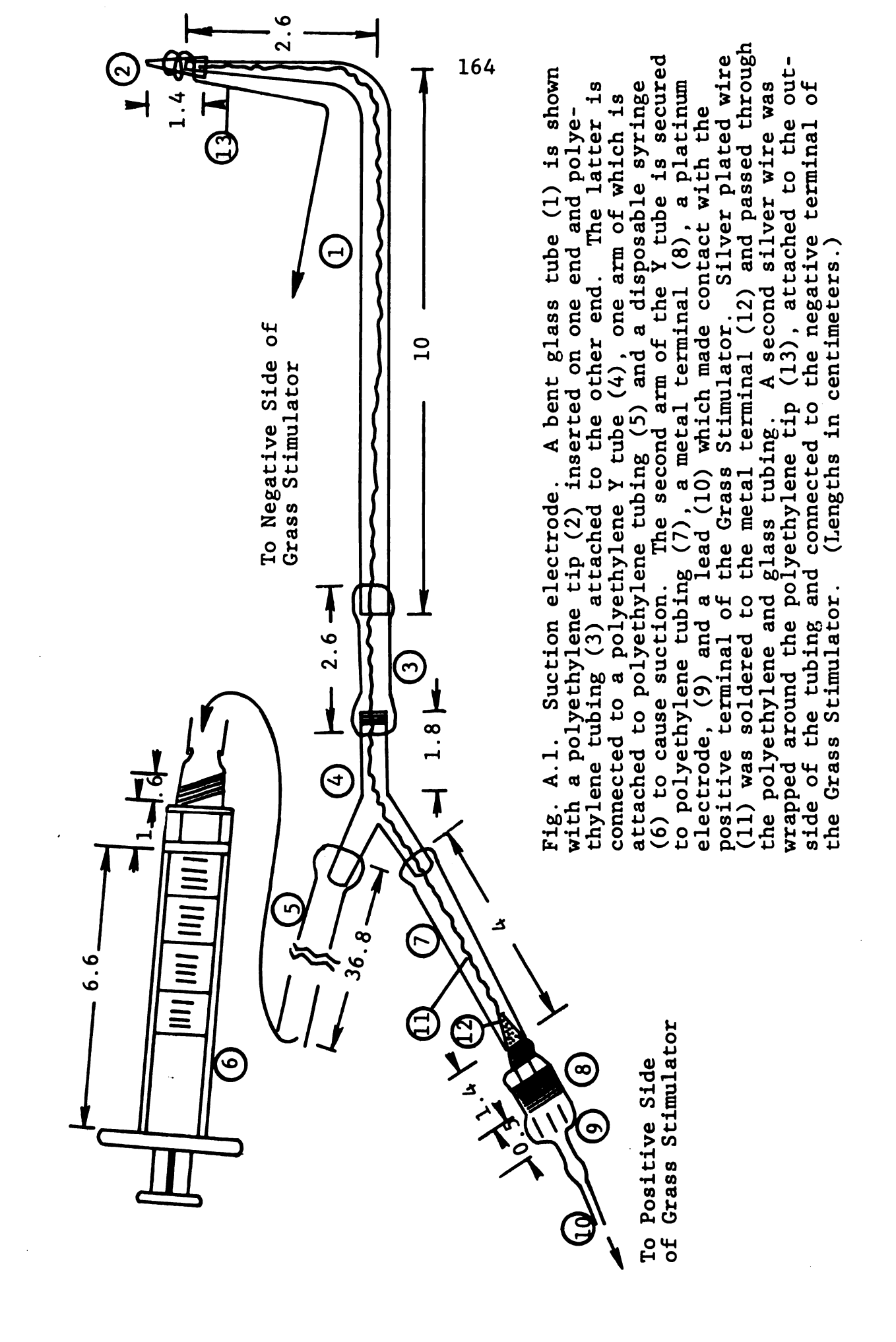
Procedure:

The polyethylene tip was inserted in the bath and placed very close to the obturator nerve segment which had been removed with the anterior gracilis muscle during surgery. The syringe plunger was slowly extended to create suction, causing the nerve to be drawn onto the tip and a small amount of Tyrode's solution to flow in and make contact with both the silver wire and nerve. The power switches on the Grass and auxiliary stimulators were turned

on and the frequency, time duration and current intensity dials were adjusted. The current path was thereby established from the silver wire within the glass tubing through the nerve segment to the ground wire in the bath.

However, the suction electrode was not used because:

1) it was difficult to maneuver in the bath; 2) its weight
pulled the nerve and affected the contractile force recordings; and 3) the resulting forces were dependent not only
upon the generated muscle response but also upon the condition of the myoneural junctions.



APPENDIX B

VISUAL TECHNIQUE FOR CLOSE MUSCLE INSPECTION

Principle:

A camera stand, composed of a camera, telemicroscope, extension tubes, and various lenses, was constructed to provide photographs of the anterior gracilis muscle at magnifications between one and fifteen power.

Equipment:

The camera stand which was designed and constructed by Jon Tyner, a mechanical engineering student, is shown in Figures B-1 a) and b). A camera (Nikon Model F, Nippon Kogaku, Tokyo, Japan) was secured to a support and gear system capable of vertical movement and the support was connected to a heavy base. A Nikon F Camera to Microscope Adapter was then attached to the front of the camera. A Nikon Sleeve was utilized to connect the adapter to the eyepiece (Bausch and Lomb Zoom 10 to 20 Power) of a telemicroscope and stand (Serial Number GB4180, Bausch and Lomb Co., Rochester, N.Y.). Extension tubes (Nikon Series K) were attached to the front of the telemicroscope stand and a reversing ring (Nikon BR-2) was placed ahead of the extension tubes to allow for the attachment of a lens for

proper magnification and space requirements. The lenses which were employed were either a 50 mm. lens (Nikkor Model S, Auto 1:1.4) or a 105 mm. lens (Nikkor Model P, Auto 1:2.5). The film utilized in the tests was Kodak High Speed Ektachrome Outdoor 35 mm. Color Film with an ASA range of 160-600. The lighting was furnished through an electronic flash (Metz Model 203, E.P.O.I., Garden City, N.J.) with color temperatures of 6000°K. and aluminum foil was wrapped around the test apparatus to provide an even distribution of the lighting.

Procedure:

A small rectangular paper grid was taped on the universal joint above the top specimen grip in the same plane as the front face of the anterior gracilis muscle. The camera stand and base were moved close to the test chamber, the adjusting knob on the telemicroscope was turned to focus upon the grid and the magnification was determined. The gear system was then used to move the camera and microscope vertically downward to focus upon the desired area of the muscle. The flash which was incorporated in place of continuous lighting to reduce the heat load, was synchronized with the camera shutter. Previously determined exposure settings (F-Stop and shutter speed) were set and photographs were taken of different regions of the muscle at magnifications between one and fifteen power.

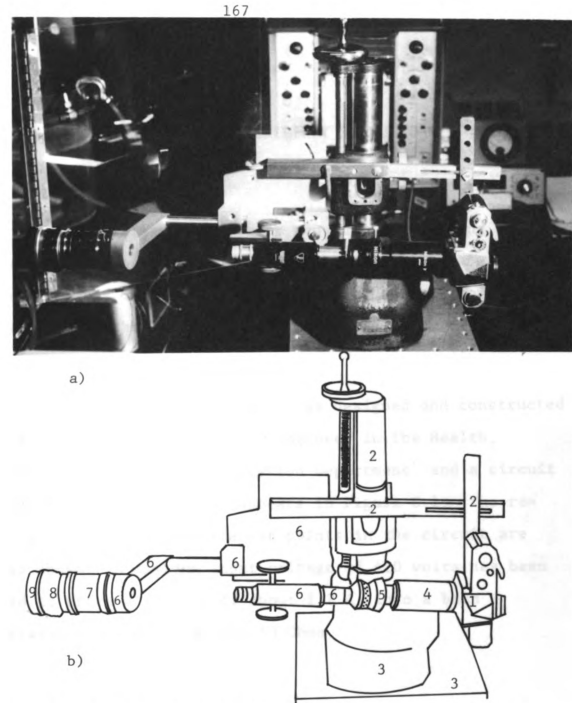


Fig. B.1. (a) Photograph of camera stand and base and (b) sketch of apparatus. The Nikon camera (1) was attached to a support and gear system (2) which rested on a heavy base (3). In front of the camera are a Nikon F Camera to Microscope Adapter (4), Bausch and Lomb Zoom 10 to 20 Power Eyeplece (5), Bausch and Lomb Telemicroscope and Stand (6), Nikon Series K Extension Tubes (7), Nikon BR-2 Reversing Ring (8) and either a Nikkor Model S 50 mm. or Model P 105 mm. lens (9).

APPENDIX C

CIRCUIT DIAGRAM FOR AUXILIARY STIMULATOR

Principle:

The auxiliary stimulator provides alternating square pulses of prescribed current level which, when used with the Grass Stimulator, produces tetanic force responses in the anterior gracilis muscle.

Equipment:

The auxiliary stimulator was designed and constructed by Robert Wells, an electical engineer in the Health, Physical Education and Recreation Department, and a circuit diagram of the stimulator appears in Figure C.1. The resulting waveforms at different points in the circuit are also shown. A maximum input voltage of +10 volts has been used to drive a current of about 1.2 A. into a bath resistance of approximately 50 Ohms.

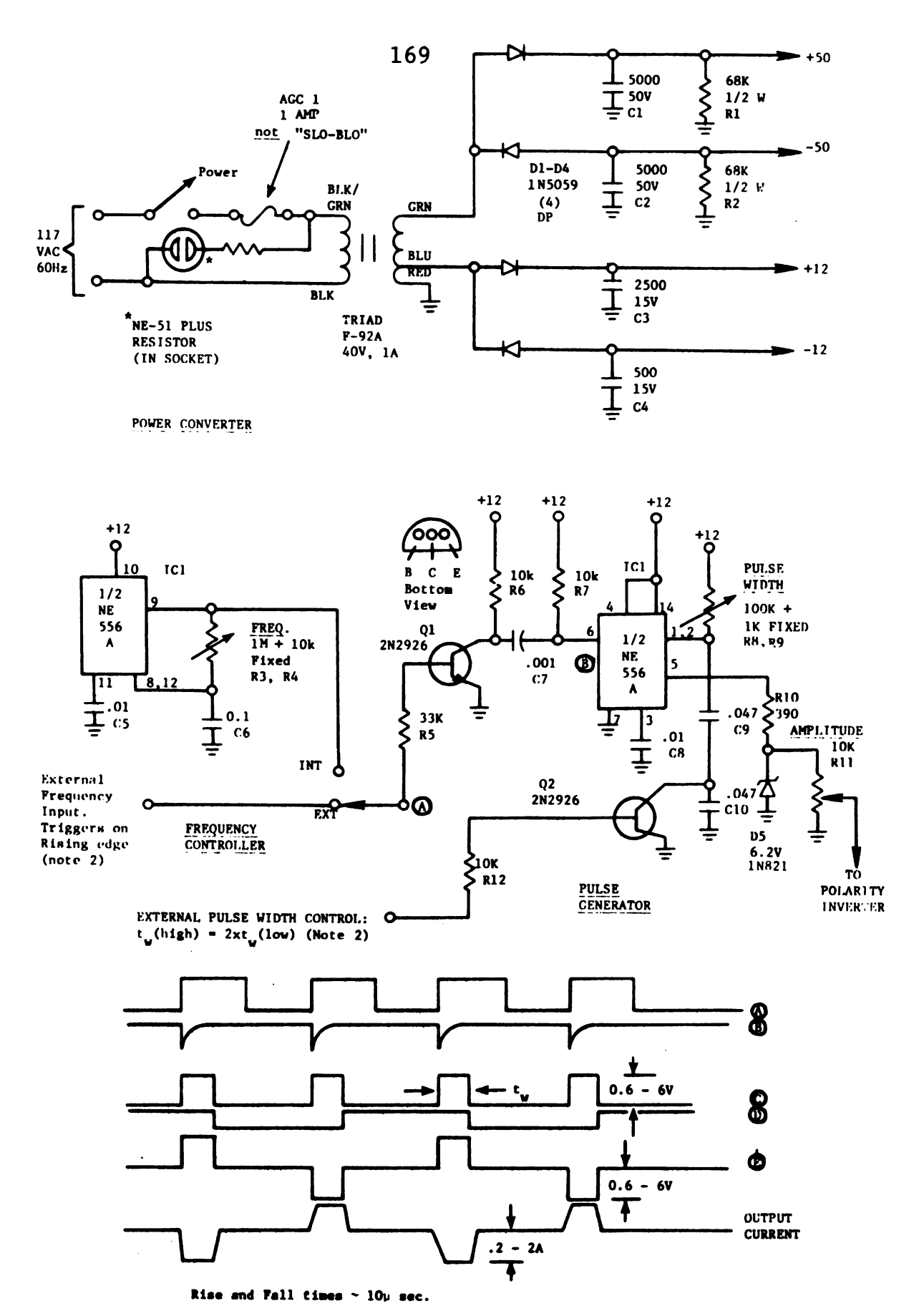


Figure C.1. Circuit diagram of auxiliary stimulator. Note waveforms at different points in the circuit.

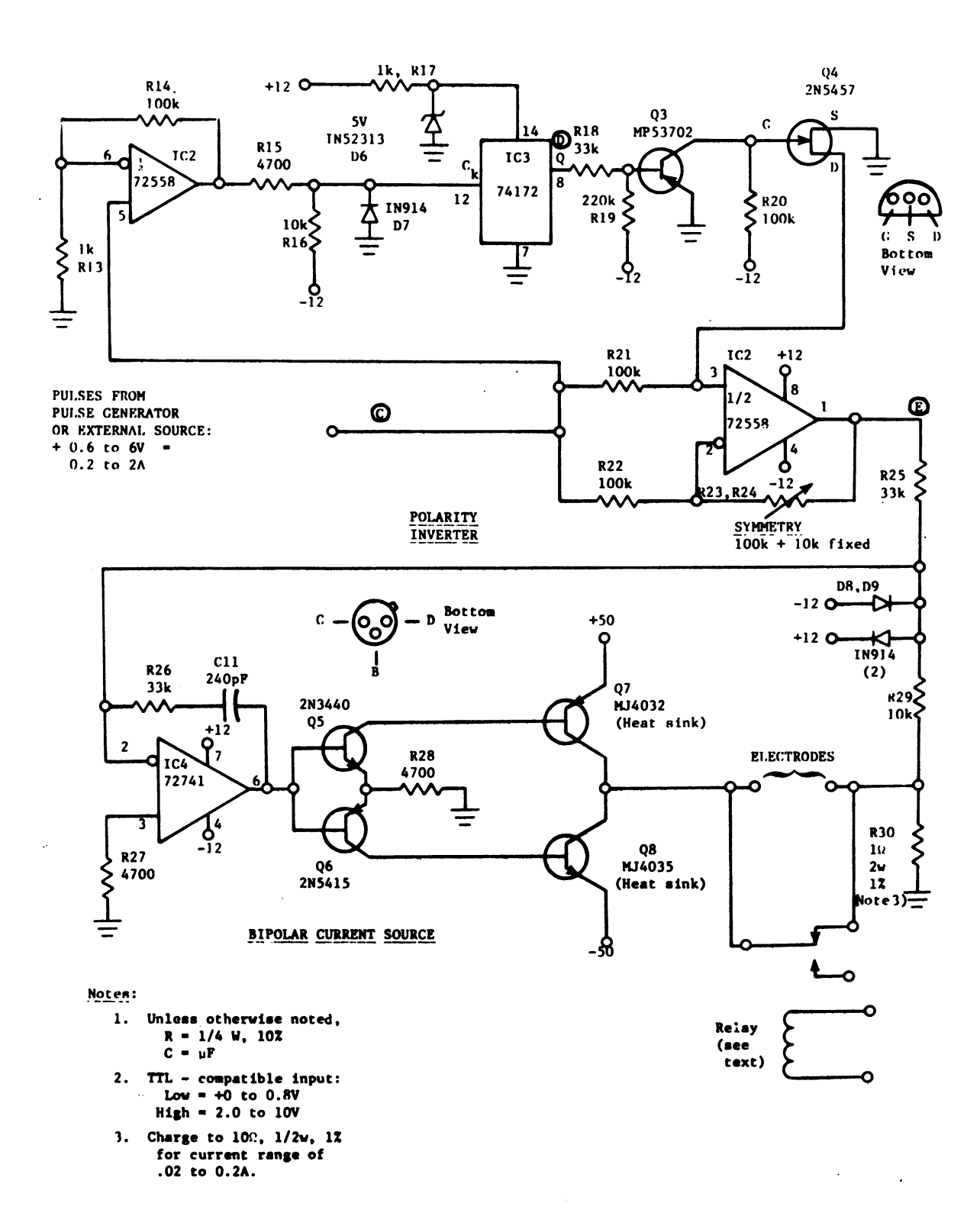


Fig. C.1. (Continued)

